The apparent mass and transmissibility of a bicycle-rider system.

MSc. Thesis Report

J.W. de Haan

Technische Universiteit Delft

TU Delft Delft University of Technology

Challenge the future

The apparent mass and transmissibility of a bicycle-rider system.

MSc. Thesis Report

by

J.W. de Haan

in partial fulfillment of the requirements for the degree of

Master of Science
in Biomedical Engineering

at the Delft University of Technology.

Student number:	4522044	
Project duration:	May 1, 2018 – June 20, 2019	
Supervisor:	Dr. ir. A.L. Schwab,	TU Delft
Thesis committee:	Dr. ir. A.L. Schwab,	TU Delft
	Dr. ir. R. Happee,	TU Delft
	Dr. ir. A.C. Schouten,	TU Delft

This thesis is confidential and cannot be made public until June 20, 2019.

TU Delft Delft University of Technology

Abstract

The objective of this research is to identify the passive response of the rider's body to translational and rotational random perturbations. A custom made bicycle mock-up equipped with a system of sensors has been developed, capable of measuring the linear accelerations, angular velocity and the rider's force responses in all translational axes of all bicycle interfaces. The bicycle mock-up is driven by a hexapod that generates coloured noise perturbations in the range 0–10 Hz. Twenty four healthy male adults participated in this study and gave informed consent according to the guidelines of the ethical committee of Delft University of Technology. The responses of all subjects are represented in the frequency domain by means of frequency response functions. More specific, the interaction of the rider's body at the seat, foot pegs and handlebars are expressed in terms of apparent mass and as seat-to-sternum transmissibility functions (STS). The apparent mass and STS transfer functions for the surge and heave motion suggest a simple underlying passive response system. For surge, a clear resonance peak was found at 2 Hz for nearly all interfaces and directions, whereas, for the heave motion a clear resonance peak at 5 Hz was found for the seat and handlebars and a resonance peak at 6 Hz for the foot pegs. The apparent mass of the pitch and yaw motion also suggest, to a certain extend, simple passive dynamics after 1 Hz characterised by resonance peaks at 1.8 and 2.3 Hz, respectively. Only the corresponding yaw STS transfer function showed a resonance peak around 2.3 Hz, as well. The sway and roll motion do not suggest simple passive dynamics showing similar trends in apparent mass characterised by an ever-decreasing gain and no resonance peaks. Finally, the surge, heave, pitch and yaw apparent mass transfer functions suggest that higher body mass in general yields higher peak magnitude and lower resonance frequency. This effect was most apparent for the surge motion.

J.W. de Haan
Delft, June 2018

Contents

1

Introduction

The bicycle-rider system is a man-machine system in which the total dynamics are determined by the integration of two individual systems: the bicycle and the rider. Two systems mean that resolving the dynamics of the uncontrolled bicycle remains a simplification of the bicycle-rider system. Current bicycle models define the rider as a point mass rigidly attached to the rear frame, or as a pendulum connected to the rear frame [1], [2]. Hence, that the bicycle-rider system is characterised by a relative high rider's mass with respect the mass of the vehicle. This means that the rider adds considerable inertial, stiffness and damping properties to the bicycle system affecting the dynamic response of the total system. Therefore, one can imagine that the dynamics of the bicycle are not only influenced by voluntary control actions (i.e. steering, pedalling and leaning), but also by the passive response of the rider's body to bicycle oscillations. For instance, with the increased number of electric bikes in the streets and higher commuting speeds observed nowadays, the effect of the rider's body to wobble must be explored. Thus, to understand better the bicycle-rider interaction and dangerous oscillatory modes such as wobble, it is prerequisite exploring the passive dynamics of the bicycle rider eventually contributing to better bicycle designs and safety.

F.C.T. van der Helm et al., 2002 [3] and *E. de Vlucht et al., 2006* [4] proofed that system identification is a valuable approach to identify the control mechanisms of the arm, whereas, *Van Drunen et al., 2015* [5] and *Van Drunen et al., 2015* [6] identified the stabilising strategies of the trunk.

The intrinsic body response of seated persons has mainly be performed in the automotive field and is extensively reported in terms of apparent mass and vibration transmissibility. Most research have been performed with respect to vertical whole-body vibrations. For instance, *T.E. Fairley and M.J. Griffin, 1989* [7] investigated the effect of several factors (i.e. footrest, backrest, posture, muscle tension and vibration magnitude) on the vertical apparent mass of seated subjects, whereas, *N. J. Mansfield and M.J. Griffin* [8] studied the non-linearities in apparent mass and transmissibility as a result of different vibration magnitudes. *S. Rakheja and I. Stiharu, 2002* [9] investigated the apparent mass characteristics of car passengers (i.e. hands-in-lap) versus car drivers (i.e. hands-on steering), and analysed the effect of body mass on resonance peaks. *W. Wang et al., 2004* [10] and *N. J. Mansfield and S. Maeda, 2005* [11] shared interests in the effect of different sitting postures on the vertical apparent mass. The first study focused on the effect of back support, hands-on steering wheel and different inclination and pan angels, while, the second study focused also on back support but, as well, on the effect of a twisted trunk and measured the apparent mass in the for-and-aft cross-axis. *M.G.R. Toward and M.J. Griffin* [12] quantified the influence of the position of both the steering wheel and footrest on the apparent mass of the human body. The effect on the vertical apparent mass of inter-subject variability together with four different backrest conditions was investigated by *M.G.R. Toward and M.J. Griffin, 2011* [13]. *J.H. Goa et al., 2011* [14] studied the vertical apparent mass in seated Chinese people and fitted a two-degrees-of-freedom biodynamic model to the experimental data. *M. Kim et al., 2012* [15] measured both the vertical and pitch cross-axis apparent mass of riders exposed to vertical vibrations in different sitting configurations.

Concerning horizontal whole body vibrations, *T.E. Fairley and M.J. Griffin, 1990* [16] analysed the effect of back support on the apparent mass of seated persons during for-and-aft and lateral perturbations . *N.J. Mansfield and R. Lundström, 1999* [17] was interested in the combined motion measuring

the apparent mass of the human body exposed to non-orthogonal vibrations in the horizontal plane. *G.J. Stein et al., 2007* [18] noticed a lack of biomechanical models able to describe the biodynamic for-and-aft interaction between the seated human body and cushioned driver seats. Therefore, they measured the for-and-aft apparent mass of drivers in a cushioned seat holding a frontal support. *Y. Qiu and M.J. Griffin* [19] defined a biomechanical model to simulate the for-and-aft apparent mass of the human body together with the transmissibility of the backrest. *Van Drunen et al., 2015* [5] conducted experiments to study the modulation of intrinsic and reflexive contributions to low-back stabilisation in different conditions.

According to rotational whole-body vibrations, *Van Drunen et al., 2015* [6] investigated neural feedback mechanisms with respect to trunk stabilisation during pitch oscillations.

In the field of two-wheeled vehicles no study has reported the apparent mass of bicycle riders. In literature, most studies report the biodynamic rider response in terms of impedance and kinematics. Rider identification is mainly performed with respect to steer, roll and yaw perturbations.

Concerning steer perturbations, *V. Cossalter et al., 2011* [20] analysed and modelled the stiffness and damping properties of the rider's arms (i.e. steering impedance) and its effect on motorcycle stability.

According to roll perturbations, *A. Doria et al., 2013* [21] measured both handlebar impedance and trunk kinematic transfer functions and fitted several biomechanical models with different degrees of freedom. *M. Bevilacqua et al., 2013* [22] measured the passive response of the rider's body based on interaction forces between the rider and the vehicle. *A. Doria and M. Tognazzo, 2014* [23] performed specific bicycle rider identification and analysed its effect on the open-loop stability of the bicycle.

According to yaw perturbations, *A. Doria and M. Tognazzo, 2012* [24] measured the kinematic transfer function of the rider's trunk and fitted a biodynamic model able to cope with yaw and steer oscillations. Next to roll oscillations, *A. Doria and M. Tognazzo, 2014* [23] performed also rider identification with respect to yaw perturbations and analysed its passive effect on bicycle stability.

The aim of this study is to identify the passive non-parametric response of the rider's body to all translational and rotational motions. The response of the rider's body is represented in the frequency domain by means of frequency response functions (FRFs). More specific, the interaction of the rider's body in the seat, handlebars and foot pegs is expressed in terms of apparents mass and as seat-to-sternum transmissibility (STS) functions. The report is structured as follows: after this brief introduction of state-of-the art research, the experimental procedure and set-up will be presented. Then, the perturbation signal design and the human identification methodology are described after which the results of this research are presented. The report ends with a discussion and conclusion reflecting on the results and findings of this study in the light of established literature.

2

Methods

2.1. Experimental procedure

Twenty four healthy male adults (i.e. mean age = 26 $\pm$ 3 years, weight = 81.7 $\pm$ 7.4 kg, height = 181 $\pm$ 7 cm) participated in this study and gave informed consent according to the guidelines of the ethical committee of the Delft University of Technology.

Two days before the start of the experiment, participants received a research information sheet together with the informed consent form. The research information sheet and informed consent are shown in Appendix A. The experiment started with a ten-minute briefing regarding the experimental procedure, safety rules and installing the participant on the experimental setup. Participants were requested, while wearing a safety harness, to sit on a bicycle mock-up placed on a hexapod motion platform, as shown in figure 2.1.

The participants were perturbed in all six DoF. More specific every participant was perturbed in all translational (surge, sway and heave) and rotational motions (roll, pitch and yaw). In figure 2.1 the axes for all motions are illustrated.

For each motion, the participant was asked to perform a relaxed task. The relaxed task was formulated as follows: *"take the posture of a bicycle rider while relaxing your entire body as good as possible, and keep focussing in front of you during the motion"*. All reaction forces generated by the rider due to the perturbation were measured at all bicycle interfaces: the seat post, the left and right handlebar and the left and right foot pegs. Furthermore, both the linear acceleration and the angular velocity were measured of the motion platform and the upper body.

Three trials were conducted for every participant: one offset trial and two perturbation trials. During the offset trial, the offset of the sensors and the static force generated by the participant on the bicycle mock-up were measured. Each trial had a duration of 60 seconds. Every participant performed 18 trails in total. After three trails the participant was asked to stand up and to stretch his body to prevent muscle stiffness and fatigue.

A "raw TLX" questionnaire was administrated after the experiment in order to evaluate its subject response.

2.2. Equipment and setup

Hexapod motion platform

The eMove eM6-670 electric motion system from E2M Technologies was used to apply perturbations to the rider. This motion system is a six degrees of freedom (DOF) hexapod typically being applied in flight and vehicle simulators. Figure 2.1 shows the motion platform. To simulate bicycle motions virtual axes had to be installed in the motion platform. The longitudinal axis (X-axis) and lateral axis (Y-axis) are placed 15 cm below the surface of the grey wooden base of the mock-up. This height was determined based on the distance between the seat post and the ground surface in a real bicycle. The vertical axis (Z-axis) runs straight through the seat post.

Figure 2.1: The experimental setup. Surge is the translation along the X-axis, sway is the translation along the Y-axis and heave is the translation along the Z-axis. Roll is the rotation around the X-axis, pitch is the rotation around the Y-axis and yaw is the rotation around the Z-axis. The virtual X- and Y-axis were placed 15 cm below the surface of the grey wooden base of the bicycle mock-up.

Bicycle mock-up

The identification of the rider's body response during perturbations requires the development of a custom-made set-up. The custom-made set-up must be able to perturb the rider's body in a wide frequency range and monitor its response. Another important requirement for the design of the set-up is its geometry. A realistic rider posture should be guaranteed, since the activation of the various muscular regions may depend on posture. An experiment with a posture different from the one of a bicyclist may lead to results that are not useful for bicycle-rider identification. To fulfil the requirements mentioned above a modular experimental set-up has been developed; it consists of a custom-made bicycle mock-up, a system of sensors, a data acquisition system and an ultra-precision hexapod. The bicycle mock-up is constructed from steel tubes combined with aluminium clamps (figure 2.2). It is equipped with standard bicycle handlebars (which cannot rotate about the steering axis), a saddle and custom made foot pegs. In contrast to a real bicycle, the foot pegs are mirrored to the bicycle plane of symmetry. Mirroring is done in order to have comparable results between the left and right leg. The frame is constructed to represent a hybrid bicycle and has a reach-to-handlebars equal to 34 cm and stack-to-handlebars equal to 75 cm. This frame geometry leads to an upper torso inclination of approximately 20 degrees (slightly bend elbows), and a knee, ankle angle of about 90 and 75 degrees, respectively. The latter applies to the body build of the 95% of the male European population. Aforementioned dimensions are shown in Figure 2.2.

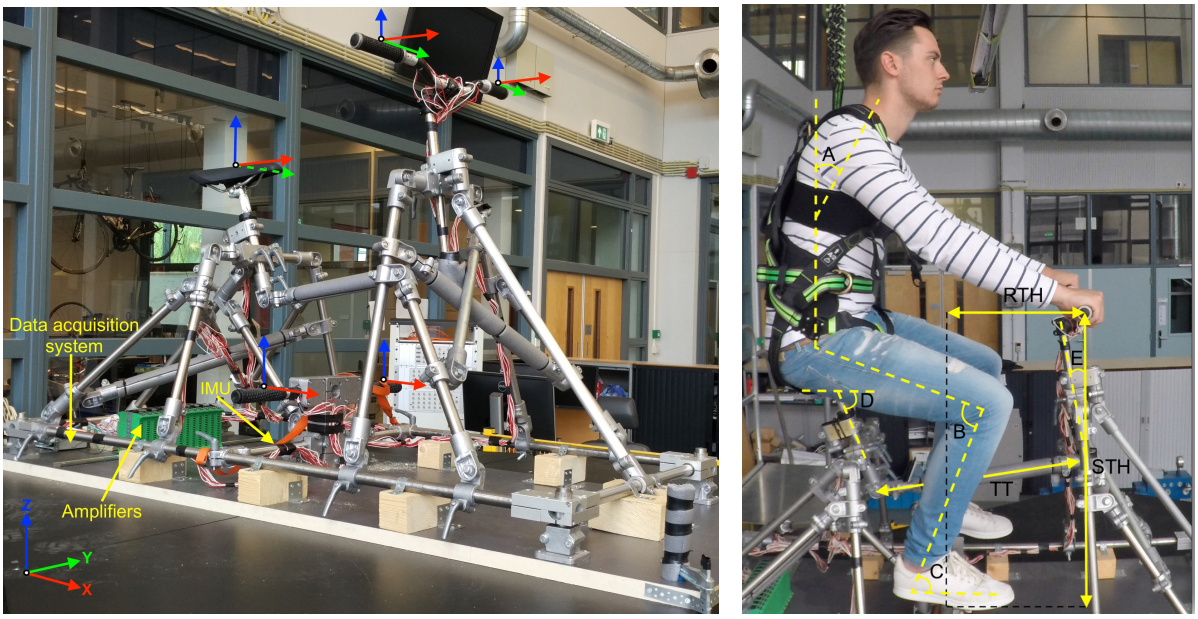

(a) Mock-up (b) Dimensions

Figure 2.2: (a) shows the bicycle mock-up with strain gauge transducers placed at five interfaces. A right-hand sided Cartesian coordinate frame defines the directions of the measured forces. Forces in forward, left and upward direction are considered as positive. Picture from [25]. (b) shows the main rider and mock-up dimensions. Angle **A** is the upper torso inclination ($\pm$ 20°), **B** is the knee angle ($\pm$ 90°) and **C** is the ankle angle ($\pm$ 75°). Angle **D** is the seat post inclination (72°), **E** is the head angle (12°), **RTH** is the reach-to-handlebars (34 cm), **STH** is the stack-to-handlebars (75 cm) and **TT** is the top tube length (68 cm).

Sensors

MTw Awinda wireless motion trackers from Xsens were used to measure linear accelerations and angular velocities. The MTw's are miniature inertial measurement units containing 3D linear accelerometers and 3D rate gyroscopes. One IMU was placed on the motion platform. Figure 2.3 shows the position of the IMU. This IMU was used to measure the input signal for the identification procedure. In the case of translational perturbations, the IMU measured linear accelerations, whereas, the IMU measured angular velocity for rotational perturbations. In the case of translational motions, the linear acceleration of the motion platform is equal to the linear accelerations at the interfaces. However, this does not hold for rotational motions. In the case of rotational motions, the angular velocity measured at the motion platform was multiplied with the position vector of the interfaces to obtain the linear velocities at all

interfaces. Table 2.1 shows the position vectors (r) of the interfaces relative to the IMU placed on the motion platform.

Table 2.1: The position vectors for all interfaces relative the IMU on the motion platform. Note, that the handlebar strain gauge transducers that measure the force in x- and z-direction are near the stem, and the strain gauge transducers that measure the force in y-direction are near the handlebars. Therefore, they have different position vectors.

	Seat post (m)	**Handlebars (m)**	**Foot pegs (m)**
r_{x-axis}	0.67	0.92(xz), 0.97(y)	0.24
r_{y-axis}	0.67	1.11(xz), 1.13(y)	0.35
r_{z-axis}	0	0.64(xz), 0.65(y)	0.31

The second IMU is placed at the infrasternal notch of the rider, and it is used to measure upper torso dynamics. Figure 2.3 for exact location. Xsense MT manager software package is used for logging and to present real-time data.

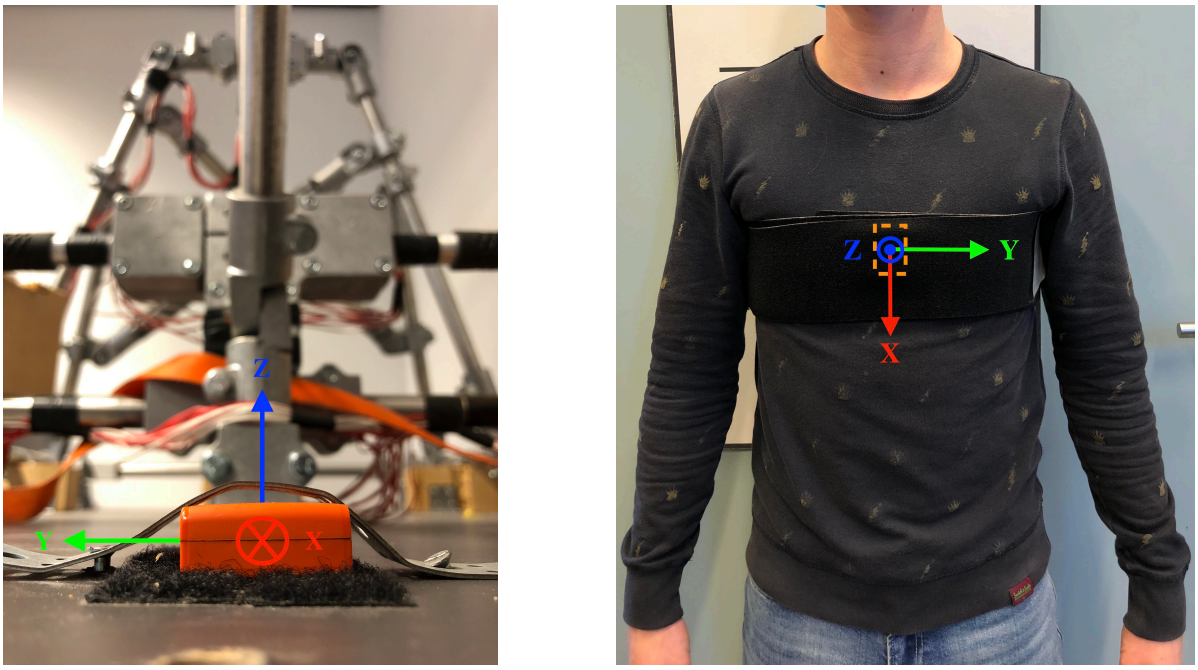

(a) Platform IMU (b) Upper body IMU

Figure 2.3: (a) shows the IMU placed on the motion platform and (b) shows the IMU placed on the sternum of the participant. For both IMU's the right-hand sided Cartesian coordinate frame is shown.

The bicycle mock-up is equipped with 52 strain gauges (3 wheatstone bridges per handlebar side, 2 per footpegs side, and 3 at seatpost) capable of measuring the rider's force response in all translational axes at the interfaces. A data acquisition system from National Instruments/LabVIEW is used for data logging the strain gauges at 100 Hz.

Calibration and sign convention

During the offset trail, the offsets of the IMUs were measured. The offset trail contains a static period of 60 seconds. Thus, during this period no linear accelerations and angular velocities were expected. However, the IMUs measured small accelerations and angular velocities. These offsets were considered as measurement errors, which were subtracted from the measured data during the analysis.

Due to temperature variations, the offset of the strain gauges can change. Therefore, each day before the start of the experiments, the offset of the strain gauges was measured in a static experimental setup without a participant. These offsets were considered as measurement errors, which were subtracted from the measured data during the analysis.

A right-handed Cartesian coordinate system was used as the global reference frame to indicate the direction of the motions and forces. The right-handed Cartesian body-fixed coordinate frame of

the motion platform, the strain gauge transducers and IMUs are shown in figure 2.1, 2.2 and 2.3, respectively. The right-handed Cartesian coordinate system indicates that a motion and a force in the forward direction (X-axis), the left direction (Y-axis) and the upward direction (Z-axis) are considered as positive. For rotational motions, this means that right-handed rotations around the X-, Y- and Z-axis can be considered as positive. In every trial, the body-fixed frame of both IMUs was aligned with the global bicycle frame, see figure 2.3 for the coordinate system of the IMUs.

2.3. Participants

In total 24 subjects participated in this study, their characteristics are shown in table 2.2. The mean weight and height of young adult European males were chosen as the reference point for our population. The mean weight of the European population (men and women combined) is 70,8 kg [26]. The mean height of young adult European males, calculated as a weighted average of 42 European Nations, is 178 cm [27]. The population had a mean age of 26, a mean weight of 81.2 kg and a mean height of 181 cm.

Table 2.2: The table shows the age, weight and height of all participants that participated in this research.

Particiapnt	Age	Weight (kg)	Height (cm)	Particiapnt	Age	Weight (kg)	Height (cm)
1	25	71.2	170	13	29	85.9	186
2	22	80.5	182	14	28	100.3	178
3	25	90.1	190	15	28	73.9	180
4	21	83.5	179	16	30	81.5	177
5	25	76.8	186	17	29	70	175
6	24	79.7	186	18	25	90.2	188
7	23	81.9	180	19	25	92.3	193
8	26	77.5	188	20	25	86.9	188
9	27	72.3	180	21	26	87	171
10	32	80.3	166	22	24	78.5	184
11	36	76.3	173	23	24	72.5	185
12	28	77.6	178	24	24	81.1	185
Mean					**26**	**81.2**	**181**
SD					**3**	**7.4**	**7**

Women did not participate in this research due to potential measurement issues concerning the upper body. As a result of a different upper body structure, and placing an IMU on the sternum different upper body motions can be measured between men and women. The potential risk is a biased identification of the upper body.

Identification task

It was decided to perform a relaxed task to identify the passive rider. For human identification, it is recommended to formulate extreme tasks such as a relaxed task or a co-contracted task. During a relaxed task, the body segments are entirely relaxed, whereas, the body segments are very stiff during a co-contracted task. The advantage of extreme tasks is that voluntary control behaviour is minimised. Note, that the real control behaviour is somewhere in between. Since the posture of a normal bicycle rider, especially for a passive rider, is close to a relaxed body posture a relaxed task was formulated as follows: *"take the posture of a bicycle rider while relaxing your entire body as good as possible, and keep focussing in front of you during the motion"*.

As aforementioned, one motion consists of three trials (one offset trail and two perturbation trials). Between the trials, the participant was allowed to release his hands from the handlebars. The participant was not allowed to change his position on the seat post and foot pegs between the three trails. This was crucial to maintain the same rider posture for every motion as good as possible. In prior-experiments, the rider was also not allowed to release his hands from the handlebars. However, in this configuration, the rider experienced stiffness in his arms, neck and upper body resulting in fatigue. Therefore, it was decided to release his hands between the trials to relax his body. The participant was asked to place his hands on roughly the same position on the handlebars to maintain the same body posture. Between the motions (thus, after three trials), the participant was allowed to stand up to stretch his entire body to prevent body stiffness.

Carryover effects

All subjects were perturbed in all 6 DoF, and a Latin square was used to randomise the sequence of the motions for each participant. Table 2.3 shows the Latin square for six motions and six participants. In a Latin square, each motion appears one time in each row and one time in each column. As a result, each motion appears exactly one time at each position in the sequence. Since we have six motions, the Latin square can maximally define the sequence for six participants and, therefore, after six participants the Latin square repeats.

Table 2.3: The Latin square for six motions and six participants. For each participant the sequence of motions is shown. After six participant the Latin square repeats. Thus, the sequence for participant number seven is equal to the sequence of participant number one.

Participant 1	surge	sway	heave	roll	pitch	yaw
Participant 2	sway	heave	roll	pitch	yaw	surge
Participant 3	heave	roll	pitch	yaw	surge	sway
Participant 4	roll	pitch	yaw	surge	sway	heave
Participant 5	pitch	yaw	surge	sway	heave	roll
Participant 6	yaw	surge	sway	heave	roll	pitch

The advantage of a Latin square is that carryover effects such as learning and fatigue can be controlled. Despite random perturbations and a relaxed task, it could be that the participant gets familiar with the experimental procedure and, therefore, can adapt his control behaviour during the experiment. The same holds for fatigue. During the experiment, it could be that muscle fatigue arises. As a result of a Latin square, the potential effect of learning and fatigue is kept the constant and minimised for each motion. Note, that the Latin square assumes that the carryover effects are constant and equal for each participant.

2.4. Passive rider control diagram

The dynamics of a system can be derived based on measured in- and output signals. The derivation can be carried out both in time and frequency domain. Figure 2.4 shows the general control diagram of a system in the time domain. In the time domain, the output signal of the system is the convolution of the system's time response with the input signal (equation 2.1). Identification of the system's time response requires deconvolution (equation 2.2), which is computationally demanding and results in a function from which the system dynamics hardly can be derived by eye.

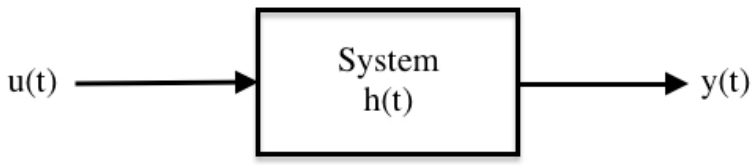

Figure 2.4: The control diagram for a system in time domain. $u(t)$ is the input signal, $h(t)$ is the system's time response (impulse response) and $y(t)$ is the output signal of the system.

$$y(t) = h(t) * u(t) = \int_{-\infty}^{\infty} h(\tau)u(t-\tau)d\tau \tag{2.1}$$

$$h(t) = u(t) * y(t) = \int_{-\infty}^{\infty} u(\tau)y(t-\tau)d\tau \tag{2.2}$$

It is known, that convolution in the time domain is equal to multiplication in the frequency domain. Thus, the output signal of the system in the frequency domain can be calculated by taking the Fourier Transform of the measured time signal $u(t)$ and the system's time response $h(t)$ followed by the multiplication of the transformed signals (equation 2.3). From multiplication follows that system dynamics are identified by the division of the in- and the output signal in the frequency domain (equation 2.4).

Therefore, derivation in the frequency domain is mathematically simple and efficient resulting in a frequency response function (FRF) from which the dynamics can be derived easily. Based on the above, it is decided to identify the passive rider in the frequency domain.

$$Y(f) = U(f)H(f) \tag{2.3}$$

$$H(f) = \frac{Y(f)}{U(f)} \tag{2.4}$$

Since we are only interested in the passive dynamics of the rider, the bicycle-rider system is considered in this study as an open loop system (there is no feedback loop from the rider to the perturbation platform). In other words, the rider can not influence the motion of the platform by applying any control action (i.e. steering or leaning). The block diagram of the bicycle rider system is presented in figure 2.5, where $p(t)$ and $u(t)$ are the input perturbation signal before and after motion cueing, $n(t)$ is the measurement noise and $y(t)$ is the rider output response. $E(t)$ and $H(t)$ are the dynamics of the platform and rider, respectively.

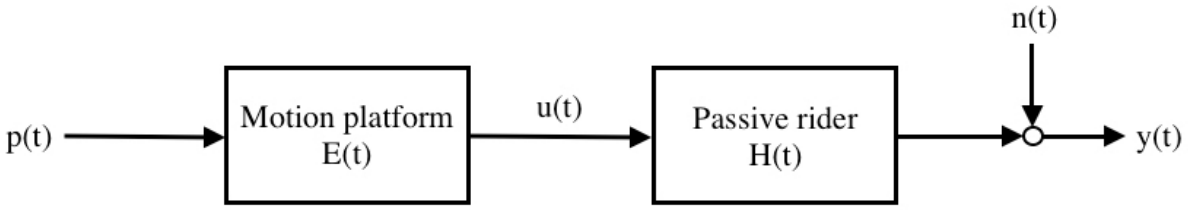

Figure 2.5: The open loop control diagram of the bicycle-rider system. $p(t)$ is the designed perturbation signal, $E(t)$ are the dynamics of the motion platform, $u(t)$ the perturbation motion applied to the rider, $H(t)$ are the passive dynamics of the rider, $n(t)$ is the measurement noise and $y(t)$ is the response of the passive rider.

In practice, $u(t)$ and $y(t)$ are measured. $u(t)$ is measured by the IMU on the motion platform. $u(t)$ resembles linear acceleration for translational motions, whereas, it resembles angular velocity for rotational motions. $y(t)$ resembles the forces measured by the strain gauge transducers at the interfaces. Based on the control diagram of the bicycle-rider system and the measured signals the passive dynamics of the rider can be derived in the frequency domain as follows:

$$Y(f) = P(f)E(f)H(f) + N(f) \tag{2.5}$$

$$H(f) = \frac{Y(f)}{P(f)E(f)} - N(f) \tag{2.6}$$

From the control diagram of the bicycle-rider system it is known that $U(f) = P(f)E(f)$, so that the dynamics can be estimated by

$$H(f) = \frac{Y(f)}{U(f)} - N(f) \tag{2.7}$$

2.5. Perturbation signal selection

In general, an optimal perturbation signal requires prior knowledge of the system to be identified, and the corresponding noise characteristics [28]. Since the dynamics of the bicycle-rider system are unknown, it was decided to use white noise perturbations signals. The advantage of white noise, in contrast to a multisine, is that it contains all frequency increments within a particular frequency bandwidth. Therefore, it excites all dynamics of an unknown system, whereas, in case of a multisine the system is excited at predetermined frequencies. In other words, one already assumes to know the dynamics of a system at frequencies that are not excited within the bandwidth of interest. Since the dynamics of the passive bicycle-rider system are unknown white noise perturbations are used to excite the system.

It is known that many physiological systems of the human are highly non-linear due to neural reflexes; geometry of muscles and tendons; changing muscle arms with the joint angle, and non-linear force-length and force-velocity muscle fibre properties. The advantage of white noise is that it is a stochastic signal, and, therefore it prevents feedforward responses from human participants. When humans anticipate, humans adapt their control dynamics, which result in non-linear control behaviour that not can be identified.

The disadvantage of white noise is that it has a bad signal-to-noise ratio (SNR) and that it is sensitive to aliasing and leakage. How we take care of these aspects, will be addressed in Section 2.6 and 2.8. Pink noise was also considered as perturbation signal. Pink noise is a signal in which the power spectral density is inverse proportional with the frequency ($1/f$). However, due to $1/f$ the perturbation signal will have very large amplitudes at very low frequencies, which can result in discomfort for the rider and non-linear control behaviour. In similar research studies, frequency sweep perturbations are typically used to identify the mechanical impedance of a rider. *A. Doria et al., 2013* [21], *M. Bevilacqua et al., 2013* [22] and *A. Doria and M. Tognazzo, 2014* [23] used frequency sweep perturbations (0.5 - 10 Hz duration of 115 s) to identify the response of the rider's body to roll oscillations. In their experiments, the amplitude of the frequency sweep was decreased at higher frequencies in order to avoid non-linear rider behaviour. However, the disadvantage of a frequency sweep signal is that the amplitude increases linear in time and, therefore, allows for feedforward responses of the rider.

Bandwidth

System identification requires that a perturbation signal continuously excites the dynamics of the system over a given measurement period [28]. Therefore, the designed signal should contain at least all frequencies at which the dynamics of the system should be identified. Since there is no prior knowledge about the dynamics of the passive rider, it is decided to identify the passive rider between 0 and 12 Hz. In this case, the perturbation signal includes the frequencies of the weave and wobble motion, which are considered as the most dominant oscillatory modes in bicycles [1], [29], [2] and [30]. Typical frequencies for weave and wobble are between 0 - 2 Hz and 0 - 8 Hz, respectively. Despite the frequencies concerning the weave and wobble mode, while during bicycling the rider is also exposed to road surface vibrations. Therefore, it is also interesting to excite the dynamics of the passive rider at frequencies outside these ranges. It was decided to identify the passive rider in a frequency range of 0 - 12 Hz.

Amplitude

The goal of this research is to identify a passive bicycle rider that resembles the passive dynamics of a rider during bicycling in real-life. The maximum perturbation amplitudes for all translational and rotational signals were based on naturalistic cycling data measured by *Van den Ouden, 2011* [31]. The finite time measurements from *Van den Ouden, 2011* [31] can be found in Appendix B. From the time measurements, the maximum accelerations for each motion were determined (surge, sway, heave, roll, pitch and yaw).

Since a Gaussian white noise has a normal distribution, the standard deviation (SD) can be used as a measure for the amplitudes of a perturbation signal. The following equation is used to determine the amplitude distribution of each perturbation signal:

$$\sigma_{pert} = \frac{\max \ddot{x}}{3} \tag{2.8}$$

in which σ_{pert} is the SD of the perturbation signal and $\max \ddot{x}$ is the maximum acceleration measured for a specific motion. The equation results in a perturbation signal in which 99.7% of the amplitudes are within 3 standard deviations of the mean (zero mean), see figure 2.6. Note, that 3 standard deviations are equal to the maximum measured acceleration and, therefore, 99.7% of the accelerations within the perturbation signal are between μ-3σ_{pert} and μ+3σ_{pert}. Note, that in the case of zero mean signals the root mean square (RMS) is equal to the SD (RMS = SD = σ_{pert}). In signal analysis one speaks of RMS in stead of SD. Therefore, in the remainder of this report the focus is on RMS.

The question remains if perturbations signals with amplitudes close to the real amplitudes in bicycling can be used for passive rider identification. For identification, it is required to identify the passive rider around its linear operation point. The rule of thumb is that amplitudes are as small as possible but

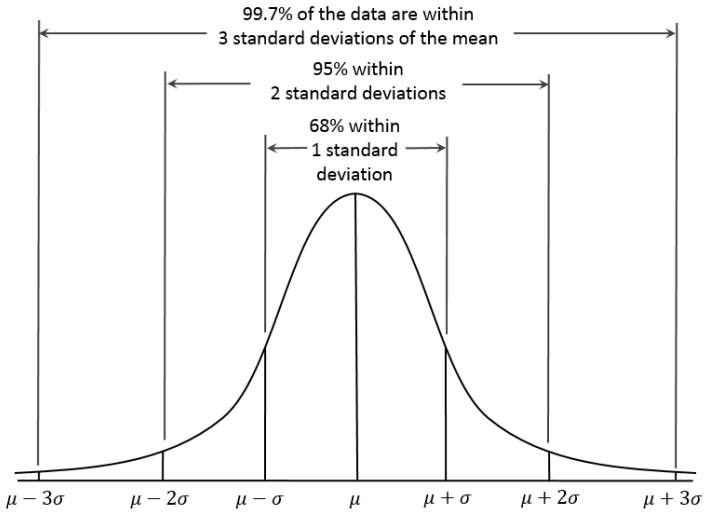

Figure 2.6: Gaussian white noise has a normal distribution.

large enough to perform rider identification. Too large amplitudes can result in discomfort and safety issues for the participant resulting in non-linear dynamics. On the other hand, too small amplitudes will not reach the threshold for particular dynamics and, therefore, cannot be identified. Another important aspect is that large amplitudes at high frequencies can induce non-linear dynamics. Therefore, the power at higher frequencies has to be reduced relative to the power at lower frequencies. The power spectrum of white noise can be adjusted with a low-pass filter. Note, that a filtered white noise is called coloured noise. To find the optimal perturbation signal for each motion it was decided to base the acceleration amplitudes on real-life bicycling acceleration amplitudes. Those perturbation signals were tested in prior experiments in which they were applied to a participant. Based on the FRF, and the coherence it was decided if the signal was proper for passive rider identification or had to be fine-tuned to an optimal perturbation signal. Coherence describes the linear relationship between the in- and the output signal and decreases by noise and non-linear dynamics. Coherence has a value between 0 and 1 in which 1 indicates a full linear relationship between in- and output. Thus, based on the coherence one can determine if the participant stays around the linear operation point when disturbed by the perturbation signal. Table 2.4 shows the determined maximum amplitudes from the measurements from *Van den Ouden, 2011* and the maximum optimal amplitudes for the final perturbation signals.

Table 2.4: The first row shows the maximum amplitudes roughly determined from the finite time measurements from *Van den Ouden, 2011*. Subsequently, the maximum amplitudes of the final perturbation signals used in this research together with the corresponding mean and RMS are shown.

	Surge (m/s²)	Sway (m/s²)	Heave (m/s²)	Roll (rad/s²)	Pitch (rad/s²)	Yaw (rad/s²)
Van den Ouden (2011)	1.5	1.0	1.0	1.0	1.0	1.0
Final max. amplitudes	0.75	0.75	1.0	1.0	0.5	1.0
Mean	-2.62e-04	-6.11e-04	4.25e-05	6.98e-04	2.96e-04	9.31e-04
RMS	0.25	0.25	0.33	0.33	0.17	0.33

2.6. Perturbation signal design

White noise

The perturbation signals were designed with a sample frequency (F_s) of 100 Hz and had a total duration (T_{pert}) of 60 seconds. To design a white noise signal, the following function was used in MATLAB:

$$p(t) = \sigma_{pert} * randn(N, 1) + \mu_{pert} \tag{2.9}$$

in which $p(t)$ resembles the designed perturbation signal (figure 2.5). σ_{pert} is the RMS of the perturbation signal (equation 2.8). $randn(N, 1)$ is a MATLAB function that generates a N-by-1 matrix with pseudorandom values drawn from a normal distribution. N is the total number of samples in

the perturbation signal and can be calculated by $N = T_{pert} * F_S$. μ_{pert} is the mean of the perturbation signal. The mean of each perturbation signal is equal to zero since a perturbation signal always operates around a stable equilibrium position in which the acceleration is equal to zero.

Coloured noise

Equation 2.9 generates a white noise signal with a frequency spectrum up to the Nygquist frequency (= $fs/2$ = 50 Hz). As aforementioned, a white noise has a bad SNR. The SNR describes the ratio between signal power and noise power. The SNR of a white noise signal can be improved by either increasing the input signal $p(t)$ or decreasing the noise $n(t)$ (Figure 2.5).

Filtering the white noise signal will increase the power of the input signal $p(t)$ resulting in a coloured noise signal. Since the white noise signal and the resulting coloured noise signal should have the same variance (i.e. the same maximum amplitude), filtering removes the unneeded frequencies from the perturbation signal, and concentrate based on Parseval's theorem the power in a limited number of frequencies. Parseval's theorem defines that the area under the power spectral density (S_{pp}) is equal to the variance (σ^2_{pert}) of the perturbation signal and is shown in equation 2.10.

$$\sigma^2_{pert} = \int p(t)^2 \, dt = \int P(f)^2 \, df \tag{2.10}$$

Since the white noise signal and the coloured noise signal have the same variance, the area under the power spectral density of both signals is the same. Therefore, in a bandwidth of 0-12 Hz, an equal-sized area is obtained by increasing the power per frequency. Figure 2.7 shows the power spectral densities of the white and the coloured noise signal. A 5-pole Butterworth filter with a cut-off frequency of 9 Hz was used to generate a coloured noise perturbation signal with a bandwidth of approximately 0 - 12 Hz.

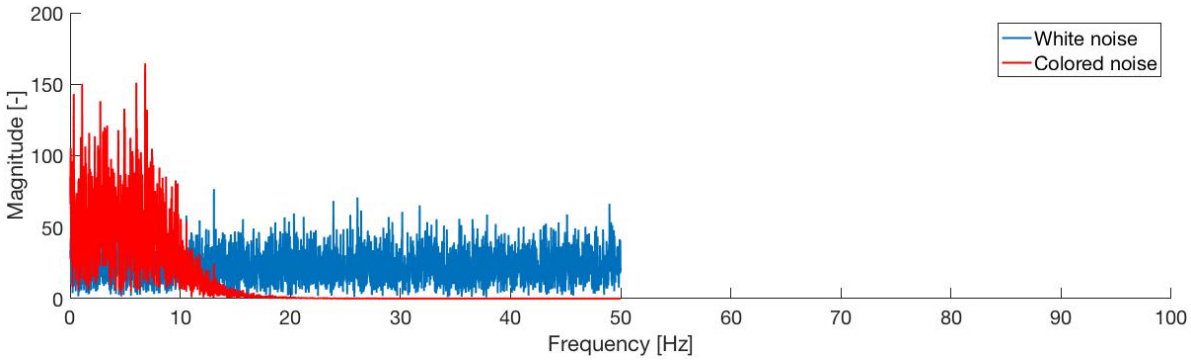

Figure 2.7: The power spectral densities of the white and the coloured noise perturbation signal for the heave motion shown up to the sampling frequency (F_s = 100 Hz). The white noise signal contains power up to the Nyquist frequency (= 50 Hz), whereas, the coloured noise signal contains power up to approximately 17 Hz. It can be seen, that the coloured noise has higher power within a bandwidth of 0 - 12 Hz.

As aforementioned (section 2.5), power had to be reduced at higher frequencies to prevent non-linear rider dynamics and discomfort. Reducing power at higher frequencies was also carried out by the Butterworth filter. For this reason, the red and blue area in figure 2.7 are not exactly equal-sized. The magnitude FRF of the Butterworth filter is shown in Appendix C. Since filters are not perfect a cutoff-frequency of 9 Hz proofed to be the most optimal frequency. As a result, the power reduction starts with minimal reductions at 3.5 Hz after which the reduction increases up to 50% at 10 Hz (Appendix C). Figure 2.8 shows the resulting colored noise perturbation signal for the heave motion.

The Butterworth filter also prevents the potential risk of aliasing. Aliasing arises when a signal is sampled with a too low frequency. As a result, high frequencies will be sampled as low frequencies resulting in a sampled signal that does not correctly resembles the original signal. The rule of thumb defines that the sampling frequency should be at least 2.5 times the cutoff frequency. In our case, the cutoff frequency is 12 Hz (actually 9 Hz for the filter), which means that we should sample at least at 30 Hz. Since both the strain gauge transducers and the IMU have a sample rate of 100 Hz, aliasing will not be a problem when using the coloured noise perturbation signal.

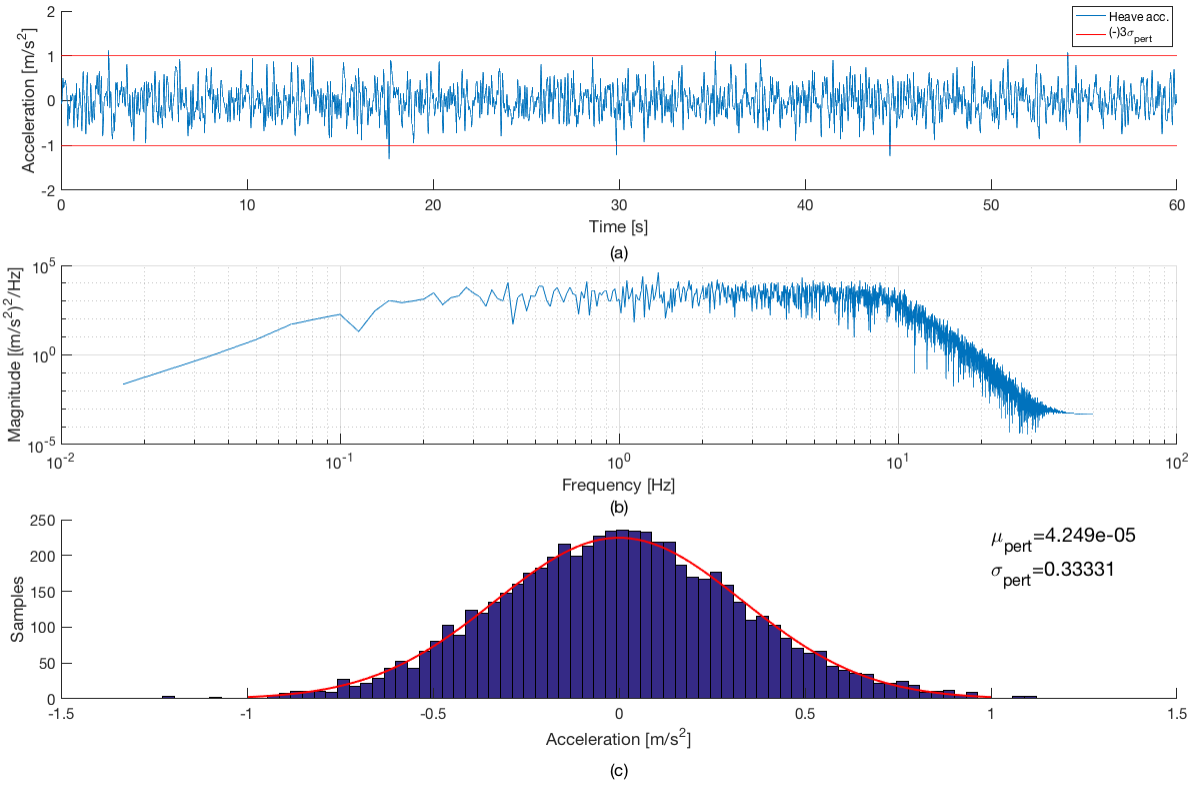

Figure 2.8: The heave perturbation signal. (a) shows the perturbation signal in time domain in which the red lines indicate μ-3σ_{pert} and μ+3σ_{pert}. (b) shows the frequency spectrum of the perturbation signal. (c) shows the amplitude distribution in the perturbation signal with the corresponding mean and RMS.

Extended perturbation signal

Due to the hardware setup, it was not possible to data log the strain gauge and IMU signals using the same real-time operational system (RTOS). There were latency issues, which affected the alignment of the in- and output signals. Two step functions were added to the final signals to solve the misalignment of the signals. The fade-in and fade-out signals had a period of 3.5 seconds and were used as a time stamp for aligning the signals. Figure 2.9 shows the extended perturbation signal for the heave motion with both step signals. The step signal is a smooth motion with a maximum acceleration of 0.25 m/s^2 or 0.25 rad/s^2 for translational and rotational perturbations, respectively. Due to this signal elongation, the total duration of the signal increased to 69 seconds, while the perturbation duration (T_{pert}) remains 60 seconds.

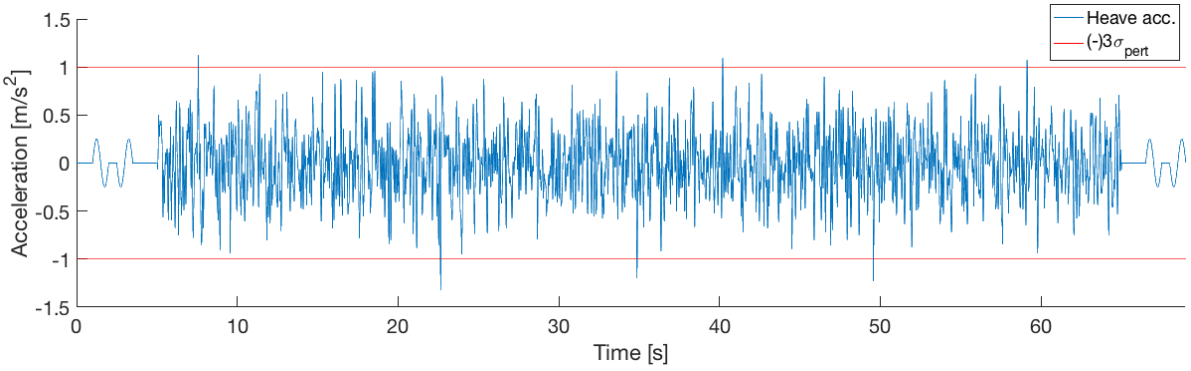

Figure 2.9: The extended heave perturbation signal with a step signal before and after the perturbation part.

Final perturbation signal

The motion platform is PVA controlled. This means that the perturbation signal is made out of three signals: an acceleration signal, a velocity signal and a position signal. The corresponding velocity and position signal were obtained by numerical integration (MATLAB-function: $cumtrapz$) of the designed acceleration signal. Numerical integration goes along with drift in the velocity and position signal due to finite time steps resulting in an estimation error. Drifts are low-frequency signals. Therefore, drift can be solved by filtering the velocity and position signal with a high-pass filter with a very low cutoff-frequency. In this research, a 2-pole Butterworth high-pass filter with a cutoff frequency of 0.2 Hz was used (the magnitude FRF of the Butterworth filter is shown in Appendix C). Figure 2.10 shows the heave and roll PVA signal to control the motion platform. The generated (PVA) signals are used to control the platform, only measured accelerations and angular velocities are used for identification of the bicycle-rider system.

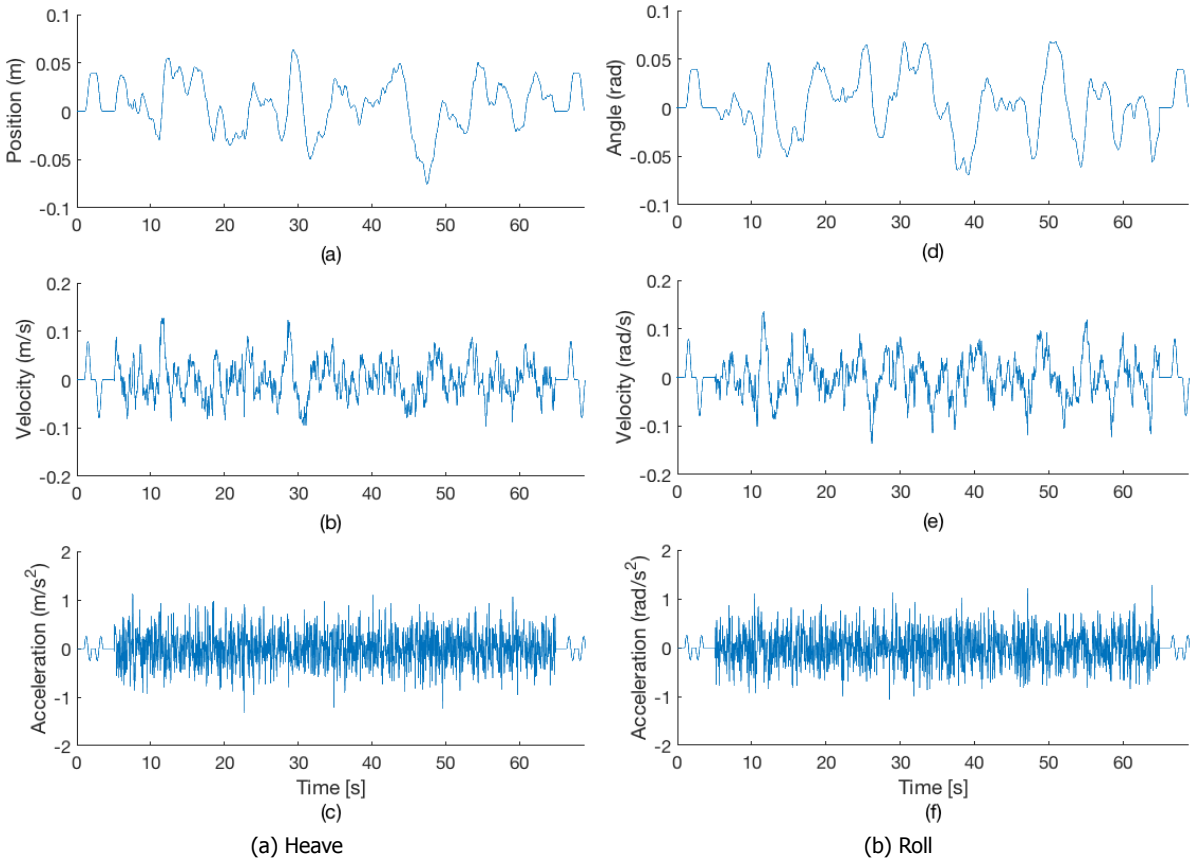

Figure 2.10: (a) and (b) show the PVA signal for the heave and roll motion, respectively. (a) (top row) and (d) show the position signal, which is the result of integrating the acceleration signal twice, (b) (mid row) and (d) show the velocity signal, which is the result of integrating ones the acceleration signal and (c) and (f) show the acceleration signal.

The perturbation design method described above is used to generate all six individual perturbation signals. The characteristics of the six individual perturbation signals are shown in Table 2.4.

2.7. Perturbation signal validation

The designed perturbation signals were validated by comparing them with the actual motion of the platform, which means that the input $p(t)$ signal was compared with the output $u(t)$. A perfect fit validates that amplitudes in the perturbation signal are not changed as a result of motion cueing. Figure 2.11 shows the fit between the designed perturbation signal and the measured perturbation signal in the time domain for the heave and roll motion.

To obtain a perfect fit, the measured perturbation signal had to be filtered to remove measurement noise (> 12 Hz). A finite impulse response (FIR) 70-pole low-pass filter with a cutoff frequency of

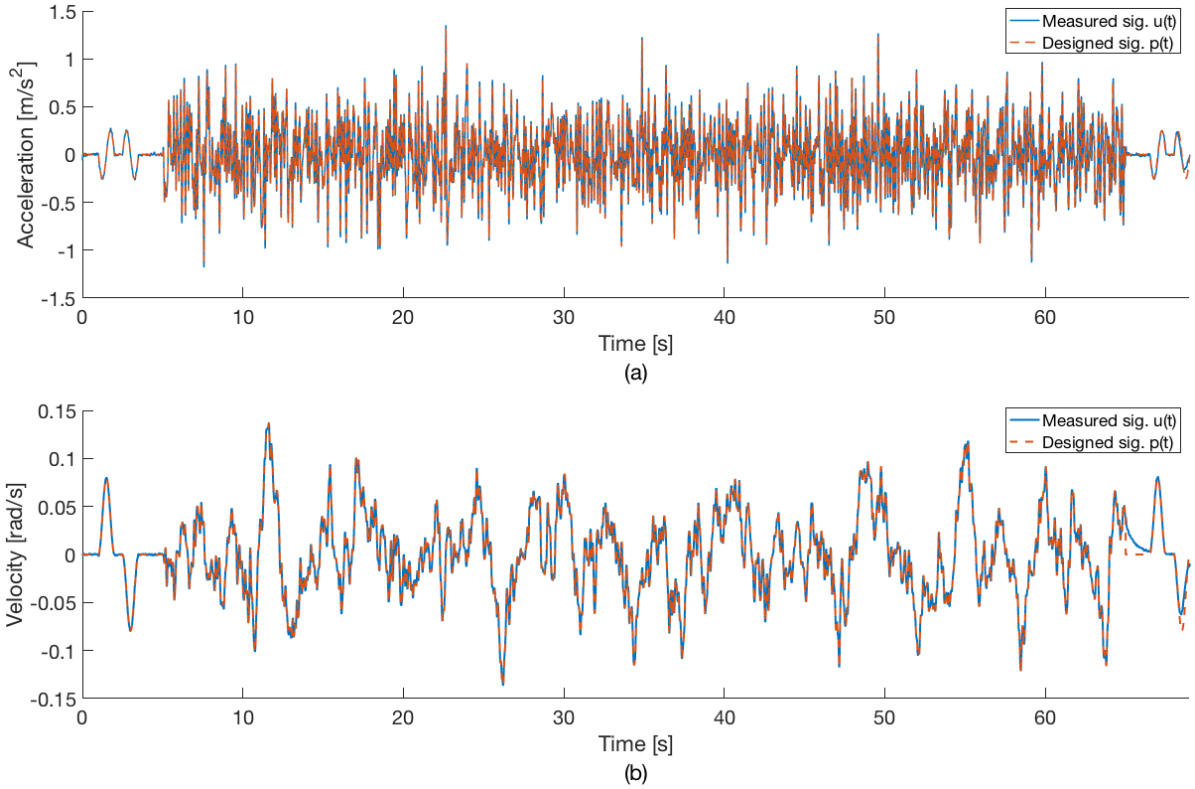

Figure 2.11: The fit between the designed perturbation signal $p(t)$ and the measured perturbation signal $u(t)$ in time domain. (a) and (b) show the fit for the heave and roll motion, respectively.

13 Hz was used to remove the measurement noise. Both perturbation signals had to be aligned due to latency issues. To find the delay between both signals the MATLAB-function $xcov(x, y)$ was used, which returns the cross-covariance of two discrete-time signals x (= $p(t)$) and y (= $u(t)$). From the cross-covariance, the difference in the number of samples between the two signals was calculated. By shifting the measured signal relative to the designed signal with the calculated number of samples, both signals can be aligned after which the fit can be checked. The measured output signal was aligned and resampled. To resample the data the MATLAB-function $resample(x, p, q)$ was used. The function resamples the original signal x (=$u(t)$) at p/q times the initial sample frequency (F_s = 100 Hz). A difference of 2 samples was found (0.02 sec) resulting in a p/q ratio of 0.99997.

For all six individual motions, a perfect fit was obtained between the designed signal and the measured perturbation signal.

2.8. System identification

Since we are only interested in the passive dynamics of the rider, the bicycle-rider system is considered in this study as an open loop system (there is no feedback loop from the rider to the perturbation platform). In other words, the rider cannot influence the motion of the platform by applying any control actions (e.g.steering or leaning). The dynamics of the passive rider are described based on FRFs of the in- and output signals.

Correlation functions were used to derive the FRF of the passive rider. Auto-correlation functions $\Phi_{uu}(\tau)$ reveal structures of signals that are not detectable in the times series. Cross-correlation functions $\Phi_{yu}(\tau)$ are used to analyse the relationship between two signals. Correlation functions in the frequency domain are called spectral densities. The auto-spectral density $S_{uu}(f)$ of a signal corresponds to the Fourier Transform of the auto-correlation in the time domain, whereas the cross-spectral density $S_{yu}(f)$ corresponds to the Fourier Transform of the cross-correlation in the time domain.

There are two ways to calculate the spectral densities of the measured signals: the indirect and the direct method. The indirect approach calculates the auto-/cross-correlation functions of time signals followed by the Fourier Transform resulting in auto-/cross-spectral densities, as shown in flow-graph

2.11. The direct method calculates the Fourier Transform of the time signals from which the auto-/cross-spectral densities are calculated, see flow-graph 2.12.

$$Indirect\ approach = \quad u(t), y(t) \quad \rightarrow \quad \Phi_{yu}(\tau) \quad \rightarrow \quad \hat{S}_{yu}(f) \tag{2.11}$$

$$Direct\ approach = \quad u(t), y(t) \quad \rightarrow \quad U(f), Y(f) \quad \rightarrow \quad \hat{S}_{yu}(f) \tag{2.12}$$

The direct method is considered computationally more efficient and for this reason, is used herein. The spectral densities of the Fourier transformed signals $U(f)$ and $Y(f)$ can be calculated as follows:

$$\hat{S}_{uu}(f) = \frac{1}{N} U(n\Delta f) U^*(n\Delta f) \tag{2.13}$$

$$\hat{S}_{yy}(f) = \frac{1}{N} Y(n\Delta f) Y^*(n\Delta f) \tag{2.14}$$

$$\hat{S}_{yu}(f) = \frac{1}{N} Y(n\Delta f) U^*(n\Delta f) \tag{2.15}$$

where $\hat{S}_{uu}(f)$ and $\hat{S}_{yy}(f)$ are the estimated auto-spectral densities of the in- and output signal, respectively, $\hat{S}_{yu}(f)$ is the estimated cross-spectral density between the in- and output signal, N is the number of samples as a result of a discrete Fourier Transform, n is an integer number, Δf is the frequency resolution and U^* and Y^* are the complex conjugates. The passive rider transfer function $H(f)$ can now be expressed as the ratio of the estimated spectral densities:

$$\hat{H}(f) = \frac{\hat{S}_{yu}(f)}{\hat{S}_{uu}(f)} - \hat{S}_{nu}(f) \tag{2.16}$$

where $\hat{S}_{nu}(f)$ is the cross-spectral density between the input $u(t)$ and noise signal $n(t)$. From the control diagram of the passive rider, see figure 2.5, it follows that the input and noise signal are uncorrelated (open loop system). Since the cross-spectral density describes the interdependency between two signals, $\hat{S}_{nu}(f)$ is equal to zero resulting in the spectral estimator of the passive rider given by:

$$\hat{H}(f) = \frac{\hat{S}_{yu}(f)}{\hat{S}_{uu}(f)} \tag{2.17}$$

Spectral estimator optimisation

A spectral estimator is an estimator that describes the 'true' relation between the in- and output signal. The performance of an estimator can be described based on bias, variance and consistency. Bias is defined as a structural error in the estimation (i.e. raw estimation of coherence). Variance is defined as a random error (i.e. noise). Consistency is defined as the ability of an estimator to converge, in probability, to the quantity being estimated as the sample size grows. The consistency of an estimator improves by reducing bias and variance in the estimator. In other words, by optimising the estimator, the estimation of the passive rider becomes more reliable.

Equation 2.17 is also known as the raw spectral estimator of the passive rider. The raw estimator is not consistent and can be optimised by Welch's method in combination with a Hanning window. The advantage of Welch's method in combination with a Hanning window is that it reduces the effect of noise and leakage in the estimation of the spectral densities. Leakage is a common problem in measured stochastic signals such as white and coloured noise. Leakage occurs when a finite time observation is made of a signal from which certain frequencies do not perfectly fit in the time window. In other words, some frequencies cannot be build-up from the frequency resolution ($\Delta f = 1/T$). As a result, frequencies that do not fit in the time window will have sharp discontinuities at the endpoints of the window, and their power will leak to neighbouring frequencies.

The effect of leakage can be minimised by windowing. Welch's method divides a finite time signal into multiple overlapping time segments. Each overlapping segment is multiplied with a Hanning window. A Hanning window is defined by:

$$w(t) = \frac{1}{2}\left(1 - cos\left(\frac{2\pi t}{T_{seg}}\right)\right) \tag{2.18}$$

In which $w(t)$ is the Hanning window function, t is the time step between each sample and T_{seg} is the duration of each segment. The essence of a Hanning window is that it gives more priority to the data close the centre of the segment than to the data at the edges. Leakage occurs at the edges and, therefore, a Hanning window minimises leakage. However, windowing remains a trade-off since amplitude reduction at the edges results in data loss causing a reduction in frequency resolution. The time segments were overlapped to mitigate the loss of frequency resolution. Finally, the spectral density of each segment is calculated followed by averaging of the individual spectral densities.

As a conclusion, windowing and Welch's averaging reduces the bias and variance in the spectral estimator. A reduction in variance means a smaller confidence interval of the estimator resulting in a more reliable estimation of the FRF and coherence of the passive rider.

The step-by-step procedure followed to calculate the final transfer functions $H(f)$ is presented employing the number points below:

1. A finite time measurement (T = 60 sec.) is obtained from the in- and output signal $u(t)$ and $y(t)$, respectively:

2. Each finite time measurement is divided into 10 segments with 50% overlap, and each segment is multiplied with a Hanning window to remove leakage (time domain):

X

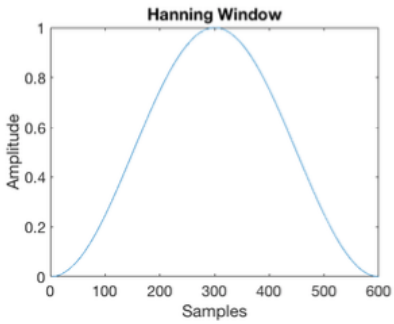

3. The Fourier Transform of each time segment is calculated (frequency domain):

4. The spectral density of each segment is calculated followed by averaging over each segment to reduce noise (frequency domain):

$$\hat{S}_{uu}(f) = \frac{1}{D}\sum_{d=1}^{D} S_{uu}(f) = \frac{1}{DN_D}\sum_{d=1}^{D} U(f)U^*(f) \tag{2.19}$$

$$\hat{S}_{yu}(f) = \frac{1}{D}\sum_{d=1}^{D} S_{yu}(f) = \frac{1}{DN_D}\sum_{d=1}^{D} Y(f)U^*(f) \tag{2.20}$$

in which D is number of segments, d is ϵ [1, 2,$\cdots$, D] and N_D is the number of samples in each segment.

5. The FRF and the coherence are calculated by dividing the correct spectral densities:

$$FRF: \quad \hat{H}(f) = \frac{\hat{S}_{yu}(f)}{\hat{S}_{uu}(f)} \tag{2.21}$$

$$Coherence: \quad \hat{\gamma}^2_{yu}(f) = \frac{|\hat{S}_{yu}(f)|^2}{\hat{S}_{yy}(f)\hat{S}_{uu}(f)} \tag{2.22}$$

Coherence

In order to analyse the coherence correctly the significance of coherence (CSL) is calculated and added to the coherence plots. The CSL indicates the threshold above which the coherence is significantly different from zero and is calculated by the following equation:

$$CSL = 1 - \alpha^{\frac{1}{L_{seg} - 1}} \tag{2.23}$$

in which α is the significance level and defines the probability of committing a Type 1 error. In other words, it defines the confidence interval of the estimator. L_{seg} is the number of independent segments. Since the spectral densities are averaged over 10 segments with 50% overlap resulting in 5 independent segments, coherence greater than 0.53 is significant with $\alpha < 0.05$. Note, that the CSL does not indicate linearity between input and output.

2.9. Transfer functions

The passive dynamics of the rider will be described by both 1D kinematic and 3D (X, Y, Z) kinetic transfer functions. The kinematic transfer functions are expressed in terms of transmissibility, which describes the transmission of vibrations between the bicycle mock-up and the rider's torso. Sub-experiments turned out that the acceleration is identical for both the hexapod base and the seat post. Therefore, in this report the torso transmissibility is referred as seat-to-sternum transmissibility (STS), which is defined as the ratio between the torso motion and the motion of the hexapod base. The STS transfer function of the translational motions is defined by the following FRF:

$$T_{trans}(f) = \frac{a_{torso}(f)}{a_{mock-up}(f)} \tag{2.24}$$

in which $T_{trans}(f)$ is the STS transfer function for translational motions, a_{torso} is the linear acceleration of the torso measured at the sternum and $a_{mock-up}$ is the linear acceleration of the mock-up measured at hexapod base. The STS transfer function of the rotational motions is defined by the following FRF:

$$T_{rot}(f) = \frac{\omega_{torso}(f)}{\omega_{mock-up}(f)} \tag{2.25}$$

in which $T_{rot}(f)$ is the STS transfer function for rotational motions, $\omega_{torso}(f)$ is the angular velocity of the torso measured at the sternum and $\omega_{mock-up}(f)$ is angular velocity of the mock-up measured at the hexapod base. Note, that the gain of the STS transfer functions is unitless since it is obtained by a division of the same units.

The kinetic transfer functions are expressed in terms of apparent mass, which is defined by the following FRF:

$$M(f) = \frac{F(f)}{a(f)} \tag{2.26}$$

in which $M(f)$ is the apparent mass transfer function, $F(f)$ are the linear forces measured in all interfaces (i.e. seat post, foot pegs and handlebars) in all directions (X, Y and Z) and $a(f)$ are the linear accelerations. Note, that the AM transfer functions of the rotational motions are also described by their linear components. Since the IMU only measures angular velocity, the measured angular velocities are differentiated with respect to time to obtain angular accelerations. The angular accelerations are multiplied with the position vectors of the interfaces to obtain the corresponding linear accelerations. Thereby, the rotational transfer functions are comparable to the translational transfer functions.

The apparent mass is a derivation of Newton's second law (i.e. $F = ma$). Therefore, the apparent mass can be described by kilograms (kg). Note, that the unit kilograms only resembles a pure mass when the dynamics of an unknown system are described by a rigid body. The transfer function of a rigid body is characterised by a gain that is not a function of frequency, and a phase of zero degrees for all accelerations and frequencies. Therefore, the apparent mass of a rigid body resembles its static mass. However, in the case of humans the apparent mass is often the result of a combination of several parameters (e.g. mass, spring and damper properties) that describe the dynamics of the underlying system. In this case, the unit kg does not resemble a pure mass but resembles the total combination of the underlying system parameters.

It should be noted, that for the yaw motion the apparent mass transfer function cannot be calculated for the seat post since the axis of rotation runs through the force measuring point and, therefore, its position vector is equal to zero. This means that the yaw angular acceleration has no linear acceleration component at the seat post where linear forces are measured. Therefore, only for this specific situation, an "apparent mass" transfer function is calculated that describes the ratio between the measured linear forces at the seat post and the corresponding yaw angular acceleration. This ratio is defined by the following FRF:

$$M_{yaw,SP}(f) = \frac{F_{SP}(f)}{\dot{\omega}_{yaw}(f)} \tag{2.27}$$

in which $M_{yaw,SP}$ is the yaw transfer function of the seat post, F_{SP} are the corresponding linear forces measured in all directions (X, Y and Z) at the seat post and $\dot{\omega}_{yaw}$ is the yaw angular velocity of the mock-up measured at the hexapod base.

Mean rider

The transfer functions will be calculated for the mean rider (i.e. mean age = 26 $\pm$ 3 years, weight = 81.7 $\pm$ 7.4 kg, height = 181 $\pm$ 7 cm). This means that the resulting transfer functions show the mean gain, phase and coherence averaged over 24 participants. Furthermore, the corresponding SD is shown indicating the variance in gain, phase and coherence between participants. To calculate the SD of the gain and phase of the mean rider the absolute values and angles of the complex numbers are used, respectively.

For simplicity and clearness, the mean apparent mass transfer functions for the foot pegs and handlebars are the average of the left and right side. Note, that this is only valid when both sides show roughly similar dynamics (i.e. similar gain and/or phase). When identical interfaces (e.g. left and ride side handlebar) show different gains and/or phases the mean is calculated for only one side. This will be explicitly mentioned Chapter 3.

3

Results

In this chapter, results will be shown based on the mean rider (i.e. mean age = 26 $\pm$ 3 years, weight = 81.7 $\pm$ 7.4 kg, height = 181 $\pm$ 7 cm). The mean rider is the average of the results of 24 participants. Results for individual participants are shown in Appendices E-K. First the results for the translational motions are discussed followed by the results for the rotational motions.

Nomenclature

In this chapter the following nomenclature will be used:

- SP = seat post
- FPL = foot peg left
- FPR = foot peg right
- HBL = handlebar left
- HBR = handlebar right
- STS = seat-to-sternum
- CSL = coherence significance level

3.1. Translational motions

In this section, the results for the translational motions (i.e. heave, surge and sway) are shown. First the force distribution is analysed. Second the transmissibility and apparent mass transfer functions are discussed based on gain, phase and coherence.

3.1.1. Force distribution

For each translational motion a force distribution is shown to understand the passive forces that the rider both statically and dynamically generates in the bicycle interfaces. The force distribution indicates which interfaces are crucial in the passive control behaviour of the rider with respect to translational motions. Furthermore, it can reveal dominant interface forces that were not expected in advance. The force distribution for heave, surge and sway is analysed, respectively and shown in table 3.1.

Table 3.1: Static and dynamic force distribution of the mean rider at the seat post (SP), foot pegs (FP) and handlebars (HB) for the heave ($\ddot{z}$), surge ($\ddot{x}$) and sway ($\ddot{y}$) motion.

Heave ($\ddot{z}$)			**Surge ($\ddot{x}$)**			**Sway ($\ddot{y}$)**		
Interface	**Static (N)**	**Dynamic (N)**	**Interface**	**Static (N)**	**Dynamic (N)**	**Interface**	**Static (N)**	**Dynamic (N)**
SP_Z	645	27	SP_Z	638	9	SP_Z	636	9
SP_X	295	14	SP_X	294	18	SP_X	296	2
SP_Y	22	1	SP_Y	28	1	SP_Y	28	11
FPL_Z	90	4	FPL_Z	90	1	FPL_Z	93	2
FPL_X	18	1	FPL_X	17	1	FPL_X	17	1
FPR_Z	88	4	FPR_Z	90	1	FPR_Z	88	2
FPR_X	0	0	FPR_X	1	1	FPR_X	0	1
HBL_Z	40	2	HBL_Z	41	2	HBL_Z	40	2
HBL_X	13	1	HBL_X	15	3	HBL_X	14	2
HBL_Y	42	1	HBL_Y	51	1	HBL_Y	40	1
HBR_Z	39	2	HBR_Z	39	2	HBR_Z	38	2
HBR_Y	32	1	HBR_X	18	3	HBR_X	16	2
HBR_X	15	1	HBR_Y	34	1	HBR_Y	28	1

Heave

Figure 3.1 shows the heave acceleration of the hexapod and the resultant force signals of the mean rider in time domain together with the corresponding mean and SD. Note, that the force signals are not zero mean. Therefore, one should speak of SD in stead of RMS to describe the distribution of the force signals. The mean of the force signals indicate the force that the rider, as a result of gravity, statically applies at the interface. The SD of the force signals indicate the amount of force dynamically generated by the rider due to the perturbation. In the case of heave the perturbation is along the z-axis.

A force distribution table is obtained for heave, see Table 3.1. From the table follows that most of the dynamic forces are generated in the vertical direction of the seat post (i.e. SP_Z) followed by the foot pegs (i.e. FPL_Z and FPR_Z) and handlebars (i.e. HBL_Z and HBR_Z). Also the seat post in longitudinal direction suggests dominant dynamics.

Finally, with the exception of the foot peg forces in longitudinal direction (i.e. FPL_X, FPR_X), similar forces are found between the left and right side interfaces.

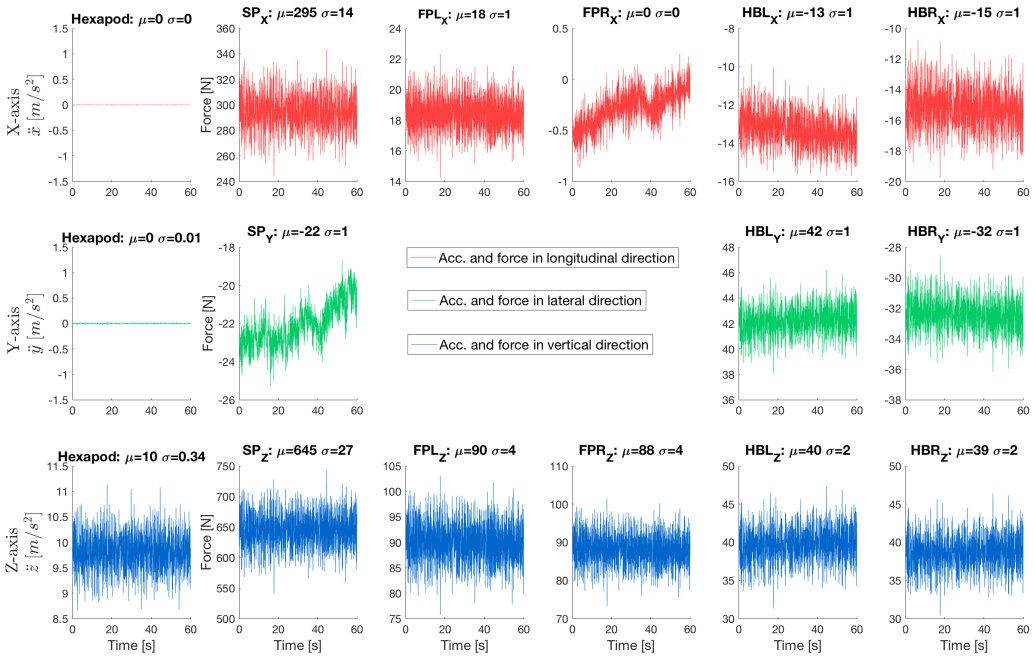

Figure 3.1: The measured heave acceleration ($\ddot{z}$) and the resultant force signals from the mean rider shown in time domain. μ and σ are the mean and the SD of each signal, respectively. In the case of heave, the acceleration is along the z-axis (blue).

Surge

Figure 3.2 shows the surge acceleration of the hexapod and the resultant force signals of the mean rider in time domain together with the corresponding mean and SD. In the case of surge, the acceleration is along the x-axis.

A force distribution table is obtained for surge, see Table 3.1. From the table follows that most of the dynamic forces are generated in the seat followed by the handlebars. Since the perturbation is along the x-axis one would expect that the dominant dynamics are in longitudinal direction. However, the SD value of the foot pegs in longitudinal direction (i.e. FPL_X and FPR_X) is low. Furthermore, dynamic forces are also observed in the vertical direction of both the seat post (i.e. SP_Z) and handlebars (i.e. HBL_Z, HBR_Z). The vertical dynamic forces in the seat post seem to be induced by the seat post inclination (72°) and the slightly forward leaned upper body, see figure 2.2. The rider configuration could also declare the vertical forces in the handlebars.

Finally, with the exception of the foot peg forces in longitudinal direction (i.e. FPL_X and FPR_X) and the handlebar forces in lateral direction (i.e. HBL_Y and HBR_Y), similar forces are found between the left and right side interfaces. On the other hand, it seems to be that the foot pegs in longitudinal direction and handlebars in lateral direction mainly differ in static force (μ). Although, the corresponding SD values do not differ, which could indicate that the left and right side show similar dynamics.

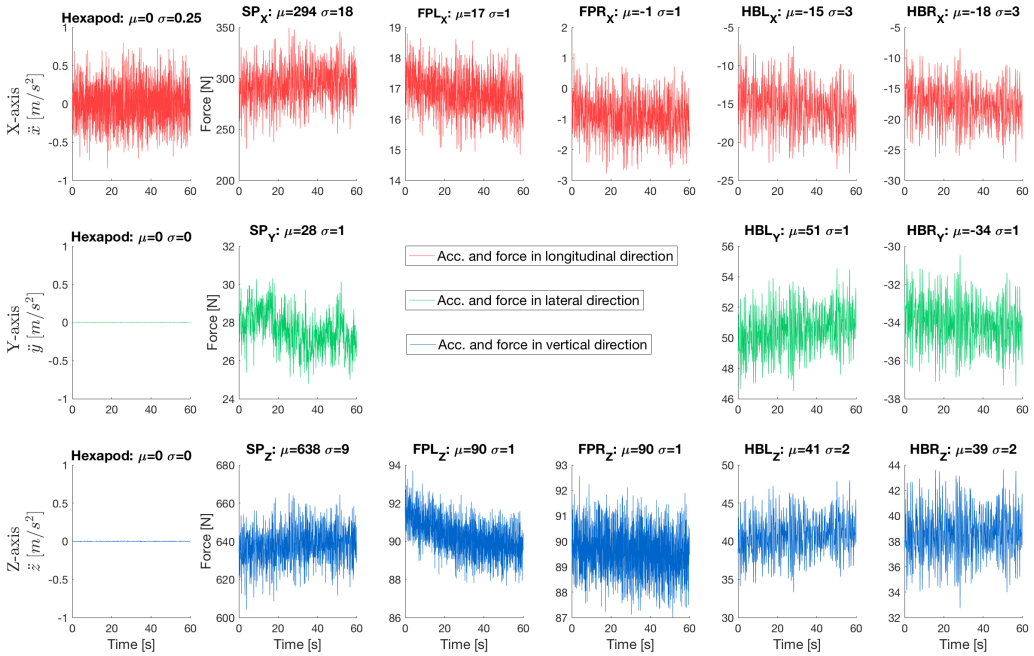

Figure 3.2: The measured surge acceleration ($\ddot{x}$) and the resultant force signals from the mean rider shown in time domain. μ and σ are the mean and the SD of each signal, respectively. In the case of surge, the acceleration is along the x-axis (red).

Sway

Figure 3.3 shows the sway acceleration of the hexapod and the resultant force signals of the mean rider in time domain together with the corresponding mean and SD. In the case of sway, the perturbation is along y-axis.

A force distribution table is obtained for sway, see Table 3.1. From the table follows that most of the dynamic forces are generated in the seat post. Also some dynamics are observed in the foot pegs and handlebars. Since the perturbation is along the y-axis one would expect that the dominant dynamics are in lateral direction. However, the dynamics in the lateral direction of the handlebars (i.e. HBL_Y and HBR_Y) seem to be low. Even more, the lateral forces in the handlebars do not significantly differ from the surge motion.

Similar to the surge motion, the SD values suggest dynamic forces both in longitudinal and vertical direction. However, for sway, the dynamic forces in the vertical direction of the foot pegs (i.e. FPL_Z and FPR_Z) seem to be higher. A reason for this could be that due to lateral trunk motion its centre of

mass is frequently located close to the centre of pressure of the feet generating higher loads in the foot pegs.

Finally, with the exception of the foot peg forces in longitudinal direction (i.e. FPL_X, FPR_X) and the handlebar forces in lateral direction (i.e. HBL_Y and HBR_Y), similar forces are found between the left and right side interfaces. However, as already suggested for surge, it could be the foot pegs and handlebars in longitudinal and lateral direction, respectively, still show similar dynamics between both sides due to similar SD values.

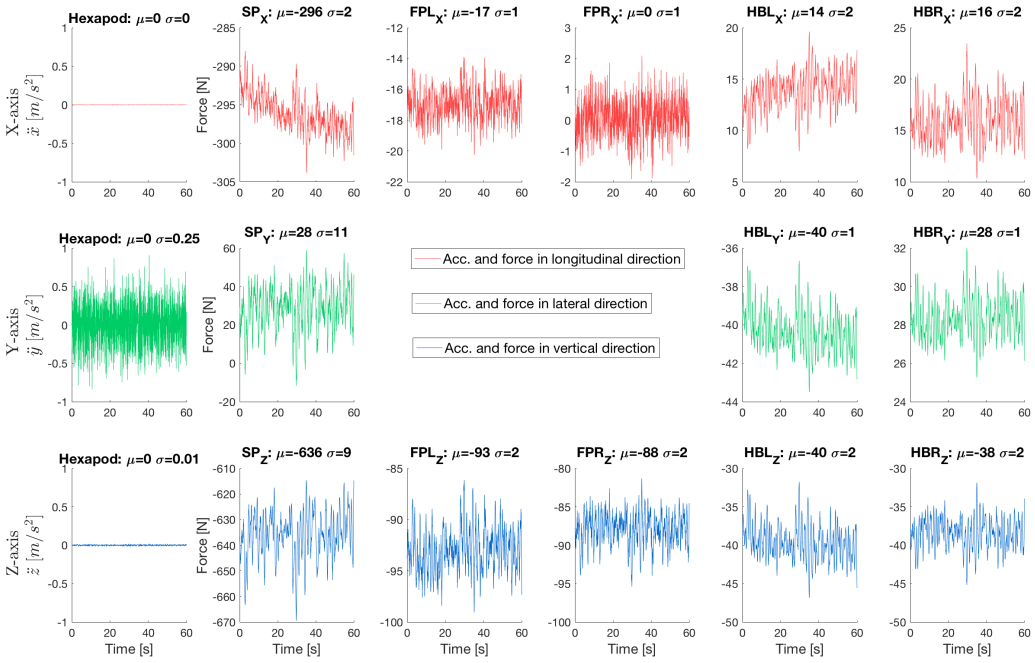

Figure 3.3: The measured sway acceleration ($\ddot{y}$) and the resultant force signals from the mean rider shown in time domain. μ and σ are the mean and the SD of each signal, respectively. In the case of sway, the acceleration is along the y-axis (green).

3.1.2. Transmissibility

In this section the translational STS transfer functions $T_{trans}(f)$ of the mean rider for heave, surge and sway are shown. The transfer functions are discussed based on the gain, phase and coherence. In the coherence plots the coherence significance level (CSL) is also shown.

Heave

The bottom row of Figure 3.4 shows the bode plot of the STS transfer function for the heave motion. The corresponding STS transfer functions for individual riders can be found in Appendix D. The coherence indicates linear correlations over almost the entire frequency range. The gain suggests a broad resonance peak around 5 Hz, which might indicate both individual rider differences and the appearance of more than one resonance peak. This observation is confirmed by the STS transfer functions of the individual riders showing a dispersion of resonance peaks between 4-8 Hz, see Appendix D. The SD shade around the resonance frequency suggests different resonance magnitudes between riders. This is also confirmed by the individual STS transfer functions, in which riders show different peak magnitudes.

Based on the gain and phase the STS transfer function suggests that the torso of the mean rider acts like rigid body below 1 Hz. At the resonance frequency the vertical acceleration of the torso is roughly twice as high the acceleration of the bicycle mock-up. After the resonance peak the gain decreases with increasing frequency. The phase shows a small phase lead between 1-4 Hz after which it shows a phase lag at higher frequencies with a maximum phase lag of roughly 70°.

Surge

The top row of Figure 3.4 shows the bode plot of the STS transfer function for the surge motion. The individual STS transfer functions can be found in Appendix D. In the range of 0.5-4 Hz high coherence

is found, whereas, the coherence after 4 Hz suggest lower, but still considerable, linear correlations. Up to 1 Hz the gain and phase remain almost constant, which indicates that the rider can easily follow the motion. Note, that the SD shade below 0.5 Hz is relatively large, therefore, it cannot be assumed that the rider acts like rigid body below 1 Hz. The gain of the trunk shows a clear resonance peak around 2 Hz. The gain of the resonance peak is around 2, which indicates that the acceleration of the trunk is twice as high the acceleration of the bicycle mock-up. After the resonance peak the gain approaches 0 indicating minimal for-and-aft motion of the trunk. The phase seems to be almost constant (roughly 0°) up to 1.5 Hz. After 1.5 Hz, the phase is characterised by a phase lag with a maximum of about 90°.

Interestingly, the individual surge STS transfer functions suggest a correlation between the rider's body mass and the main resonance peak, whereas, this was not apparent for the heave motion. Appendix D shows that riders with a high body mass show lower resonance frequencies but higher resonance magnitudes with respect to lightweight riders.

Sway

The middle row of Figure 3.4 shows the bode plot of the STS transfer function for the sway motion. The individual STS transfer functions can be found in Appendix D. The STS transfer function shows relative high coherence between 0.7-6.5 Hz. At 0.7 Hz the gain suggests that the lateral acceleration of the trunk is about twice as high the acceleration of the bicycle mock-up. This motion is characterised by a phase lag of 63°. After roughly 1 Hz the gain decreases below 1 and approaches 0 with increasing frequency, whereas, the phase lag reduces and becomes positive after 7 Hz showing a phase lead at high frequencies. This indicates that the trunk motion in lateral direction decreases with increasing frequency.

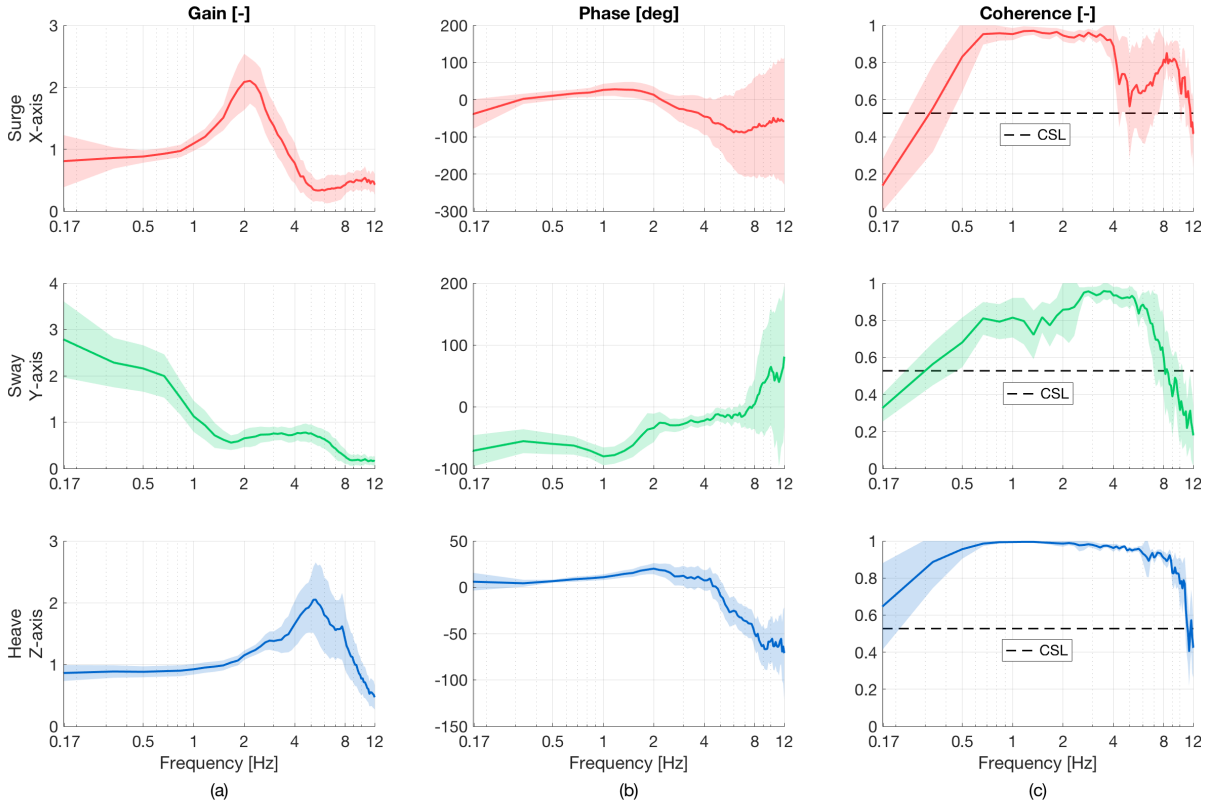

Figure 3.4: The translational seat-to-sternum (STS) transfer functions $T_{trans}(f)$ of the mean rider for the heave (Z, vertical), surge (X, longitudinal) and sway (Y, lateral) motion. (a) gain, (b) phase and (c) coherence. The coloured shade shows the SD between individual participants. The black dashed line in the coherence plots indicates the CSL (= 0.53).

3.1.3. Apparent mass

In this section the apparent mass transfer functions $M(f)$ of the mean rider for heave, surge and sway are shown. The transfer functions are discussed based on the corresponding gain, phase and

coherence. To analyse the gain and phase plots correctly, one should only focus on the interfaces with high coherence (> 0.8). In the coherence plots the coherence significance level (CSL) is also shown.

Heave

Figure 3.5 shows the gain, phase and coherence for the heave apparent mass transfer functions. The corresponding individual transfer functions can be found in Appendix E. It should be noted, that for the handlebars in lateral direction only the mean of the left side is shown since the left and right side show opposite phases, see Appendix E. Furthermore, for the foot pegs in longitudinal direction only the mean of the left side is shown since the right side seems to be noisy and, therefore, can be erroneous.

Figure 3.5c suggests high coherence for the seat post both in longitudinal and vertical direction, and the foot pegs in vertical direction over almost the entire frequency bandwidth. The handlebars show mainly high coherence in mid-frequencies, whereas, the handlebars in longitudinal direction show a drop between 1.5-3 Hz. The coherence of the the seat post in lateral direction, and the foot pegs in longitudinal direction suggests only relative good coherence at higher frequencies.

Figure 3.5a and 3.5b show the gain and phase, respectively, for all interfaces. The seat post and foot pegs in vertical direction show a clear resonance peak around 5 and 6 Hz, respectively, whereas, the handlebars in vertical direction show a broader resonance peak around 5 Hz. Similar resonance peaks are found in the longitudinal direction of the foot pegs (i.e. at 6.5 Hz) and the lateral direction of the handlebars (i.e. at 5 Hz). The seat post and handlebars in longitudinal direction suggest also the appearance of resonance peaks. However, the peaks seem to be more dispersed indicating individual differences between riders, see Appendix E. After the resonance peaks the gain approaches 0 with increasing frequency for all interfaces. Note, that the apparent mass transfer function of the seat post in vertical direction shows a similar resonance frequency (i.e. 5 Hz) as the heave STS transfer function, see figure 3.4. However, the apparent mass transfer function shows a clear resonance peak, whereas, the STS resonance peak seems to be more distributed.

With the exception of both the seat post and handlebars in longitudinal direction, all interfaces are characterised by a 0 phase at low frequencies followed by a small phase lead between 0.5-6 Hz. At higher frequencies all interfaces show a phase lag in which the seat post, the foot pegs and the handlebars in vertical direction show a maximum phase lag of roughly 60°, 80° and 160°, respectively. Note, that the phase in the longitudinal direction of the handlebars starts from roughly -180°, respectively. According to the right-hand sided Cartesian coordinate frame, this means that the longitudinal force in this interface is always in opposite direction of the heave motion. As aforementioned, for the handlebars in lateral direction only the phase of one side is shown indicating that the lateral forces in the left and right side are always in opposite direction with respect to each other. This means that phase of one side starts from from roughly 0°, whereas, the other side starts from roughly -180°, see Appendix E.

Interestingly, the gain and phase of the vertical interfaces indicate a nearly constant gain and a phase of almost 0° below 1 Hz. Therefore, it seems to be that the rider acts like a rigid body below 1 Hz. This was also observed for the heave STS transfer function, see figure 3.4. The vertical gain in the seat post, the foot peg and the handlebar at 0.5 Hz (high coherence) are 55.1 kg, 7.3 kg and 5.1 kg, respectively. This results in a total apparent mass of 79.9 kg. Note, that the gains of the foot peg and handlebar are added twice. Since the total body mass of the mean rider is equal to 81.2 kg, the total apparent mass below 1 Hz in vertical direction can be considered as a pure mass. Thus, the rider can be considered as a rigid body in vertical direction below 1 Hz. At the resonance frequency the vertical apparent mass is roughly twice as high the vertical supporting weight in each interface.

The individual apparent mass transfer functions suggest a correlation between the rider's body mass and the main resonance peak, see Appendix E. Riders with higher body mass show slightly lower resonance frequencies, and higher resonance magnitudes with respect to lightweight persons. It should be noted, that this correlation was mainly observed in the vertical direction of all interfaces. Remarkably, the correlation between the rider's body mass and the corresponding main resonance peak seems not to be apparent for the heave STS transfer function. The individual STS transfer functions of riders with specific body weights suggest different peak offsets, but do not significantly differ in magnitude, see Appendix E.

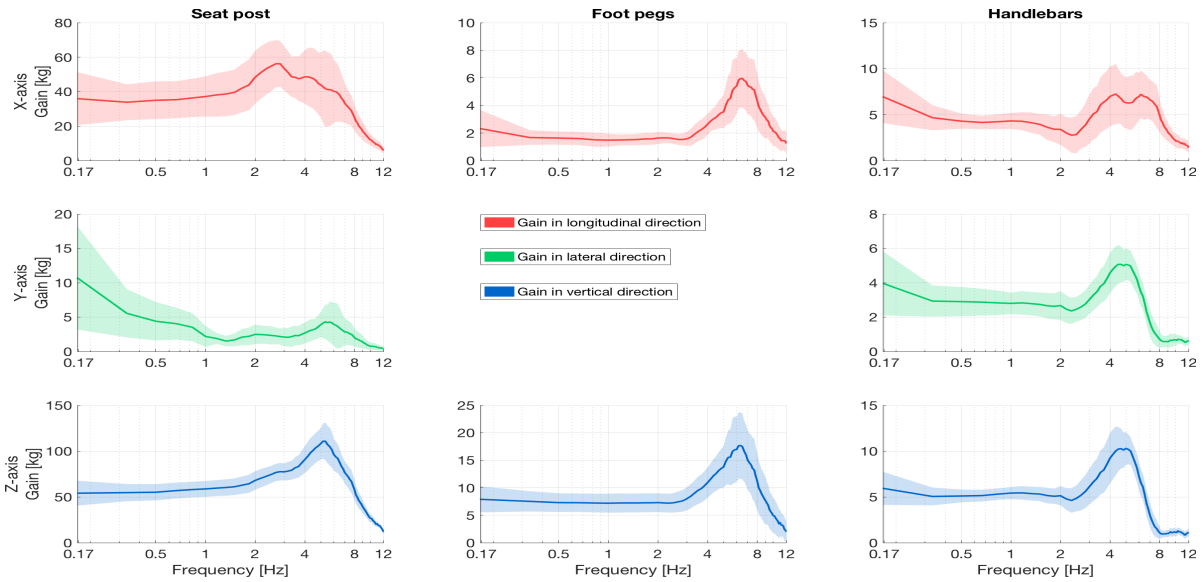

(a) Gain

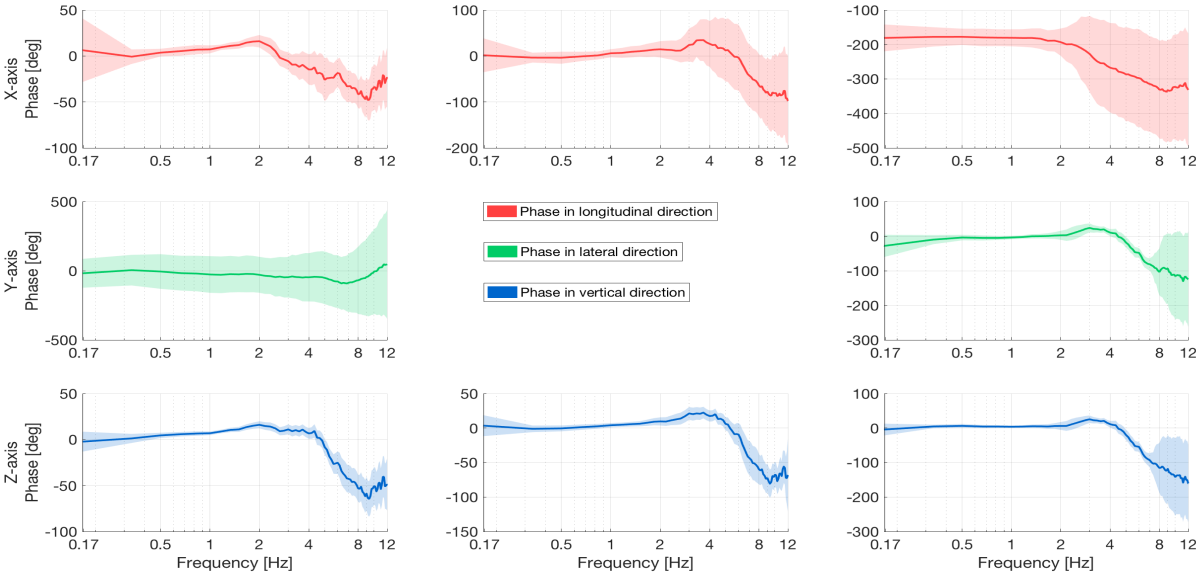

(b) Phase

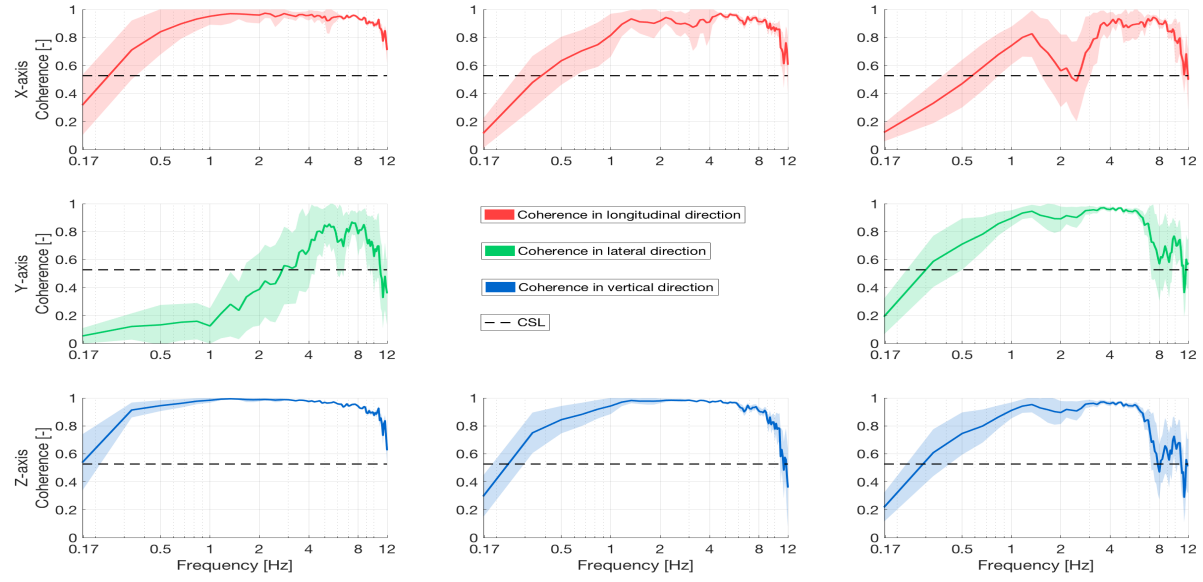

(c) Coherence

Figure 3.5: The apparent mass transfer functions $M(f)$ of the mean rider for the heave motion (Z, vertical) at the seat post, foot pegs and handlebars. (a) gain, (b) phase and (c) coherence. The coloured shade shows the SD between individual participants. The black dashed line in the coherence plots indicates the CSL (= 0.53).

Surge

Figure 3.6 shows the gain, phase and coherence for the surge apparent mass transfer functions. The corresponding individual transfer functions can be found in Appendix F. It should be noted that for the handlebars in lateral direction only the mean of the right side is shown since the left and ride side show opposite phase, see Appendix F.

Figure 3.6c suggests, with the exception of the seat post in lateral direction, high coherence in all interfaces. Especially, in the longitudinal direction of the seat post linear correlations are expected over almost the entire frequency range, whereas, other interfaces show high coherence only in specific frequency regions. The foot pegs and handlebars in longitudinal direction are characterised by a drop between 2-4 and 4-6 Hz, respectively. The handlebars both in lateral and vertical direction are characterised by two drops. The main drop is between 4-6 Hz followed by a smaller drop between 6-9 Hz. Note, that the handlebars in lateral and vertical direction show similar trends.

Figures 3.6a shows the gain in all interfaces. With the exception of the seat post in lateral direction (low coherence) and the foot pegs in vertical direction, all interfaces show a main resonance peak at 2 Hz. Note, that this resonance frequency was also found for the surge STS transfer function, see figure 3.4. The SD shade around the resonance peak suggests different apparent masses between individual riders. Interestingly, the foot pegs in longitudinal direction also show a second peak around 5 Hz, whereas, the handlebars both in lateral and vertical direction show an additional peak at 5.5 Hz. After the resonance peak the apparent mass approaches 0 with increasing frequency in all interfaces.

According to figure 3.6b the phase seems to be constant for almost all interfaces up to 1.5 Hz. After 1.5 Hz, the phase in longitudinal direction of both the seat post and the handlebars is characterised by a small phase lag but leads after 8 Hz. This trend is also observed in both the lateral direction of the handlebars. For the foot pegs in longitudinal direction, the phase remains decreasing after 1.5 Hz with a maximum phase lag of roughly 130°. This trend is found, as well, in the vertical direction of both the seat post and foot pegs with a maximum phase lag of approximately 50° and 300°, respectively. Note, that the phase in the vertical direction of both the foot pegs and handlebars starts from roughly -180° and -200°, respectively. According to the right-hand sided Cartesian coordinate frame, this means that the vertical forces in these interfaces are always in opposite direction of the surge motion. As aforementioned, for the handlebars in lateral direction only the phase of one side is shown indicating that the lateral forces in the left and right side are always in opposite direction with respect to each other. This means that phase of one side starts from from roughly 0°, whereas, the other side starts from roughly -180°, see Appendix F

The gain and phase below 1 Hz suggest that the dynamics of the rider are close to the ones of a rigid body (almost constant gain and nearly 0° phase). However, if the rider acts like a rigid body, for instance in the longitudinal direction, the sum of the gains should be equal to the total static mass in these interfaces. The sum of the longitudinal gains at 0.5 Hz (high coherence) results in a total apparent mass of 136 kg. This apparent mass cannot be equal to the total static mass in these interfaces since the total body mass of the mean rider is 81.2 kg. Therefore, the rider cannot be considered as a rigid body below 1 Hz at any interface. This was also found for the surge STS transfer function.

Concerning the interfaces with high coherence, the gain of the individual apparent mass transfer functions suggest a similar correlation between the rider's body mass and the main resonance peak as found for the surge STS transfer function, see Appendix D. Appendix F shows that riders with a high body mass show both lower resonance frequencies and higher resonance magnitudes with respect to lightweight riders. There seems to be a difference of roughly 1 Hz in resonance frequency between the heaviest and lightest person. Concerning the phase, this effect seems apparent. However, it seems to be that it is characterised by both a lower frequency offset of the phase lag, and a larger phase lag for increasing body mass.

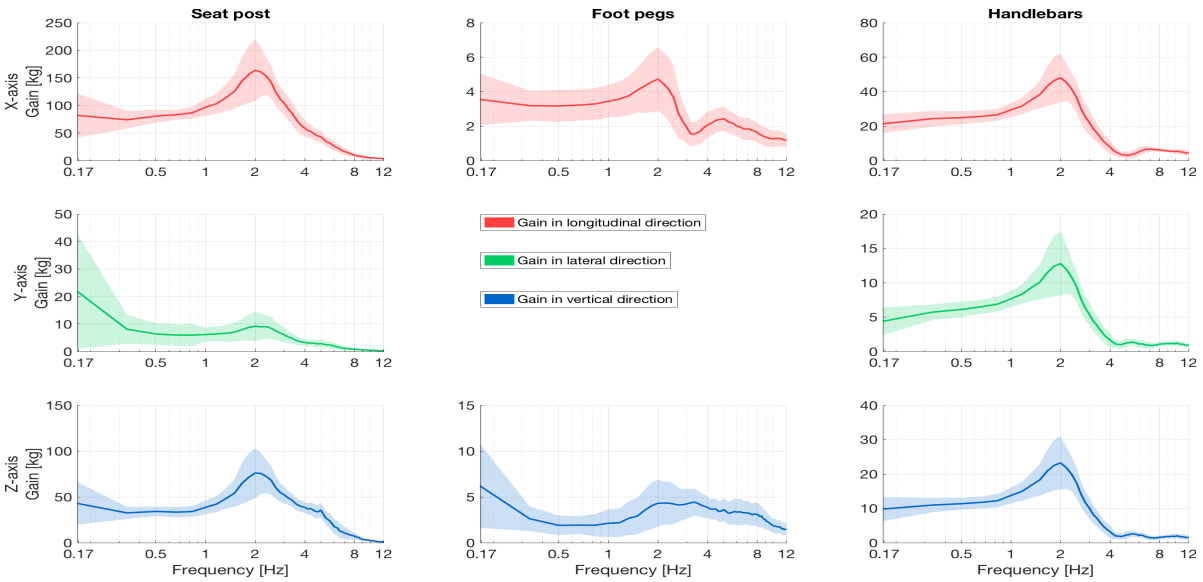

(a) Gain

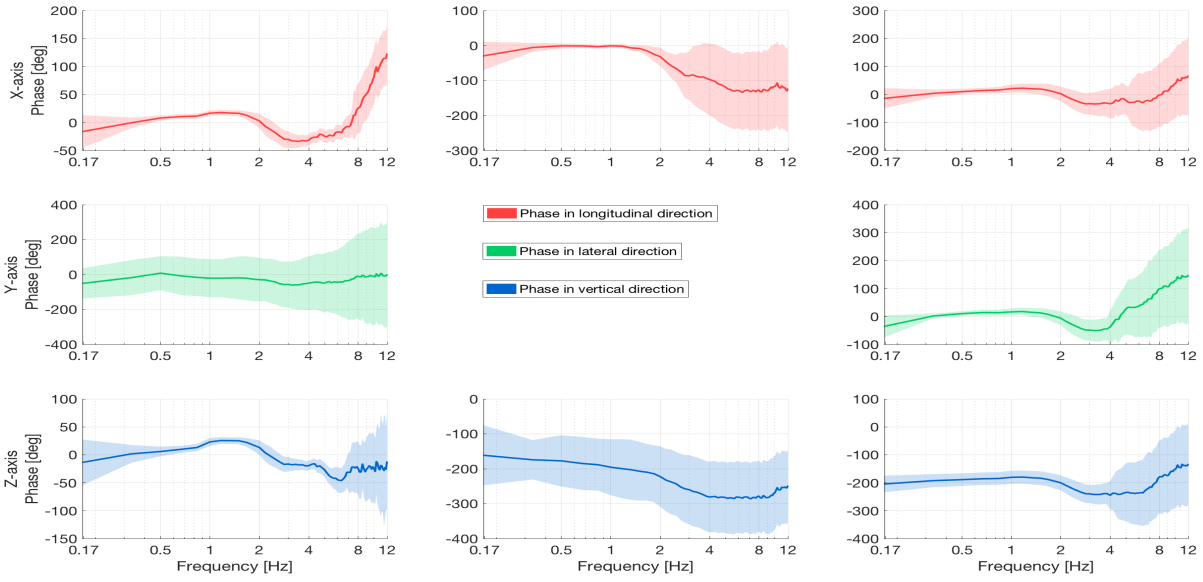

(b) Phase

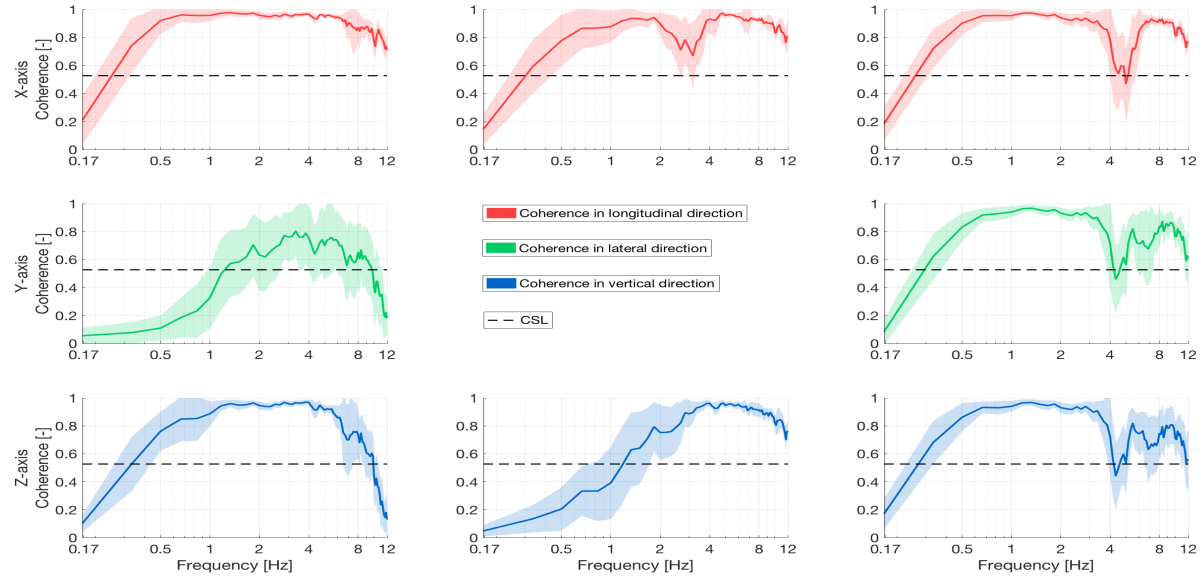

(c) Coherence

Figure 3.6: The apparent mass transfer functions $M(f)$ of the mean rider for the surge motion (X, longitudinal) at the seat post, foot pegs and handlebars. (a) gain, (b) phase and (c) coherence. The coloured shade shows the SD between individual participants. The black dashed line in the coherence plots indicates the CSL (= 0.53).

Sway

Figure 3.7 shows the gain, phase and coherence for the sway apparent mass transfer functions. The corresponding individual transfer functions can be found in Appendix G. It should be noted that for the foot pegs in longitudinal and vertical direction only the mean of the right side is shown since the left and ride side show opposite phases, see Appendix G. The same holds for the handlebars, for the longitudinal direction only the mean of the left side is shown, whereas, for the vertical direction only the right side is shown.

Figure 3.7c suggests linear correlations (coherence > 0.8) in the lateral direction of the seat post and in both the longitudinal and vertical direction of the foot pegs after roughly 1 Hz. Note, that the coherence of the other interfaces is relatively low, whereas, the coherence for the seat post in longitudinal direction is even below the CSL level over almost the entire frequency bandwidth. For the remaining interfaces the coherence suggests no linear correlations for the mean rider. Although, the SD shade suggests that some individual participants show relative high coherence in specific frequency regions.

Figure 3.7a and 3.7b show the gain and phase for all interfaces, respectively. Based on the coherence the seat post in lateral direction, and the foot pegs in both the longitudinal and vertical direction can only be analysed after 1 Hz. The interfaces are characterised by an ever-decreasing apparent mass suggesting a small resonance peak at roughly 2 Hz after which the gain approaches 0 with increasing frequency. With the exception of the seat post in longitudinal direction and the handlebars in lateral direction, the all phases show a phase lag at 1 Hz of roughly 60° after which the phase increases rapidly resulting in large phase leads at high frequencies. The gain and phase trends of the seat post in lateral direction are comparable to the trends of the sway STS transfer function. Note, that the phase of the handlebars in the lateral direction starts from roughly 180°. According to the right-hand sided Cartesian coordinate frame, this means that the lateral force in the handlebars is always in opposite direction of the sway motion. It seems that the same relationship holds for the seat post in longitudinal direction, however, this phase can be considered as erroneous since the coherence is below the CSL level over almost the entire frequency range. As aforementioned, for the foot pegs and handlebars in longitudinal and vertical direction only the phase of one side is shown indicating that the corresponding forces in the left and right side are always in opposite direction with respect to each other. This means that phase of one side starts from from roughly 0°, whereas, the other side starts from roughly 180°, see Appendix G.

Interestingly, the apparent mass of the foot pegs both in longitudinal and vertical direction show high coherence. Furthermore, the apparent mass transfer function of the seat post in the lateral direction, and the STS transfer function show relative high coherence, as well. Indicating that all are linearly related with the sway motion. Due to the lateral motion of the trunk its centre of mass is frequently swaying between both feet with its centre of mass close the centre of pressure of the feet suggesting that the feet might play an important role in lateral rider balancing. It should be noted, that the lateral apparent mass in the foot pegs is not measured meaning that the lateral dynamics of the legs remain unknown. Therefore, one cannot assume that the supposed relationship between the trunk and the feet are solely determined by the motion of the trunk.

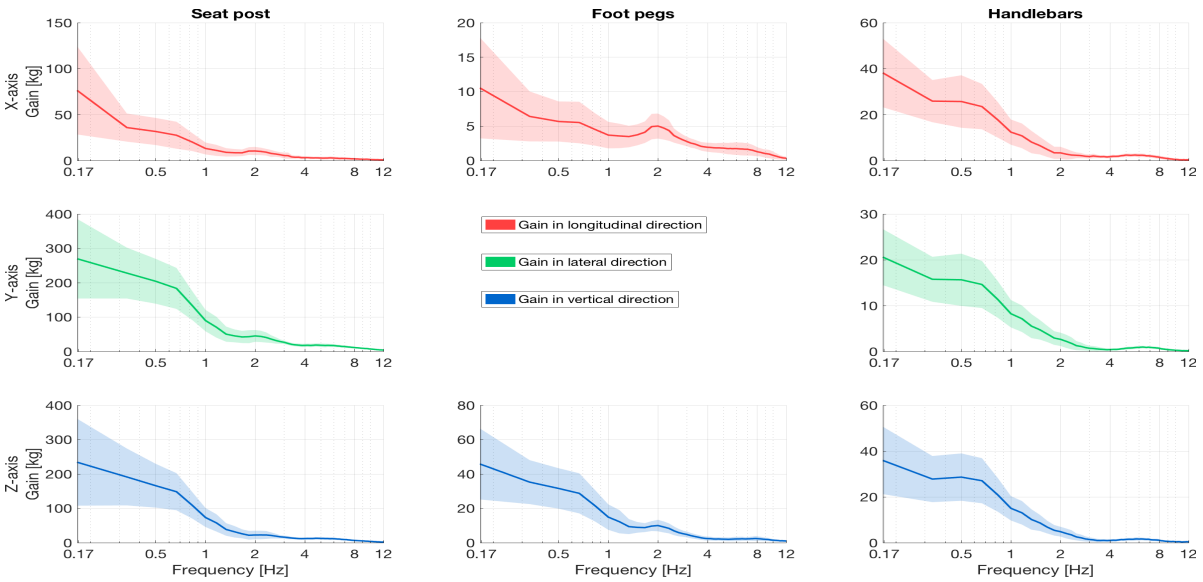

(a) Gain

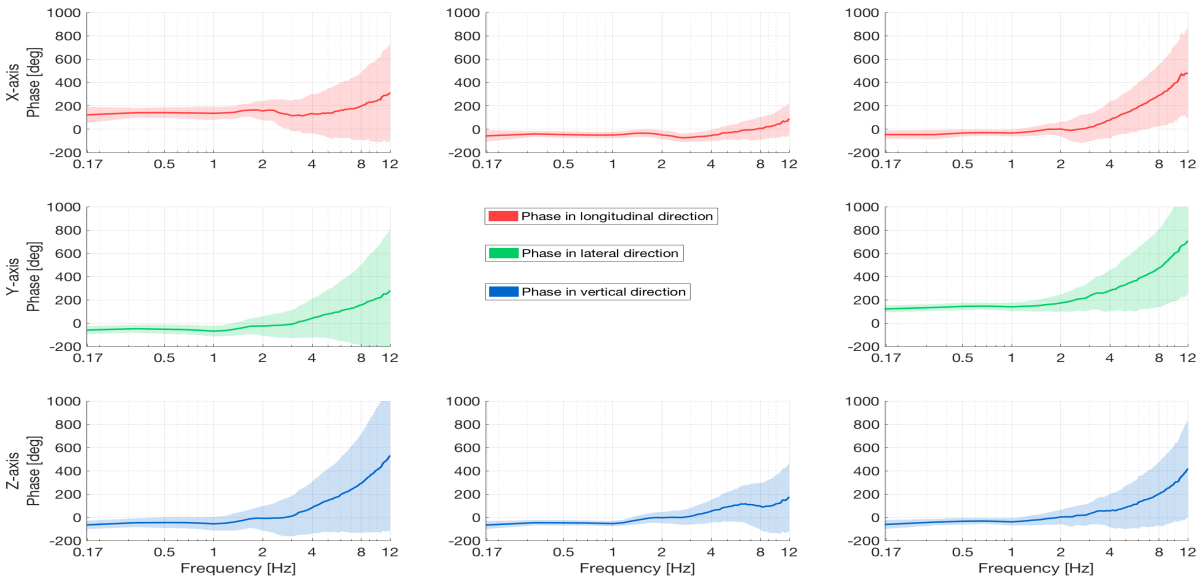

(b) Phase

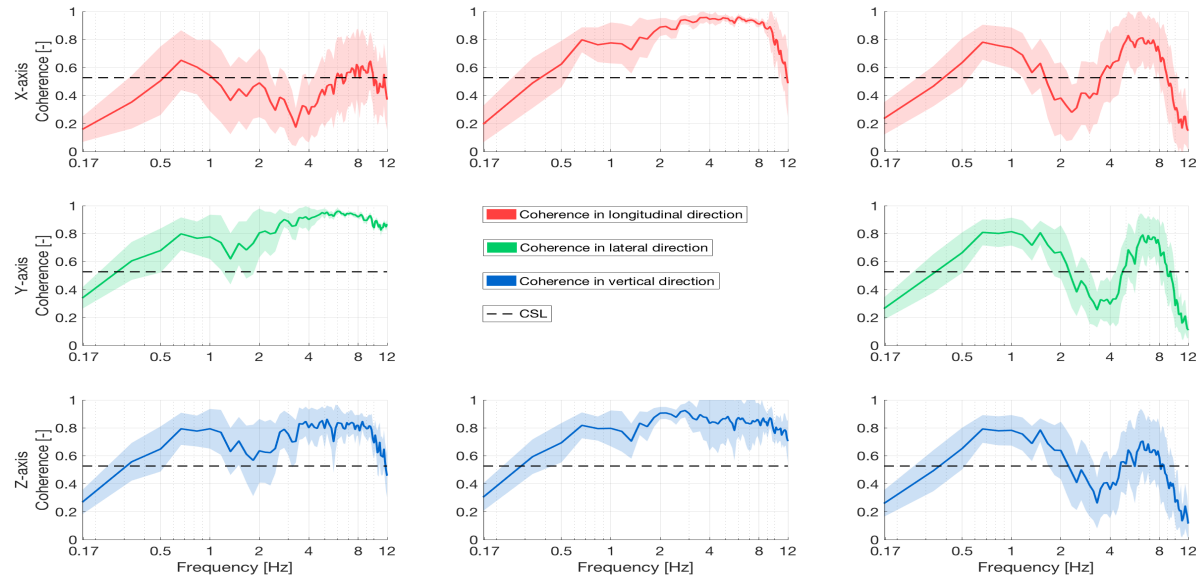

(c) Coherence

Figure 3.7: The apparent mass transfer functions $M(f)$ of the mean rider for the sway motion (Y, lateral) at the seat post, foot pegs and handlebars. (a) gain, (b) phase and (c) coherence. The coloured shade shows the SD between individual participants. The black dashed line in the coherence plots indicates the CSL (= 0.53).

3.2. Rotational motions

In this section, the results for the rotational motions (i.e. roll, pitch and yaw) are shown. First the force distribution is analysed. Second the transmissibility and apparent mass transfer functions are discussed based on gain, phase and coherence.

3.2.1. Force distribution

For each rotational motion a force distribution is shown to understand the passive forces that the rider both statically and dynamically generates in the bicycle interfaces. The force distribution indicates which interfaces are crucial in the passive control behaviour of the rider with respect to rotational motions. Also it can reveal dominant interface forces that were not expected in advance. The force distribution for roll, pitch and yaw is analysed, respectively, and shown in Table 3.2.

Table 3.2: Static and dynamic force distribution of the mean rider at the seat post (SP), foot pegs (FP) and handlebars (HB) for the roll ($\ddot{\phi}$), pitch ($\ddot{\theta}$) and yaw ($\ddot{\psi}$) motion.

Roll ($\ddot{\phi}$)			**Pitch ($\ddot{\theta}$)**			**Yaw ($\ddot{\psi}$)**		
Interface	**Static (N)**	**Dynamic (N)**	**Interface**	**Static (N)**	**Dynamic (N)**	**Interface**	**Static (N)**	**Dynamic (N)**
SP_Z	639	20	SP_Z	640	9	SP_Z	644	3
SP_X	298	7	SP_X	295	19	SP_X	296	2
SP_Y	26	32	SP_Y	24	1	SP_Y	23	3
FPL_Z	90	5	FPL_Z	94	1	FPL_Z	92	0
FPL_X	17	2	FPL_X	18	1	FPL_X	19	0
FPR_Z	87	5	FPR_Z	90	1	FPR_Z	92	0
FPR_X	0	1	FPR_X	0	1	FPR_X	0	0
HBL_Z	39	6	HBL_Z	40	3	HBL_Z	40	1
HBL_X	14	4	HBL_X	14	4	HBL_X	15	1
HBL_Y	44	2	HBL_Y	48	2	HBL_Y	52	0
HBR_Z	37	6	HBR_Z	39	2	HBR_Z	38	0
HBR_X	16	5	HBR_X	17	4	HBR_X	16	1
HBR_Y	30	3	HBR_Y	34	2	HBR_Y	33	0

Roll

Figure 3.8 shows the roll acceleration ($\ddot{\phi}$) and the resultant force signals of the mean rider in time domain together with the corresponding mean and SD. In the case of roll, the rotation is around the x-axis.

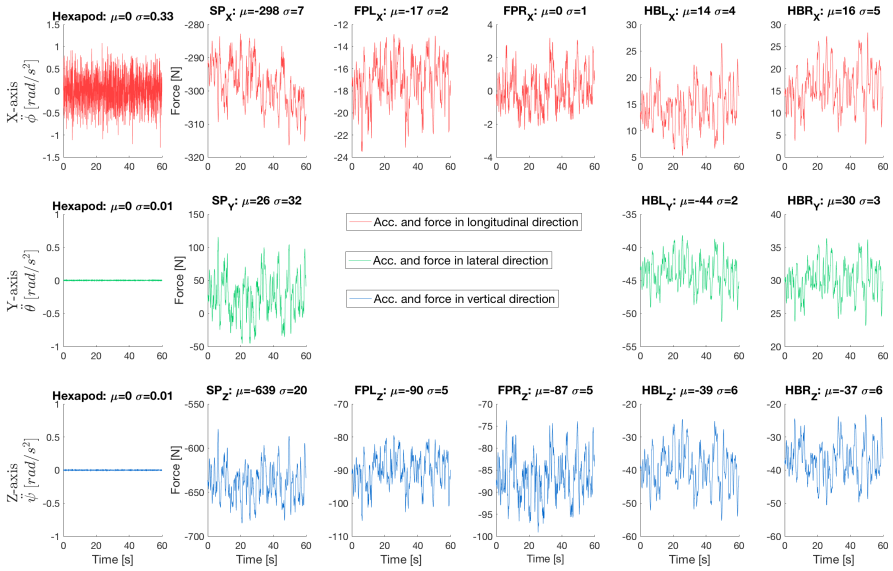

Figure 3.8: The measured roll acceleration ($\ddot{\phi}$) and the resultant force signals from the mean rider shown in time domain. μ and σ are the mean and the SD of each signal, respectively. In the case of roll, the acceleration is around the x-axis (red).

From figure 3.8 a force distribution table is obtained for roll, see Table 3.2. The table suggests many dynamics in several interfaces, which is remarkable with respect to other motions. The dominant dynamic forces are found in the seat post, especially, in the lateral and vertical direction (i.e. SP_Y and SP_Z). Concerning the foot pegs and handlebars, the dynamics are mainly observed in the vertical direction (i.e. FPL_Z, FPR_Z, HBL_Z and HBR_Z). Interestingly, despite a lateral rotation, the dynamics in the lateral direction of the handlebars (i.e. HBL_Y and HBR_Y) seem to be small relative to other interfaces.

In comparison with the force distribution for the sway motion, both motions show an almost similar interface distribution despite different force magnitudes. This suggests that the same interfaces play a dominant role in the force distribution of the rider during the sway and roll motion.

Finally, some similar interfaces suggest differences in dynamics between the left and right side (i.e. HBR_X and HBL_X; HBR_Y and HBL_Y; FPL_X and FPR_X), which was minimally observed in the translational motions.

Pitch

Figure 3.9 shows the pitch acceleration ($\ddot{\theta}$) and the resultant force signals of the mean rider in time domain together with the corresponding mean and SD. In the case of pitch, the rotation is around the y-axis.

From figure 3.9 a force distribution table is obtained for pitch, see Table 3.2. The table suggests that most dynamic forces are generated in the longitudinal and vertical direction of the seat post (i.e. SP_X and SP_Z). The seat post is followed by the handlebars in which the dominant dynamics seem to be in the longitudinal and vertical direction (i.e. HBL_X, HBR_X, HBL_Z and HBR_Z). Relative high forces in the lateral direction of the handlebars (i.e. HBL_Y and HBR_Y) are found. Remarkably, despite a for-and-aft rotation the dynamics in the longitudinal and vertical direction of the foot pegs seem the be low (i.e. FPL_X, FPR_X, FPL_Z and FPR_Z).

In comparison with the force distribution of the surge motion, both motions show an almost similar interface distribution despite different force magnitudes.

Finally, with the exception of the handlebars in vertical direction (i.e. HBL_Z and HBR_Z) all interfaces suggest similar dynamics between the left and right side.

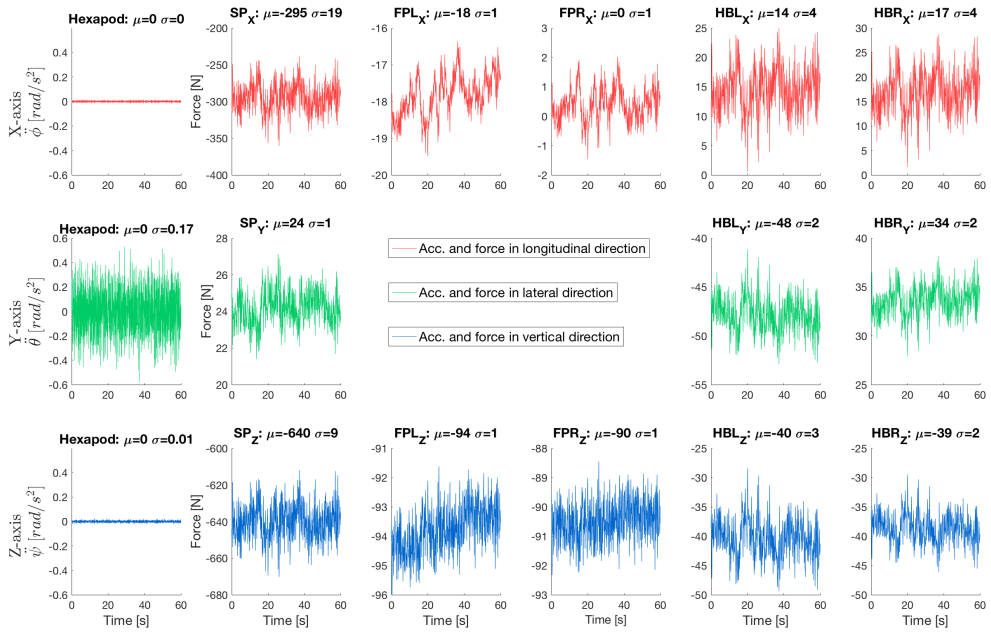

Figure 3.9: The measured pitch acceleration ($\ddot{\theta}$) and the resultant force signals from the mean rider shown in time domain. μ and σ are the mean and the SD of each signal, respectively. In the case of pitch, the acceleration is around the y-axis (green).

Yaw

Figure 3.10 shows the yaw acceleration ($\ddot{\psi}$) and the resultant force signals of the mean rider in time domain together with the corresponding mean and SD. In the case of yaw, the rotation is around the z-axis.

From figure 3.10 a force distribution table is obtained for yaw, see Table 3.2. In general, the table suggests that minimal or no dynamics are observed in all interfaces. The dominant dynamic forces are mainly generated in the seat post, especially in the lateral and vertical direction (i.e. SP_Y and SP_Z). The handlebars show some dynamic forces in the longitudinal and vertical direction (i.e. HBL_X, HBR_X and HBL_Z).

Probably, the low amount of dynamic forces during the yaw perturbation can be clarified by the fact the axis of rotation crosses roughly the centre of mass of the rider's trunk. More specific, it runs at least through the centre of mass of the lower trunk expecting no or minimal relative trunk motion.

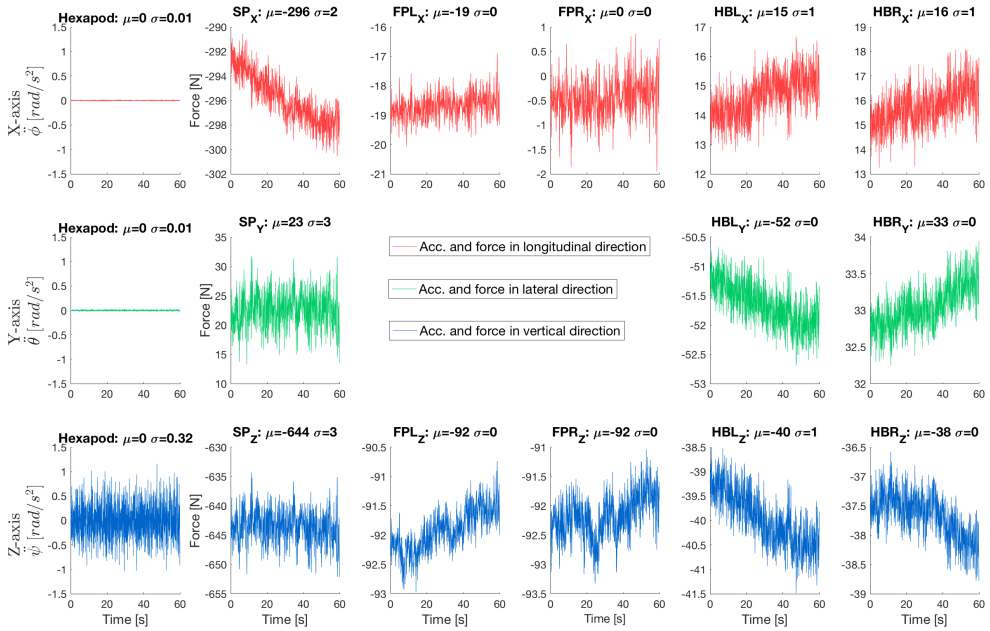

Figure 3.10: The measured yaw acceleration ($\ddot{\psi}$) and the resultant force signals from the mean rider shown in time domain. μ and σ are the mean and the SD of each signal, respectively. In the case of yaw, the acceleration is around the z-axis (blue).

3.2.2. Transmissibility

In this section the rotational STS transfer functions $T_{rot}(f)$ of the mean rider for roll, pitch and yaw are shown. The transfer functions are discussed based on the gain, phase and coherence. In the coherence plots the coherence significance level (CSL) is also shown.

Roll

The top row of figure 3.11 shows the bode plot of the roll STS transfer function. The corresponding individual transfer functions can be found in Appendix H. The coherence of the mean STS transfer function suggests only a linear correlation between 1-2 Hz. In this range the gain shows a magnitude of roughly 3 indicating that the lateral angular velocity of the trunk is 3 times higher as the lateral angular velocity of the bicycle mock-up. At 1 Hz the phase has a phase lag of about 70° and reduces to a phase lag of roughly 0° at 3 Hz. After 3 Hz the phase shows phase lead and increases with increasing frequency. From these results, it cannot be concluded that the broad peak in the gain plot can be considered as a resonance since the frequencies outside the range of 1-2 Hz show low coherence. In comparison with the sway motion, the STS transfer function seems to be totally different, especially with respect to the gain plot.

Pitch

The middle row of figure 3.11 shows the bode plot of the pitch STS transfer function. The corresponding individual transfer functions can be found in Appendix H. In general, the coherence suggests moderate linear correlations between the mock-up angular velocity and the angular velocity of the trunk since the coherence is mainly below 0.8 over almost the entire frequency range. Despite this coherence, a gain of roughly 1 and a corresponding phase of nearly 0° is observed up to 1 Hz. This suggests that the relative angular velocity between the mock-up and the rider's trunk is almost 0 suggesting that trunk can follow the pitch motion of the mock-up almost perfectly up to 1 Hz. After 1 Hz, the gain increases up to 9 Hz indicating that the relative torso angular velocity increases with increasing frequency. The gain suggests two wide resonances between 2-4 Hz and 6-9 Hz for the mean rider, however, for the individual STS transfer functions this seems to be less apparent where only some participants show a clear resonance around 2 Hz, see Appendix H.

Yaw

The bottomr row of figure 3.11 shows the bode plot of the yaw STS transfer function. The corresponding individual transfer functions can be found in Appendix H. The STS transfer function shows mainly high coherence below 1 Hz and low coherence after roughly 3 Hz. Up to 1.5 Hz the gain shows a magnitude of almost 1 with a corresponding phase of nearly 0°. After 1.5 Hz the gain shows a resonance peak at 2.3 Hz with a magnitude of roughly 1.5, whereas, the phase decreases with increasing frequency. The gain also suggests an additional resonance peak at 8.7 Hz, however, the coherence is below the CSL level indicating that the gain should be considered as erroneous.

The individual STS transfer functions suggest a correlation between body mass and the main resonance peak, see Appendix H. However, the effect seems to be mainly characterised by a lower resonance frequency, than a difference in resonance magnitude.

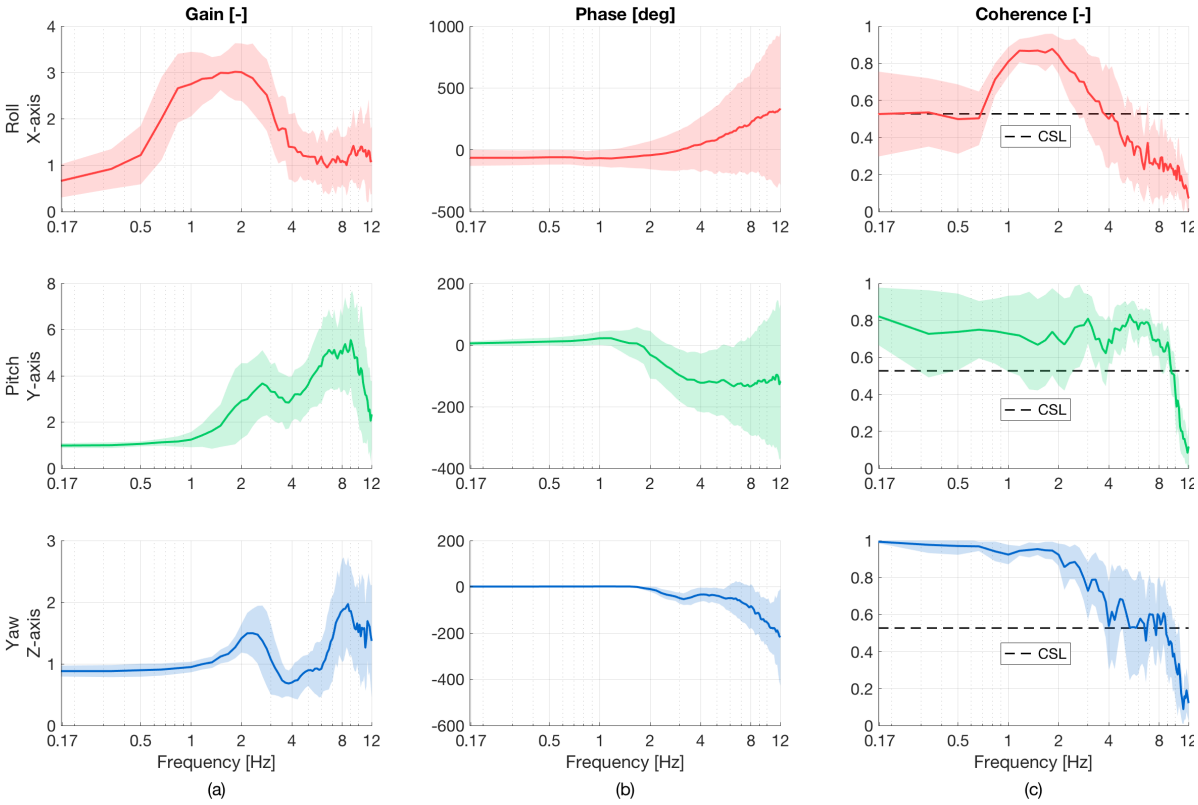

Figure 3.11: The rotational seat-to-sternum (STS) transfer functions $T_{rot}(f)$ of 24 individual riders for the roll (around X-axis), pitch (around Y-axis) and yaw motion (around Z-axis). (a) gain, (b) phase and (c) coherence. The coloured lines indicate riders with specific body weights. The black dashed line in the coherence plots indicates the CSL (= 0.53).

3.2.3. Apparent mass

In this section the apparent mass transfer functions $M(f)$ of the mean rider for roll, pitch and yaw are shown. The transfer functions are discussed based on the corresponding gain, phase and coherence. The analyse the gain and phase plots correctly, one should focus on the interfaces with high coherence (> 0.8). In the coherence plots the coherence significance level (CSL) is also shown.

Roll

Figure 3.12 shows the gain, phase and coherence, respectively, for the roll apparent mass transfer functions. The corresponding individual transfer functions can be found in Appendix I. It should be noted that for the footpegs in longitudinal and vertical direction only the mean of the right side is shown since the left and ride side show opposite phases, see Appendix I. The same holds for the handlebars. For the longitudinal direction only mean of the left side is shown, whereas, for the vertical direction only the right side is shown. Note, that this interface relationship is similar to the sway motion.

Figure 3.12c suggests that only high coherence is observed in the lateral direction of the seat post between roughly 1.5-11 Hz. The SD shade suggests that some participants show relative good coherence in the vertical direction of the seat post, and in both the longitudinal and vertical direction of the foot pegs. All handlebar directions show low coherence, whereas, the seat post in longitudinal direction shows a coherence below the CSL over almost the entire frequency range.

Figure 3.12a and 3.12b show the gain and phase, respectively, for all interfaces. Despite the fact that the seat post in the lateral direction seems to be most linear (relative high coherence), it does not show any clear characteristics like resonance. The gain shows an ever-decreasing gain approaching 0 at higher frequencies. This trend is also observed in all other interfaces.

The seat post in lateral direction shows a small phase lag of roughly 40° at 1.5 Hz. At approximately 3 Hz the phase becomes positive after which the phase lead increases rapidly with increasing frequency with a maximum phase lead of about 250° at 11 Hz. Note, that the phase of the handlebars in the lateral direction starts from roughly 180°. According to the right-hand sided Cartesian coordinate frame, this means that the lateral force in the handlebars is always in opposite direction of the roll motion. It seems that the same relationship holds for the seat post in longitudinal direction, however, this phase can be considered as erroneous since the coherence is below the CSL level over the entire frequency range. As aforementioned, for the foot pegs and handlebars in longitudinal and vertical direction only the phase of one side is shown indicating that the corresponding forces in the left and right side are always in opposite direction with respect to each other. This means that phase of one side starts from from roughly 0°, whereas, the other side starts from roughly 180°, see Appendix I. Despite that other interfaces suggest hardly linear correlations, similar phase trends are observed with respect to the seat post in lateral direction.

In comparison with the apparent mass transfer functions of the sway motion, roughly similar gain and phase trends are found. The difference between both motions is mainly characterised by higher gain magnitudes for the roll motion. Beside this, the sway motion suggests a small resonance peak around 2 Hz in the lateral direction of the seat post, and in both the longitudinal and vertical direction of the foot pegs. Similar phase trends are found as well.

Remarkably, the apparent mass and the STS transfer function for the roll motion do not have similar trends, whereas, similar trends between both transfer functions were found for the sway motion.

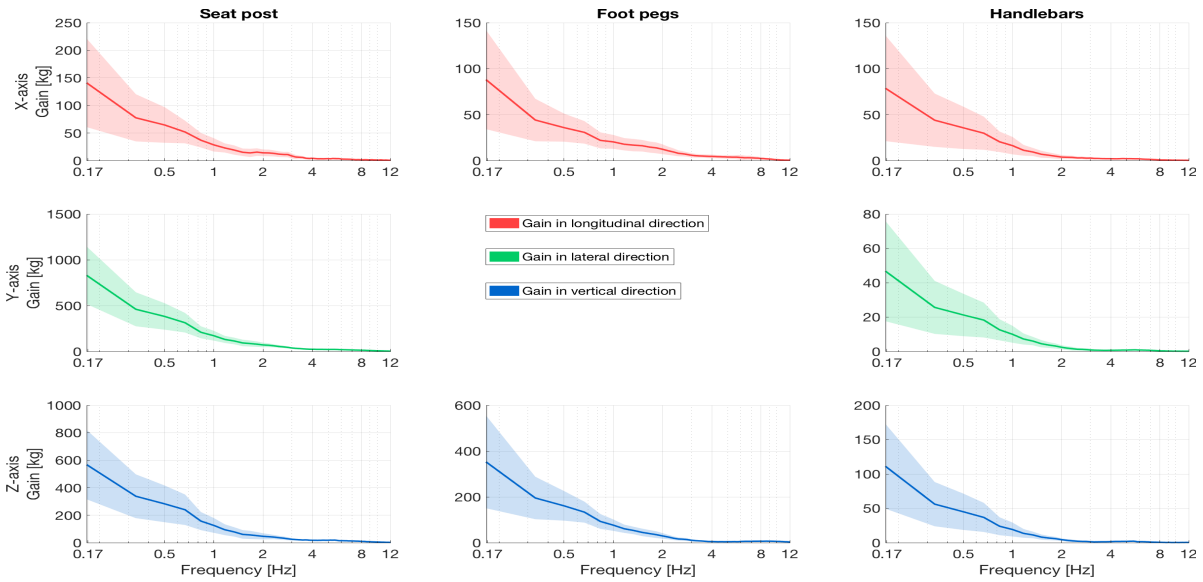

(a) Gain

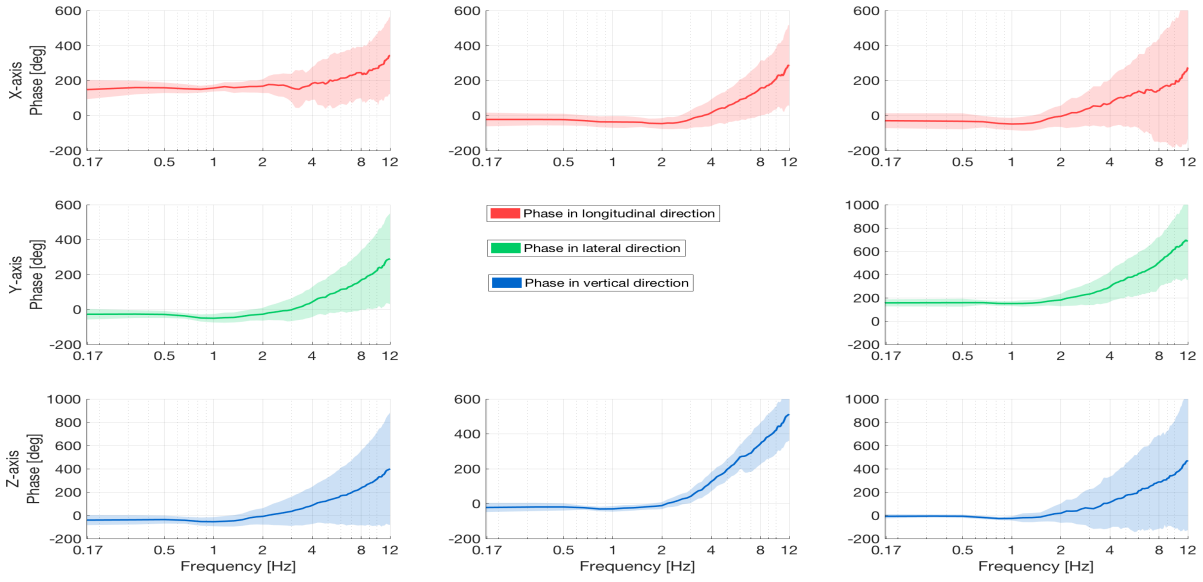

(b) Phase

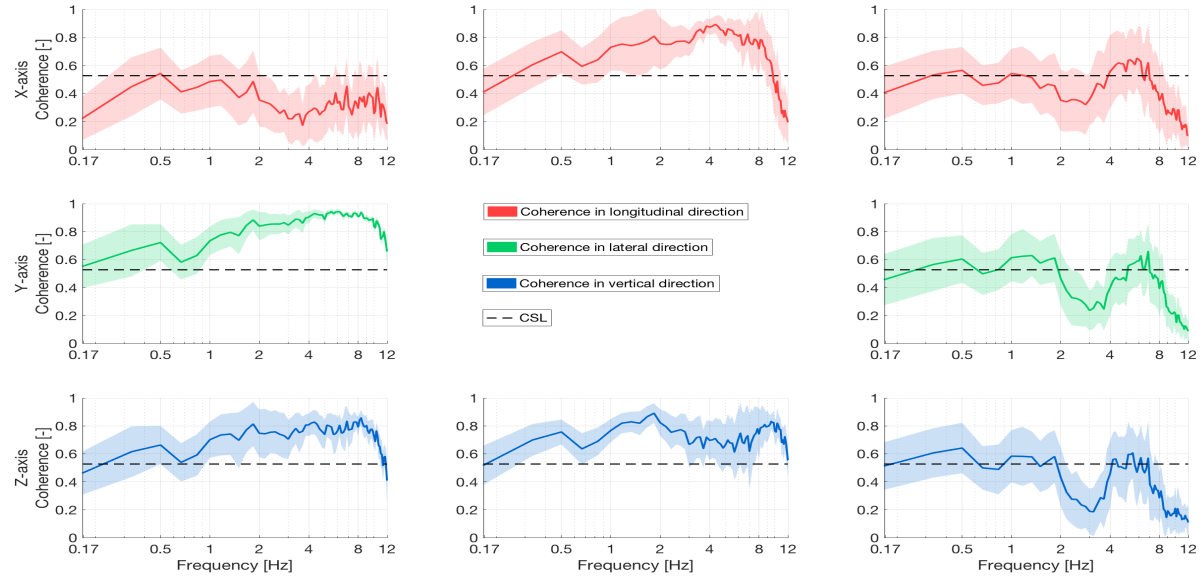

(c) Coherence

Figure 3.12: The apparent mass transfer functions $M(f)$ of the mean rider for the roll motion (around X-axis) at the seat post, foot pegs and handlebars. (a) gain, (b) phase and (c) coherence. The coloured shade shows the SD between individual participants. The black dashed line in the coherence plots indicates the CSL (= 0.53).

Pitch

Figure 3.13 shows the gain, phase and coherence, respectively, for the pitch apparent mass transfer functions. The corresponding individual transfer functions can be found in Appendix J. It should be noted that for the handlebars in lateral direction only the mean of the right side is shown since the left and ride side show opposite phases, see Appendix J. Note, that this interface relationship is similar to the surge motion.

Figure 3.13c suggests that the highest coherence is found in the seat post and handlebars. The seat post in longitudinal direction shows a high coherence between 0.3-9 Hz, whereas, the seat post in vertical direction suggests linear correlations between 0.3-5.5 Hz. In general, the handlebars show good coherence in all directions, however, they are characterised by a drop between 4.5-6 Hz. The foot pegs in vertical direction show only good coherence between 1.5-4.5 Hz. Finally, the seat post in lateral direction suggest no linear correlations over the entire frequency bandwidth, whereas, the coherence for the foot pegs in longitudinal direction is mainly below 0.8.

Figure 3.13a and 3.13b show the gain and phase, respectively, for all interfaces. Interfaces with high coherence are characterised by relative high gains at low frequencies (> 0.3 Hz). The high gains decrease rapidly and become flat around 1 Hz. After 1 Hz the gain increases and suggests a small resonance peak at 1.8 Hz for at least the interfaces with good coherence. After the resonance peak the gain approaches 0 with increasing frequency for all interfaces.

The handlebars show an almost constant phase of 0° up to roughly 1.5 Hz in all directions. The phase of the seat post both in longitudinal and vertical direction increase slightly resulting in a small phase lead up to 1.5 Hz. After 1.5 Hz the phase of all interfaces decreases and shows a phase lag in which the seat post in longitudinal direction shows a maximum phase lag of about 35° and the handlebars a phase lag of roughly 60-70°. Note, that the phase in the vertical direction of both the foot pegs and handlebars starts from roughly -200° and -180°, respectively. According to the right-hand sided Cartesian coordinate frame, this means that the vertical forces in these interfaces are always in opposite direction of the pitch motion. As aforementioned, for the handlebars in lateral direction only the phase of one side is shown indicating that the lateral forces in the left and right side are always in opposite direction with respect to each other. This means that phase of one side starts from from roughly 0°, whereas, the other side starts from roughly -180°, see Appendix J

Interestingly, the individual apparent mass transfer functions suggest a correlation between the rider's body mass and the main resonance peak at least in the interfaces with high coherence, see Appendix J. Riders with a high body mass show lower resonance frequencies but higher resonance magnitudes with respect to lightweight riders. According to the phase, this effect is less apparent. Although, the phase suggests that this effect is characterised by both a lower frequency offset of the phase lag, and a faster decreasing phase around the resonance frequency for heavy riders. Remarkably, the correlation between body mass and resonance peak was not found for the individual STS transfer functions, see Appendix H.

In comparison with the surge motion, the gain and phase of the pitch apparent mass transfer function show roughly similar trends, especially for the phase. Although, the pitch apparent mass transfer function show much higher gains at lower frequencies. Furthermore, the resonance peaks at 1.8 Hz seem to be wider and more damped.

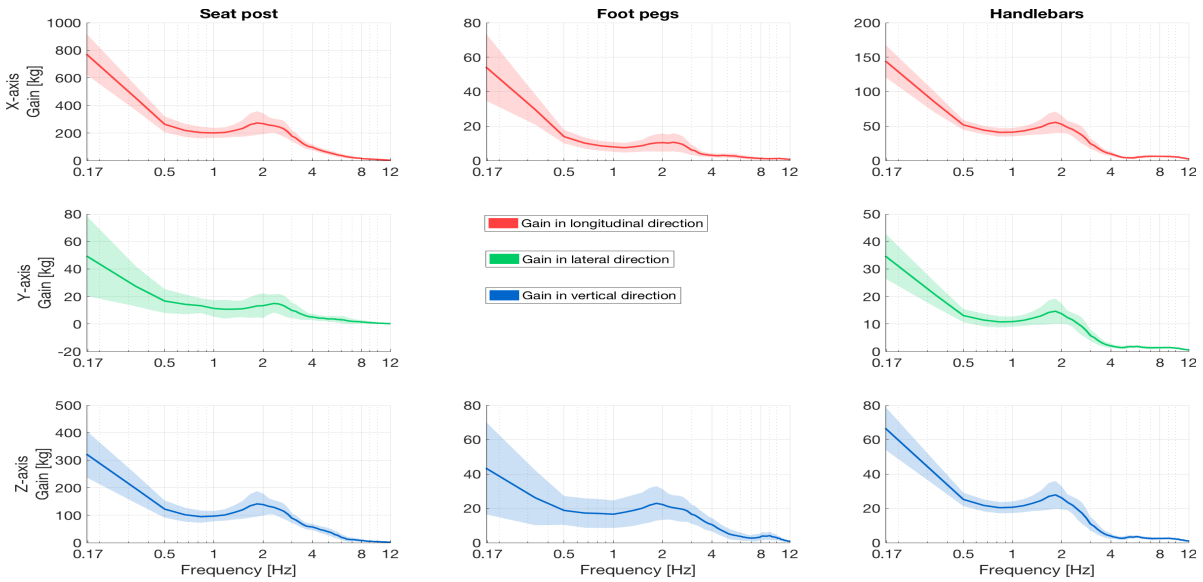

(a) Gain

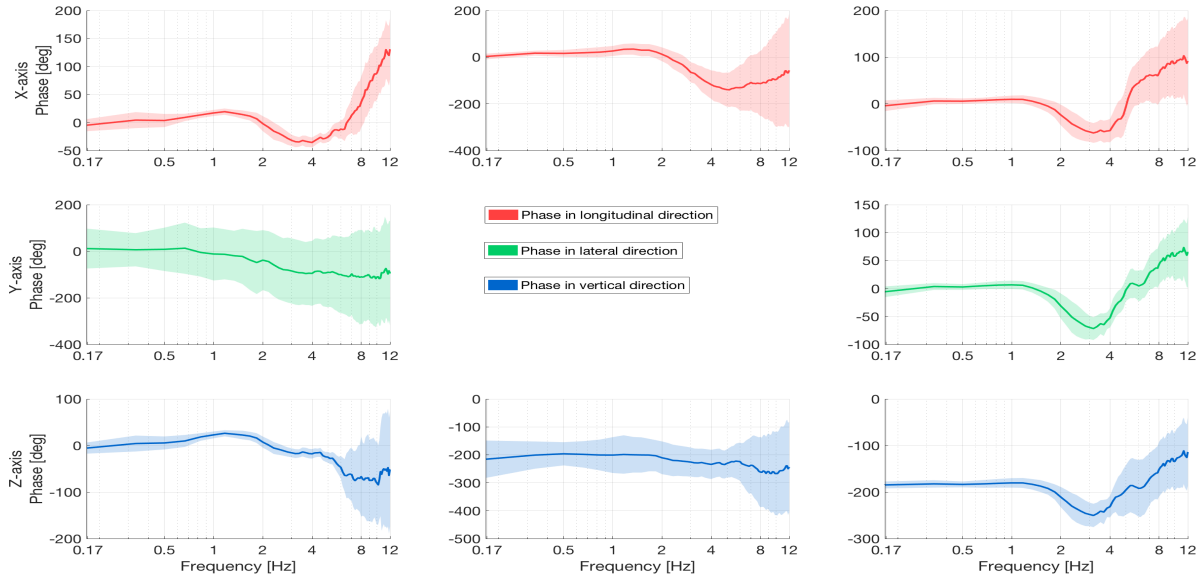

(b) Phase

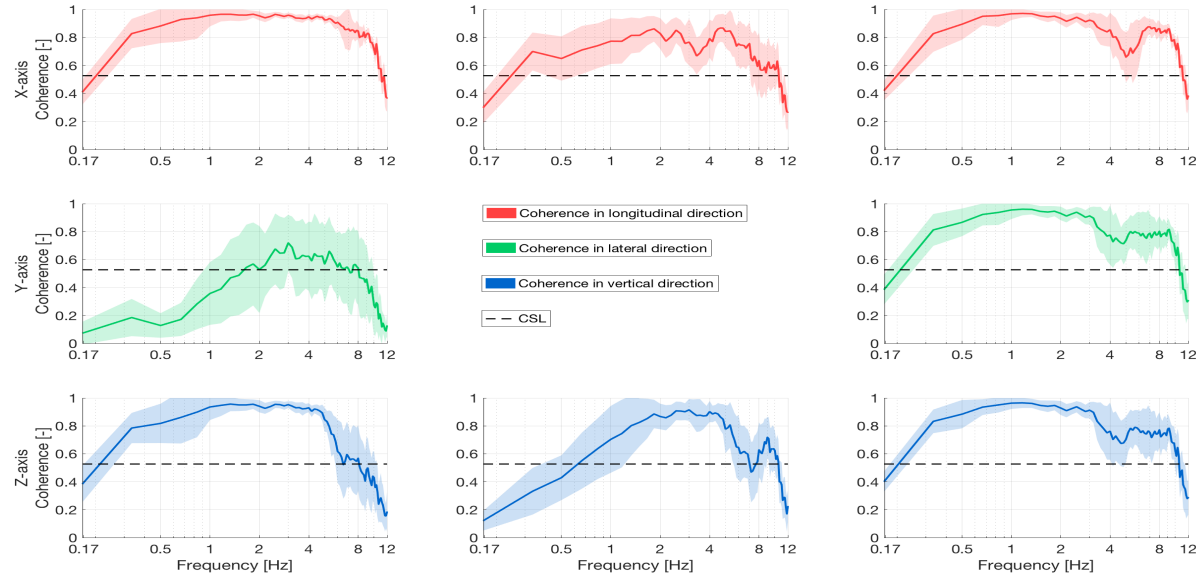

(c) Coherence

Figure 3.13: The apparent mass transfer functions $M(f)$ of the mean rider for the pitch motion (around Y-axis) at the seat post, foot pegs and handlebars. (a) gain, (b) phase and (c) coherence. The coloured shade shows the SD between individual participants. The black dashed line in the coherence plots indicates the CSL (= 0.53).

Yaw

Figure 3.14 shows the gain, phase and coherence, respectively, for the yaw apparent mass transfer functions. The corresponding individual transfer functions can be found in Appendix K. It should be noted, that for the foot pegs in longitudinal direction only the mean of the right side is shown since the left and right side show opposite phases, see Appendix K. The same holds for the handlebars in which the longitudinal and lateral direction show the mean of the right side, while, the vertical direction shows the left side.

Figure 3.14c suggests that good linear correlations are observed in the lateral direction of the seat post between 1-9 Hz, and in the foot pegs in longitudinal direction between 1-8 Hz. Other interfaces show only good coherence in specific frequency regions. For instance, the handlebars in longitudinal direction between 1-5-2.5 and 4-10 Hz; the handlebars in lateral direction between 4.5-9 Hz; the foot pegs in vertical direction between 6-10 Hz and the seat post in vertical direction between 1-3.5 Hz. The seat post in longitudinal direction and the handlebars in vertical direction suggest no linear correlations. Remarkably, whereas, the apparent mass transfer functions show low coherence below 1 Hz the corresponding yaw STS transfer function shows high coherence below 1 Hz.

Figure 3.14a and 3.14b show the gain and phase, respectively, for all interfaces. Note, that the gains of the seat post transfer functions are defined in Ns^2/rad since the corresponding position vector is equal to 0 indicating that there is no linear acceleration component for the seat post. All other interfaces show the apparent mass defined in kg. In all interfaces, the gain and phase below 1 Hz cannot be analysed due to low coherence. The interfaces with relative high coherence are characterised by a resonance peak at 2.3 Hz. According to the individual transfer functions an additional small resonance peak is found for some participants around 8 Hz in the foot pegs, see Appendix K. After the main resonance peak the gain decreases and approaches 0 with increasing frequency. The gain of the handlebars is characterised by an almost flat gain.

Considering the interfaces with relative good coherence, the foot pegs in longitudinal direction show a constant phase of roughly 0° up to 2 Hz. After 2 Hz, the phase decreases and shows a maximum phase lag of 60° around the resonance frequency. After this minimum, the phase shows an ascending phase lead with increasing frequency. Note, that the phase in the lateral and vertical direction of the seat post starts from roughly -180°. According to the right-hand sided Cartesian coordinate frame, this means that the the forces in these interfaces are always in opposite direction of the yaw motion. As aforementioned, for the foot pegs in longitudinal direction and the handlebars in all directions only the phase of one side is shown indicating that the corresponding forces in the left and right side are always in opposite direction with respect to each other. This means that phase of one side starts from roughly 0°, whereas, the other side starts from roughly -180°, see Appendix K.

At least for the interfaces with relative high coherence, the individual apparent mass transfer functions suggest a correlation between body mass and the main resonance peak indicating a lower resonance frequency, but higher resonance magnitude for heavy riders. In the individual phases this effect does not show specific characteristics. Note, that this correlation was also found for the yaw STS transfer function.

In general, the results for the yaw motion can be considered as erroneous due to overall low coherence and low power force signals. This suggests that results are affected by noise. Therefore, one should not draw conclusions from the yaw results.

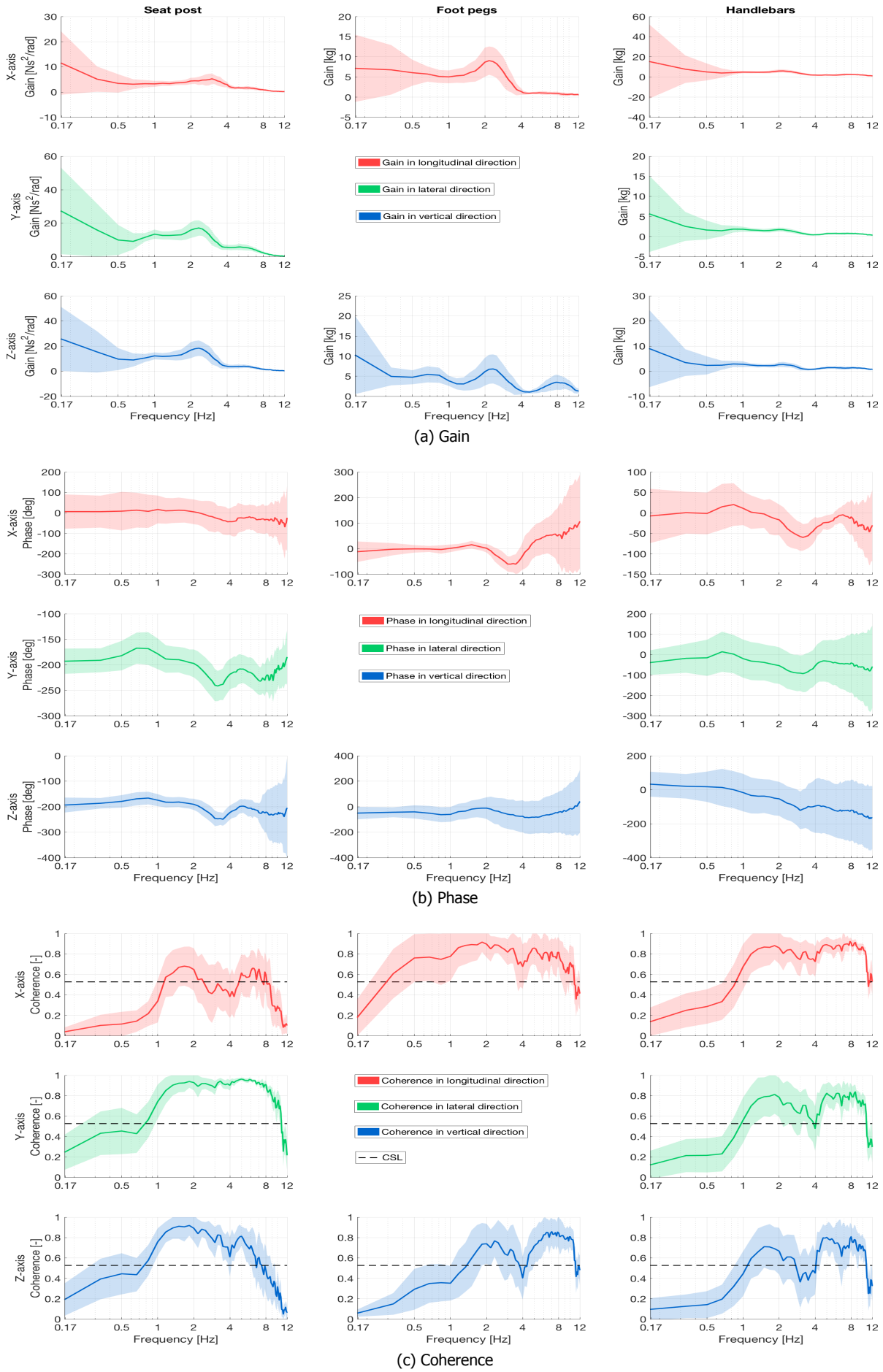

Figure 3.14: The apparent mass transfer functions $M(f)$ of the mean rider for the yaw motion (around Z-axis) at the seat post, foot pegs and handlebars. (a) gain, (b) phase and (c) coherence. The coloured shade shows the SD between individual participants. The black dashed line in the coherence plots indicates the CSL (= 0.53).

3.3. General results

In this section, results will be discussed that were observed for the greater part of the motions.

First of all, the force distribution for all motions showed relative high static forces in the lateral direction of the handlebars, while these are not expected. Sub-experiments turned out that applying a force in vertical or in longitudinal direction result in a lateral deformation of the steering assembly due to its shape. Concerning the rider configuration, one can imagine that the rider already generates relative high longitudinal and vertical loads due to the slightly forward leaned upper body causing a lateral deformation of the steer, see figure 2.2. Furthermore, the lateral and vertical apparent mass transfer functions of the handlebars show almost identical phases an coherence for all motions. Therefore, it can be suggested that the high lateral forces both statically and dynamically are mainly the result of longitudinal and vertical forces applied by the rider. In other words, it cannot be suggested that the lateral force in the handlebars is generated by a pure lateral force of the rider.

Second, the force distribution suggests also relative high lateral forces in the seat post, especially static forces. A reason for this could be that participants sit not perfectly symmetric relative to plane of symmetry of the bicycle mock-up. Another reason could be that lateral forces are generated due to the structure of the saddle.

4

Discussion and Conclusion

The aim of this study is to identify the passive non-parametric response of the rider's body to all translational and rotational motions in terms of apparent mass and STS transmissibility.

In general, the surge and heave motion showed a clear passive response system that could be simulated by a mass-spring-damper system. The apparent mass during the surge motion is mainly characterised by a resonance peak at 2 Hz both in the main (i.e. longitudinal) and cross-axes. The same resonance peak was found in the corresponding STS transfer function. According to for-and-aft whole body vibration studies in literature, no study reported a main resonance peak at exactly 2 Hz. Only, *N.J. Mansfield and R. Lundström, 1999* [17] found resonances between 2-3 Hz, whereas, *N. Nawayseh and M.J. Griffin, 2005* [32], *G.F. Stein et al., 2007* [18] and *M.G.R. Toward and M.J. Griffin, 2011* [13] reported main peaks between 2-6 Hz. These studies also reported the existence of additional resonance peaks in the seat, however, in this research this was only minimally observed in the foot pegs. It should be noted, that the results from literature are with respect to upright seated persons weather or not with a back and frontal support. This makes it hard to compare results since the passive response is mainly determined by the rider's configuration. Differences in resonance frequencies could also be explained by the fact that resonance frequencies decrease with increasing vibration magnitudes as found by *G.F. Stein et al., 2007* [18] during for-and-aft whole body vibration and by *N. J. Mansfield and M.J. Griffin, 2000* [8], *S. Rakheja and I. Stiharu, 2002* [9] and *M.G.R. Toward and M.J. Griffin, 2011* [13] for vertical whole-body vibration.

The heave motion showed similar trends as the surge motion, but revealed differences in resonance frequencies between interfaces. The apparent mass in the seat post and handlebars is mainly characterised by a resonance peak at 5 Hz, whereas, the foot pegs showed resonance around 6 Hz. The corresponding STS transfer function showed a resonance peak around 5 Hz, as well, but seemed to be more dispersed. In general, vertical whole-body vibration studies in literature, such as *N. J. Mansfield and M.J. Griffin, 2002* [33], *W. Wang et al., 2004* [10], *M.G.R. Toward and M.J. Griffin, 2011* [13] and *J.H. Goa et al., 2011* [14] showed seat resonance frequencies close to ones found in this research. However, in literature are also different resonance frequencies reported since they are influenced by posture configuration, vibration magnitude and rigid supports (e.g. backrest and steer). For instance, *S. Rakheja and I. Stiharu, 2002* [9], *W. Wang et al., 2004* [10] and *M.G.R. Toward and M.J. Griffin* [12] showed that in general holding the steering wheel lowers both the resonance frequency and magnitude with respects to a hands-in-lap configuration. Finally, the heave motion proofed that the rider acts like a rigid body below 1 Hz since the sum of all vertical apparent masses equalises roughly the body weight of the mean rider (i.e. 79.9 kg vs 81.2 kg). Latter could not be concluded for the surge motion.

The pitch and yaw motion also show, to a certain extend, mass-spring-damper characteristics. However, at very low frequencies relative high gains and low coherence was observed indicating complex control behaviour of the rider. After 1 Hz, interfaces with good coherence were characterised by a main resonance peak at 1.8 and 2.3 Hz for pitch and yaw, respectively. Only in the yaw motion a similar resonance frequency was found in the STS transfer function. In literature, no studies have reported pitch and yaw apparent masses with respect to seated rider configurations. Only *A. Doria and M. Tognazzo, 2012* [24] and *A. Doria and M. Tognazzo, 2014* [23] reported transmissibility transfer functions of two-wheeled riders showing resonance frequencies around 2 Hz, but the corresponding

trend at high frequencies was significantly different from the yaw STS tranfer function obtained in this research.

The sway and roll motion showed similar trends but suggest no simple mechanical characteristics. It seems to be that the rider's body response was a combination of both passive and voluntary control actions. One can imagine that due to the rider configuration the rider is less rigid/stable in lateral direction relative to the longitudinal and vertical direction. Hence, that the rider might be restricted to active control mechanisms (i.e. co-contraction and neural reflexes) for stability and comfort reasons. Activation of these mechanisms result in non-linear control dynamics that hardly can be simulated with a simple biomechanical system. In the field of trunk and head stabilisation *Van Drunen et al., 2015* [5] and *Van Drunen et al., 2015* [6] already showed that humans can modulate between different stabilising mechanisms depending on task instructions and frequency bandwidth. Remarkably, in the field of lateral whole-body vibration, *T.E. Fairley and M.J. Griffin, 1990* [16] and *N.J. Mansfield and R. Lundström, 1999* [17] reported clear resonance frequencies in the apparent mass. This cannot be concluded for the sway apparent mass transfer function in this research. Furthermore, in the field of rider identification with respect to two-wheeled vehicles, *A. Doria et al., 2013* [21], *M. Bevilacqua et al., 2013* [22] and *A. Doria and M. Tognazzo, 2014* [23] reported roll transmissibility transfer functions indicating resonance frequencies both around 2 and 5 Hz. This cannot be concluded for the roll STS transfer function in this research. Therefore, it can be suggested that the riders in this research were not able to stay around their linear operation point during sway and roll perturbations.

The apparent mass for the surge, heave, pitch and yaw motion suggest a correlation between the rider's body mass and the corresponding main resonance peak in interfaces with high coherence. It was found that higher body weight in general yields higher peak magnitude and lower resonance frequency with respect to lightweight riders, which was also reported by *S. Rakheja and I. Stiharu, 2002* [9] and *M.G.R. Toward and M.J. Griffin, 2011* [13]. This relationship was mainly observed in the apparent mass transfer functions, but was less apparent in the STS transfer functions. Although, the STS transfer function for surge indicates this relationship.

As a conclusion, the heave and surge motion suggest simple underlying passive dynamics both in the apparent mass and STS transfer functions of almost all interfaces and directions. The yaw and pitch apparent mass transfer functions suggest simple passive dynamics for several interfaces and directions, as well, but only after 1 Hz. The sway and roll motion showed no characteristics of simple passive dynamics both in the apparent mass and STS transfer function. Finally, the surge, heave, pitch and yaw apparent mass transfer functions showed that higher body mass in general yields higher peak magnitude and lower resonance frequency. This effect was most apparent for the surge motion. In the future, studies should focus on fitting the experimental results obtained in this research with simple mechanical systems, such as a mass-spring-damper systems, or if needed with more complex biomechanical models. Adding these biomechenical characteristics of the rider to current bicycle models shows high potential to understand better bicycle-rider interaction and improve bicycle designs and safety.

Bibliography

[1] J. Meijaard, J. M. Papadopoulos, A. Ruina, and A. Schwab, *Linearized dynamics equations for the balance and steer of a bicycle: a benchmark and review,* Proceedings of the Royal Society A: Mathematical, Physical and Engineering Sciences **463**, 1955 (2007).

[2] M. Plöchl, J. Edelmann, B. Angrosch, and C. Ott, *On the wobble mode of a bicycle,* Vehicle System Dynamics **50**, 415 (2012).

[3] F. C. van der Helm, A. C. Schouten, E. de Vlugt, and G. G. Brouwn, *Identification of intrinsic and reflexive components of human arm dynamics during postural control,* Journal of Neuroscience Methods **119**, 1 (2002).

[4] E. de Vlugt, A. C. Schouten, and F. C. van der Helm, *Quantification of intrinsic and reflexive properties during multijoint arm posture,* Journal of Neuroscience Methods **155**, 328 (2006).

[5] P. van Drunen, Y. Koumans, F. C. van der Helm, J. H. van Dieën, and R. Happee, *Modulation of intrinsic and reflexive contributions to low-back stabilization due to vision, task instruction, and perturbation bandwidth,* Experimental Brain Research (2015), 10.1007/s00221-014-4151-2.

[6] P. van Drunen, F. C. T. van der Helm, J. H. van Dieën, and R. Happee, *Trunk stabilization during sagittal pelvic tilt: from trunk-on-pelvis to trunk-in-space due to vestibular and visual feedback,* Journal of Neurophysiology (2015), 10.1152/jn.00867.2015.

[7] T. E. Fairley and M. J. Griffin, *The apparent mass of the seated human body: Vertical vibration,* Journal of Biomechanics (1989), 10.1016/0021-9290(89)90031-6.

[8] N. J. Mansfield and M. J. Griffin, *Non-linearities in apparent mass and transmissibility during exposure to whole-body vertical vibration,* Journal of Biomechanics (2000), 10.1016/S0021-9290(00)00052-X.

[9] S. Rakheja, I. Stiharu, and P. É. Boileau, *Seated occupant apparent mass characteristics under automotive postures and vertical vibration,* in *Journal of Sound and Vibration* (2002).

[10] W. Wang, S. Rakheja, and P. É. Boileau, *Effects of sitting postures on biodynamic response of seated occupants under vertical vibration,* International Journal of Industrial Ergonomics (2004), 10.1016/j.ergon.2004.04.009.

[11] N. J. MANSFIELD and S. MAEDA, *Effect of Backrest and Torso Twist on the Apparent Mass of the Seated Body Exposed to Vertical Vibration,* Industrial Health (2005), 10.2486/indhealth.43.413.

[12] M. G. Toward and M. J. Griffin, *Apparent mass of the human body in the vertical direction: Effect of a footrest and a steering wheel,* Journal of Sound and Vibration (2010), 10.1016/j.jsv.2009.11.015.

[13] M. G. R. Toward and M. J. Griffin, *Apparent mass of the human body in the vertical direction: Inter-subject variability,* Journal of Sound and Vibration (2011), 10.1016/j.jsv.2010.08.041.

[14] G. Jianghua, H. Zhichao, H. Le, and X. Qunsheng, *Vertical vibration characteristics of seated human bodies and a biodynamic model with two degrees of freedom,* Science China Technological Sciences (2011), 10.1007/s11431-011-4461-6.

[15] M. S. Kim, G. J. Jeon, J. Y. Lee, S. J. Ahn, W. S. Yoo, and W. B. Jeong, *Human response of vertical and pitch motion to vertical vibration on whole body according to sitting posture,* Journal of Mechanical Science and Technology (2012), 10.1007/s12206-012-0626-x.

[16] T. E. Fairley and M. J. Griffin, *The apparent mass of the seated human body in the fore-and-aft and lateral directions,* Journal of Sound and Vibration (1990), 10.1016/0022-460X(90)90890-C.

[17] N. J. Mansfield and R. Lundström, *The apparent mass of the human body exposed to non-orthogonal horizontal vibration,* Journal of Biomechanics (1999), 10.1016/S0021-9290(99)00135-9.

[18] G. J. Stein, P. Múčka, R. Chmúrny, B. Hinz, and R. Blüthner, *Measurement and modelling of x-direction apparent mass of the seated human body-cushioned seat system,* Journal of Biomechanics (2007), 10.1016/j.jbiomech.2006.06.012.

[19] Y. Qiu and M. J. Griffin, *Modelling the fore-and-aft apparent mass of the human body and the transmissibility of seat backrests,* Vehicle System Dynamics (2011), 10.1080/00423111003695594.

[20] V. Cossalter, A. Doria, R. Lot, and M. Massaro, *The effect of rider's passive steering impedance on motorcycle stability: Identification and analysis,* Meccanica **46**, 279 (2011).

[21] A. Doria, M. Tognazzo, and V. Cossalter, *The response of the rider's body to roll oscillations of two wheeled vehicles; experimental tests and biomechanical models,* Proceedings of the Institution of Mechanical Engineers, Part D: Journal of Automobile Engineering (2013), 10.1177/0954407012457508.

[22] M. Bevilacqua, A. Doria, and M. Tognazzo, *Interaction Forces Between the Rider and the 2-Wheeled Vehicle and Biomechanical Models,* in *Volume 1: 15th International Conference on Advanced Vehicle Technologies; 10th International Conference on Design Education; 7th International Conference on Micro- and Nanosystems*, Vol. 1 (2013) p. V001T01A020.

[23] A. Doria and M. Tognazzo, *The influence of the dynamic response of the rider's body on the open-loop stability of a bicycle,* Journal of Mechanical Engineering Science (2014), 10.1177/0954406214527073.

[24] A. Doria and M. Tognazzo, *Identification of the Biomechanical Parameters of the Riders of Two-Wheeled Vehicles by Means of Vibration Testing,* in *Volume 1: 24th Conference on Mechanical Vibration and Noise, Parts A and B* (ASME, 2012) p. 223.

[25] T. Prats Cardona, *Passive Impedance of a Bicycle Rider*, Tech. Rep. (Technical University of Delft, Delft, 2017).

[26] S. C. Walpole, D. Prieto-Merino, P. Edwards, J. Cleland, G. Stevens, and I. Roberts, *The weight of nations: an estimation of adult human biomass,* BMC Public Health **12**, 1 (2012).

[27] P. Grasgruber, J. Cacek, T. Kalina, and M. Sebera, *The role of nutrition and genetics as key determinants of the positive height trend,* Economics and Human Biology **15**, 81 (2014).

[28] B. E. Maki, *Selection of perturbation parameters for identification of the posture-control system,* Medical & Biological Engineering & Computing **24**, 561 (1986).

[29] J. D. G. Kooijman, A. L. Schwab, and J. P. Meijaard, *Experimental validation of a model of an uncontrolled bicycle,* Multibody System Dynamics **19**, 115 (2008).

[30] G. Magnani, N. M. Ceriani, and J. Papadopoulos, *On-road measurements of high speed bicycle shimmy, and comparison to structural resonance,* in *2013 IEEE International Conference on Mechatronics, ICM 2013* (2013) pp. 400–405.

[31] J. H. Van den Ouden, *Master Thesis*, Tech. Rep. (Technical University of Delft, 2011).

[32] N. Nawayseh and M. J. Griffin, *Tri-axial forces at the seat and backrest during whole-body fore-and-aft vibration,* Journal of Sound and Vibration **281**, 921 (2005).

[33] N. J. Mansfield and M. J. Griffin, *Effects of posture and vibration magnitude on apparent mass and pelvis rotation during exposure to whole-body vertical vibration,* in *Journal of Sound and Vibration* (2002).

A

Appendix A: Informed Consent

Author: J.W. de Haan Last edit: 14-08-18

Passive Rider Identification

Research information sheet

Purpose of the research

The purpose of this research is to increase our understanding of how the rider's body passively responds to translational and rotational oscillations when riding a bicycle. Passively means that the rider is not able to steer, to pedal and to show active/voluntary body motion in response to these oscillations. More specific, we will try to identify the apparent mass and mechanical impedance of the rider when subject to these oscillations. The apparent mass is the mass that is perceived at the contact surfaces of two objects while both objects are accelerating. Mechanical impedance indicates the body stiffness when the body is perturbed(= a motion/oscillation that moves you out of your reference position) in a particular direction with a certain frequency. From these measurements, we will try to identify the dynamics of a passive bicycle rider in general.

Experimental procedure

As a participant, you will be requested to wear a safety harness and to sit on a bicycle mock-up which is placed on a hexapod motion platform.

During the experiment, you will be perturbed in six individual directions: three translational and three rotational directions. The translational directions consist of surge, which is a for- and backward motion; sway, which is a lateral motion (side-to-side) and heave, which is an up- and downward motion. The rotational directions consist of roll, which is a lateral rotation around the horizontal axis that is crossing the road contact point of both the front and rear wheel; pitch, which is a for- and backward rotation around the horizontal axis directed in lateral direction placed underneath the seat post and yaw, which is a lateral rotation around the axis that is running vertically through the seat post.

Before each motion, you will be asked to take the posture of a bicycle rider and to relax your entire body as good as possible. Furthermore, you will be asked to focus on an orientation point in front of you and keep focusing on this point during the motions.

For each motion, you will perform an offset trial in order to obtain the offset of the sensors and your initial/static force. This is followed by two trials in which you will be perturbed in a particular direction. Each trial has a duration of 60 seconds. Thus, for each motion you perform three trials, which means that you have performed 18 trials in total at the end of the experiment. Between three or six trials will be a rest period of 2-3 minutes.

During a trial, we will measure the reaction forces at the seat post, foot pegs and handlebars generated by the participant as a result of the perturbation motion. Furthermore, we will measure the motion of the upper body of the participant. Therefore, you will be asked to wear an IMU sensor which will be placed on the sternum (chest).

After the experiment, the participant will be asked the fill in a questionnaire.

Benefits and risks of participating

Benefits: by giving insight into your dynamics as a bicycle rider you will provide valuable information to understand the fundamental dynamics of a passive bicycle rider in general. Potentially, this can lead to further improvement of bicycle designs, rider control strategies and bicycle safety. Furthermore, it could be valuable for cycling sports in order to improve performance.

The experiments will take place on a motion platform which could be a ones-in-lifetime experience.

Risks: during the motions, there is a chance to experience dizziness, motion sickness and fatigue. Since the amplitudes of the motions are small the chance will be low. However, when this might happen the trial will be stopped immediately. The participant can take a break to recover after which will be decided whether or not the experiment will be continued.

TU Delft

Withdrawal from the study

The participant has the right to withdraw from the study at any time before the official publication of the paper corresponding to this research. The participant is not required to give a reason for withdrawal. After publication, results and conclusions with respect to this research cannot be changed. After publication, a participant can still request for destroying the research data that corresponds to him or her. Withdrawal from the study can be obtained by contacting the researchers.

Data usage and protection

Personal data that will be collected contain the name, e-mail, gender, age, body weight, body length, cycling hours per week and hobbies/sports. Hence, that the name of the participant will only be used by the researchers in order to match the correct research data with the corresponding participant. In the light of the research and the potential publication, participants will be assigned to a participant code (e.g. sub01). The e-mail address will only be used by the researchers for contacting the participants and will not be disseminated. Age, body weight and body length will be used to calculate the mean age, body weight and body length for the general rider from which we will identify the dynamics and from which we will derive our results and conclusions.

During the experiment, body motions of the participant as a result of the applied perturbations will be recorded by two GoPro's. One is placed in front of you and one is placed on your right side. The footage will be used to help the researchers to analyse the measured data. For instance, the footage can be used to clarify particular trends in the bode plots (gain and phase plots). On the other hand, it can be useful to check if participants show voluntary/active motions or to find similarities within motions between participants.

Obtained research data that corresponds to you will be solely available for the researchers and you as a participant of this research. Participants have the right to request access to and rectification or erasure of personal data at any time.

After publication, all research data will be given to the principal researcher **Dr. ir. A.L. Schwab**. After this, his representatives in this research **G. Dialynas** and **J.W. de Haan** will destroy all research data that they possess. The way how research data (except the name, e-mail and footage) is archived, reused and disseminated is determined by the principal researcher. The use and dissemination of name, e-mail and footage for practical purposes other than for this research will always be submitted to and requires prior consent of the corresponding participant. The retention period for the research data will be infinite for the principal researcher.

How to file a complaint

A complaint can be filed by officially contacting via e-mail the principal researcher or one of its representatives. See for more information the contact details.

Contact details

Principal researcher:
Dr. ir. A.L. Schwab
BioMechanical Engineering
Delft University of Technology
Mekelweg 2, 2628 CD Delft, The Netherlands
Mail: a.l.schwab@tudelft.nl
Phone: +31 15 27 82701

Project leader:
G. Dialynas
BioMechanical Engineering
Delft University of Technology
Mekelweg 2, 2628 CD Delft, The Netherlands
Mail: G.Dialynas@tudelft.nl
Phone: +31 6 38 44 98 68

MSc student:
J.W. de Haan
BioMedical Engineering
Delft University of Technology
Mekelweg 2, 2628 CD Delft, The Netherlands
Mail: J.W.deHaan@student.tudelft.nl
Phone: +31 6 12 95 11 14

TU Delft

Author: J.W. de Haan Last edit: 14-08-18

Consent Form for passive rider identification

Please tick the appropriate boxes	**Yes**	**No**
Taking part in the study		
I have read and understood the study information dated 14/08/2018, or it has been read to me. I have been able to ask questions about the study and my questions have been answered to my satisfaction.	□	□
I consent voluntarily to be a participant in this study and understand that I can refuse to answer questions and I can withdraw from the study at any time, without having to give a reason.	□	□
I understand that taking part in the study involves body measurements (forces, accelerations, velocities and positions) with respect to six individual perturbations; film recording of body motions; and a questionnaire completed by myself (the participant) in which I will provide my name, e-mail, gender, age, body weight, body length, cycling hours per week and hobbies/sports.	□	□
Risks associated with participating in the study		
I understand that taking part in the study involves the following risks: dizziness, motion sickness and fatigue.	□	□
Use of the information in the study		
I understand that information I provide (except of my name and e-mail) will be used for a master thesis report and potential publications directly related to this research.	□	□
I understand that personal information collected about me that can identify me, such as my name or e-mail, will not be shared beyond the study team.	□	□
Future use and reuse of the information by others		
I give permission for the research data (except my name, e-mail and footage) that I provide to be anonymized archived (i.e. data is prescribed to the participant code and not to participant name) in the data repository of the principal researcher so that it can be used for future research and learning. I give permission to archive e-mail and footage corresponding to me in the data repository of the principal researcher, however, future use and dissemination of e-mail and footage corresponding to me has to be submitted to and requires prior consent from me.	□	□

Signatures

_____	_____	_____
Name of participant	Signature	Date

I have accurately read out the information sheet to the potential participant and, to the best of my ability, ensured that the participant understands to what they are freely consenting.

_____	_____	_____
Researcher name	Signature	Date

Study contact details for information: *J.W. de Haan, +31 612951114,* J.W.deHaan@student.tudelft.nl

TU Delft

B

Appendix B: Data J.H. van den Ouden

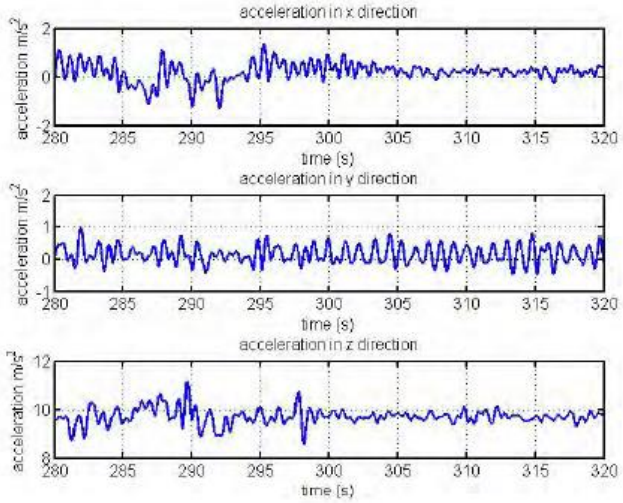

(b) Measured acceleration from the orientation sensor located on the luggage carrier of the bicycle. Test subject A

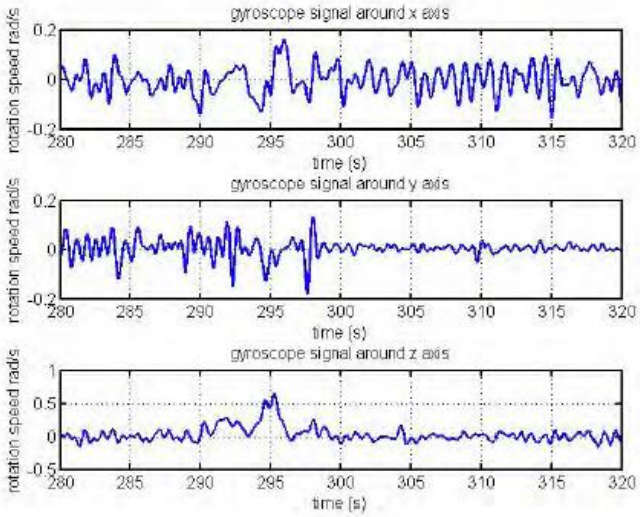

(a) Measured angular velocity from the orientation sensor located on the luggage carrier of the bicycle. Test subject A.

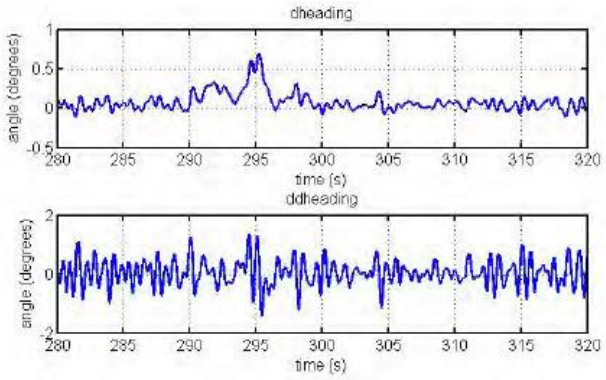

(a) The angular velocity and the angular acceleration of the orientation of the bicycle in the yaw angle direction. In this report referred to as respectively $\dot{\psi}$ and $\ddot{\psi}$. Test subject A.

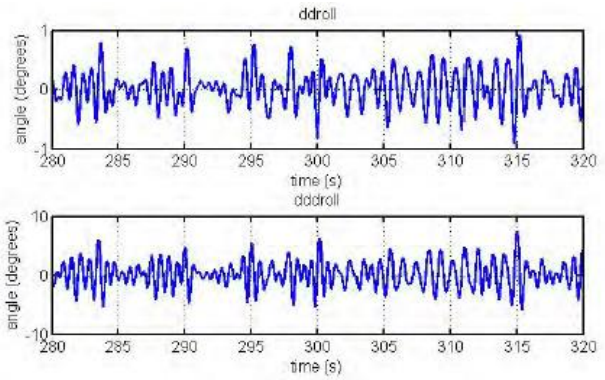

(b) The angular velocity and the angular acceleration of the orientation of the bicycle in the roll angle direction. In this report referred to as respectively $\dot{\phi}$ and $\ddot{\phi}$. Test subject A.

C

Appendix C: Filter characteristics

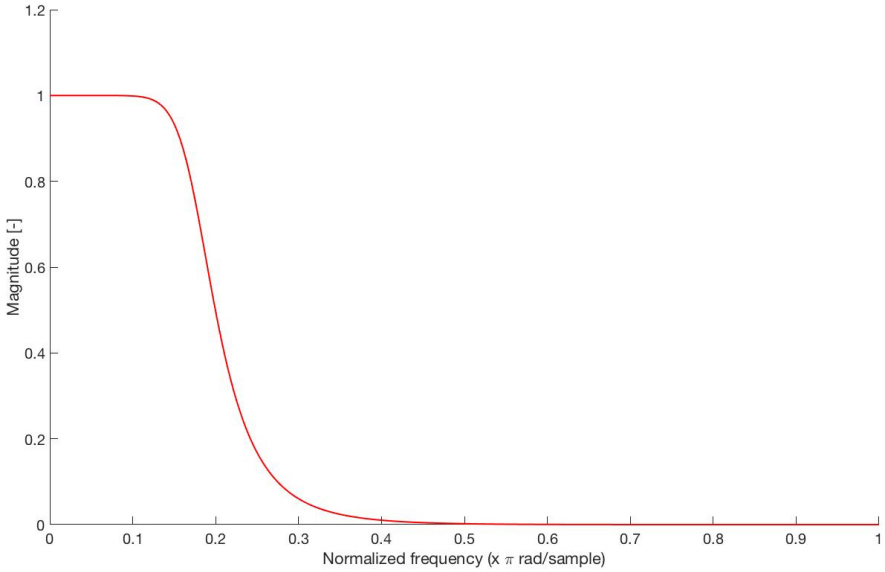

Figure C.1: The magnitude FRF of the Butterworth low-pass filter. The frequencies are normalised with respect to the Nyquist frequency (= 50 Hz). Thus, a normalised frequency of 1 corresponds to 50 Hz, whereas, a normalised frequency of 0.2 corresponds to 10 Hz.

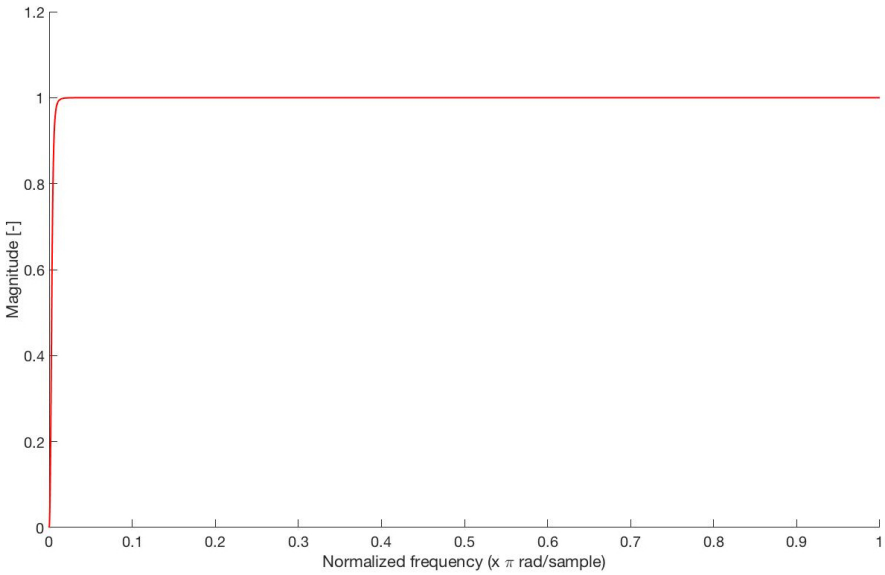

Figure C.2: The magnitude FRF of the Butterworth high-pass filter. The frequencies are normalised with respect to the Nyquist frequency (= 50 Hz). Thus, a normalised frequency of 1 corresponds to 50 Hz, whereas, a normalised frequency of 0.2 corresponds to 10 Hz.

D

Appendix D: Individual translational STS transfer functions

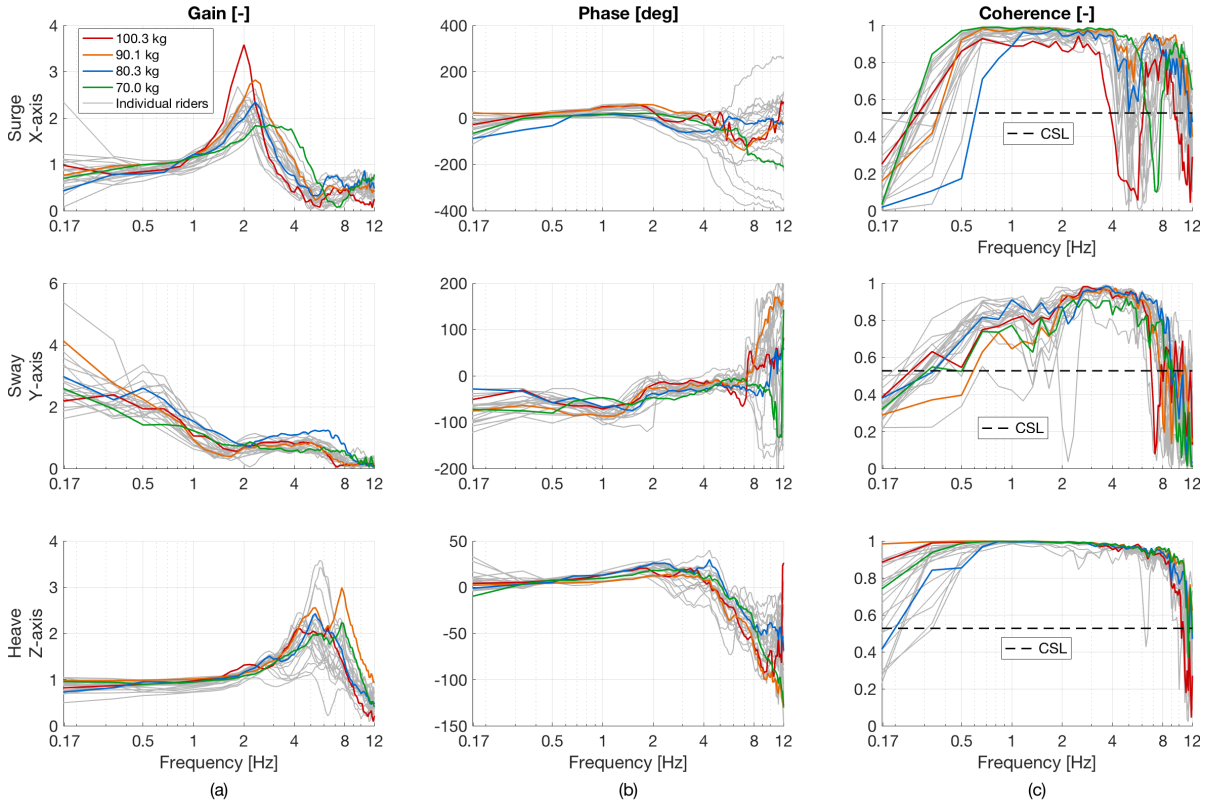

Figure D.1: The translational seat-to-sternum (STS) transfer functions $T_{trans}(f)$ of 24 individual riders for the heave (Z, vertical), surge (X, longitudinal) and sway (Y, lateral) motion. (a) gain, (b) phase and (c) coherence. The coloured lines indicate riders with specific body weights. The black dashed line in the coherence plots indicates the CSL (= 0.53).

E

Appendix E: Heave individual apparent mass transfer functions

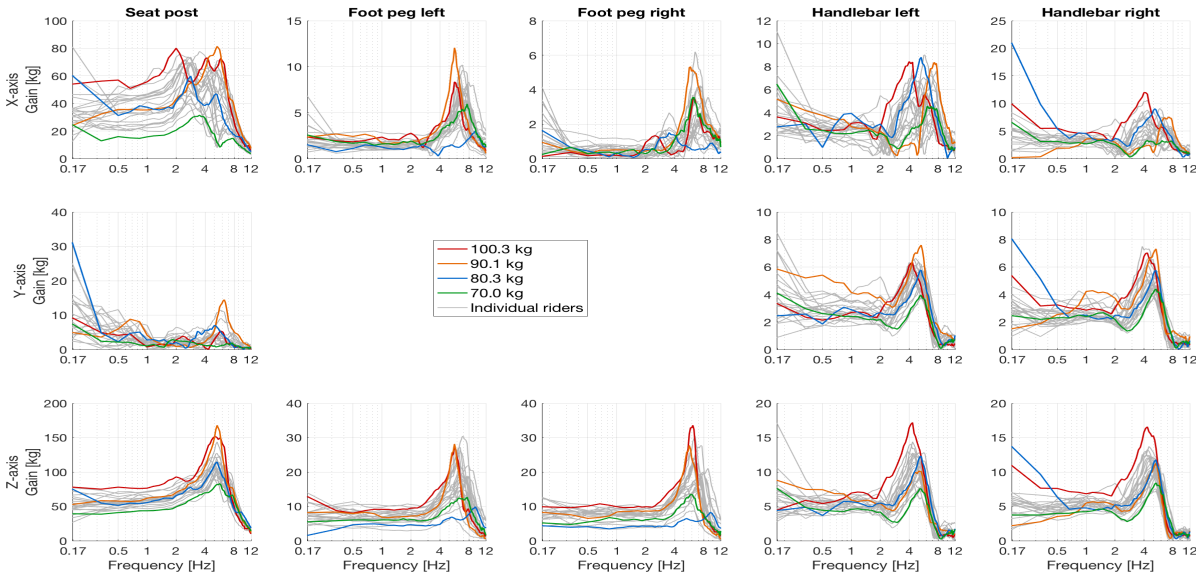

(a) Gain

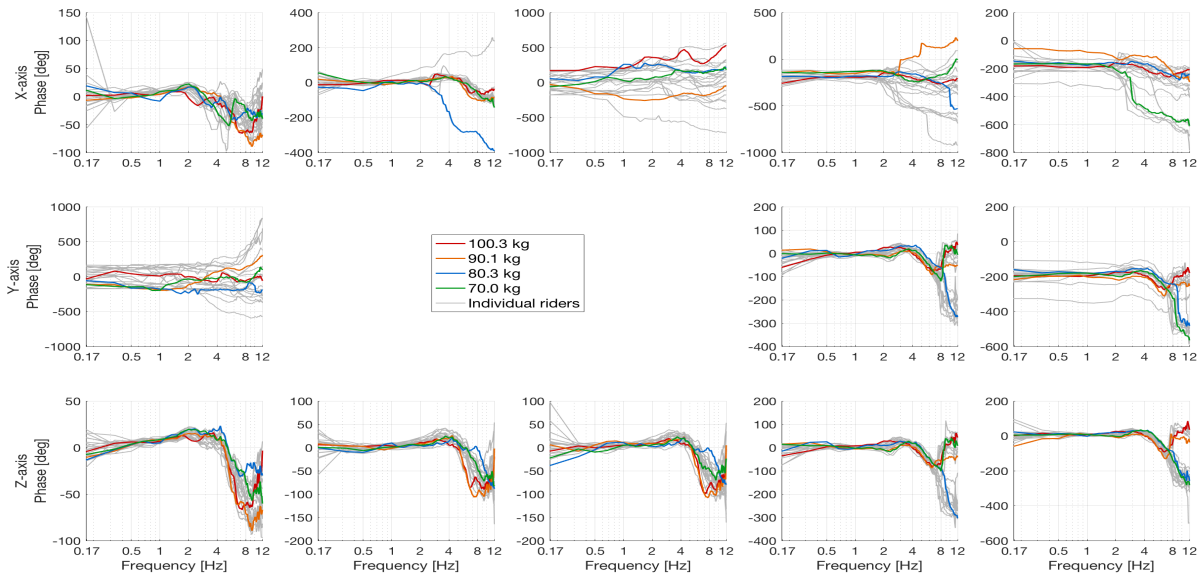

(b) Phase

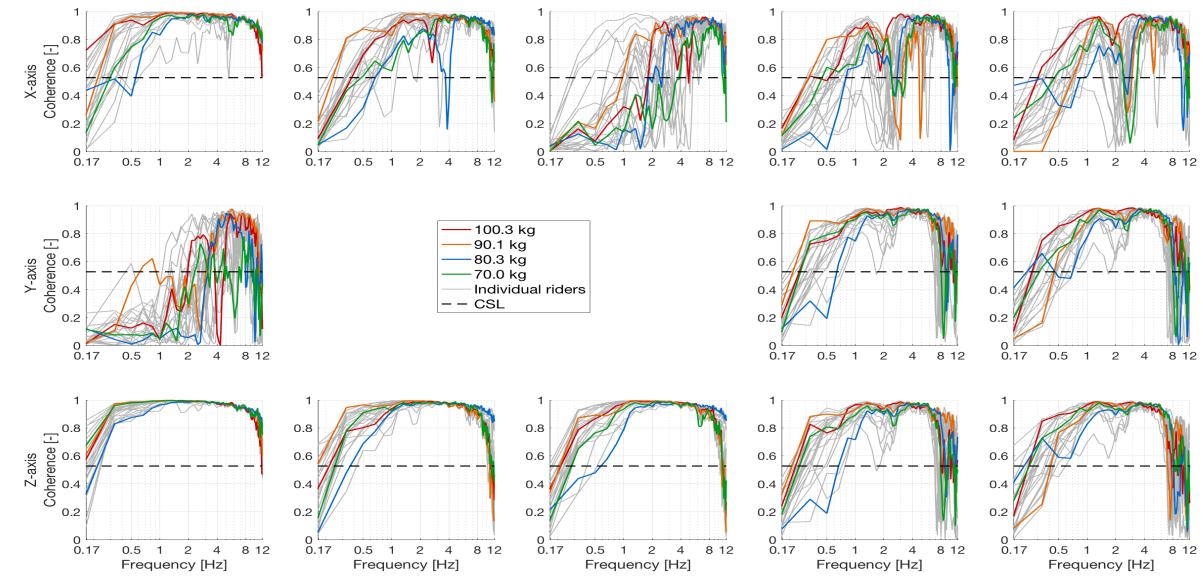

(c) Coherence

Figure E.1: The apparent mass transfer functions $M(f)$ of 24 individual participants for the heave motion (Z, vertical) at the seat post, foot pegs and handlebars. (a) gain, (b) phase and (c) coherence. The coloured lines indicate participants with specific body weights. The black dashed line in the coherence plots indicate the CSL (= 0.53).

F

Appendix F: Surge individual apparent mass transfer functions

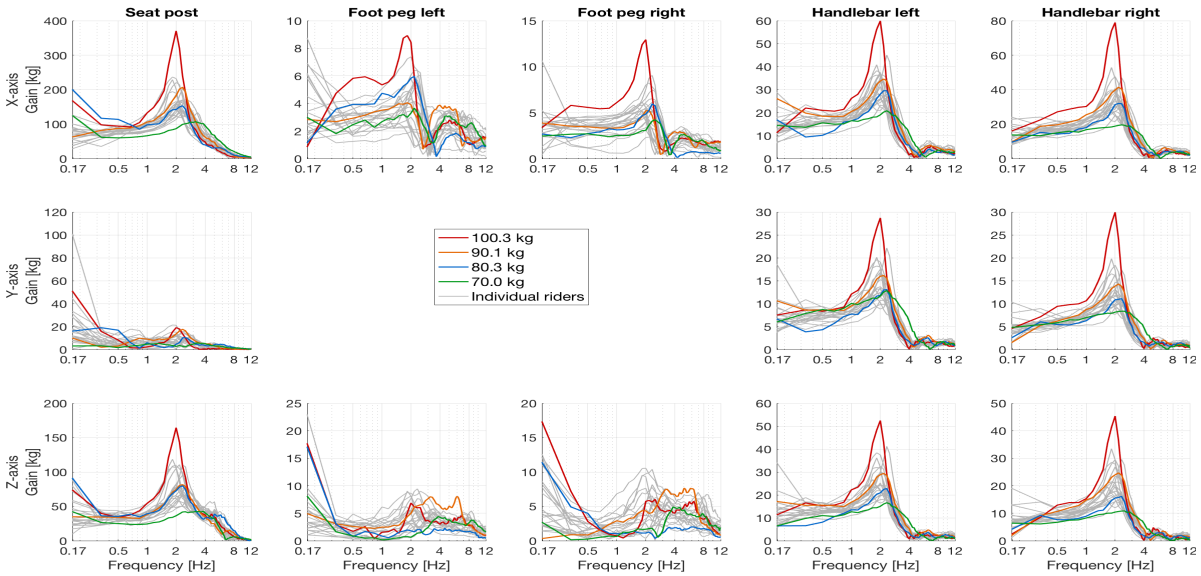

(a) Gain

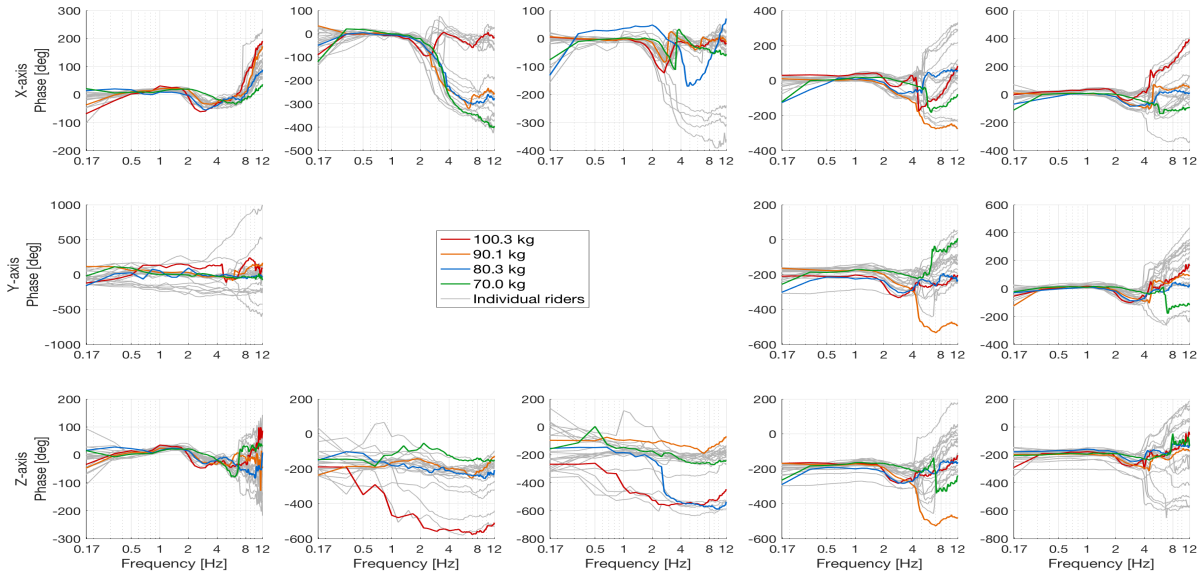

(b) Phase

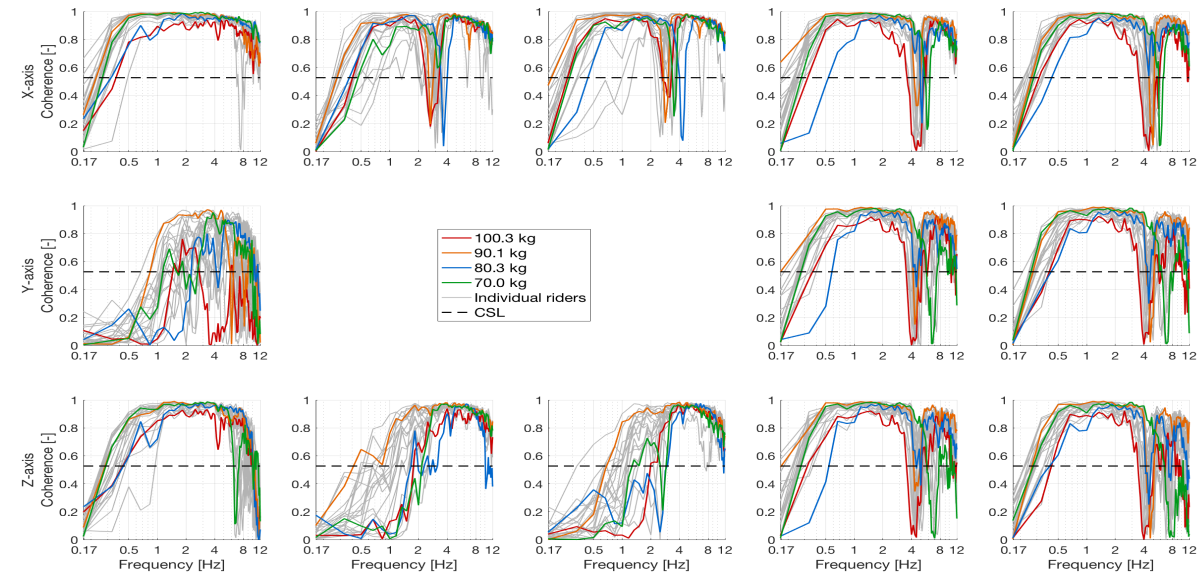

(c) Coherence

Figure F.1: The apparent mass transfer functions $M(f)$ of 24 individual participants for the surge motion (X, longitudinal) at the seat post, foot pegs and handlebars. (a) gain, (b) phase and (c) coherence. The coloured lines indicate 4 riders with specific body weights. The black dashed line in the coherence plots indicate the CSL (= 0.53).

G

Appendix G: Sway individual apparent mass transfer functions

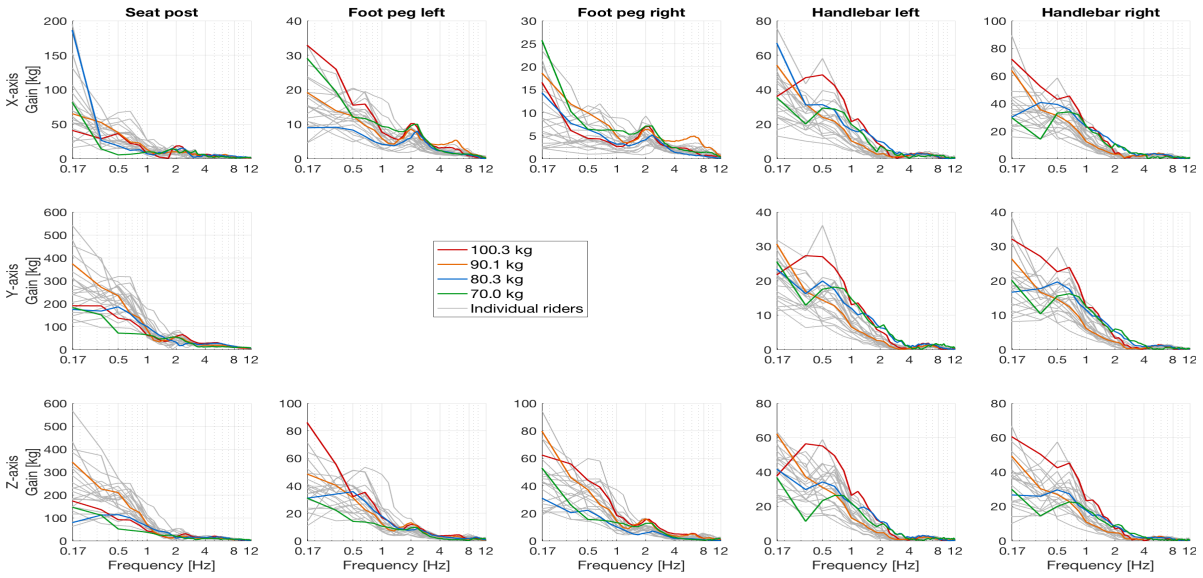

(a) Gain

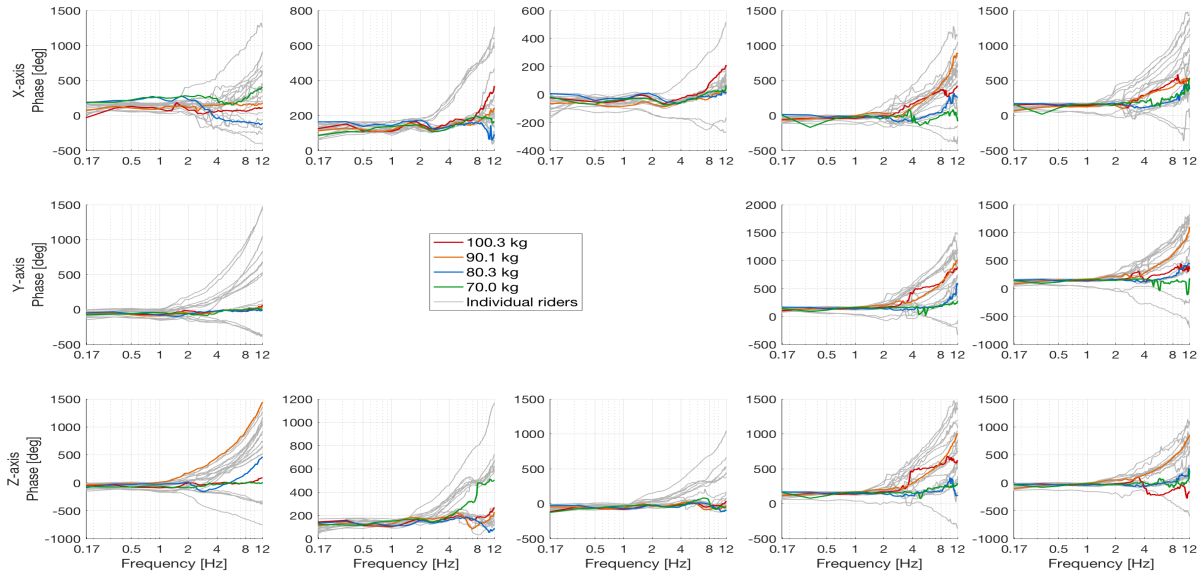

(b) Phase

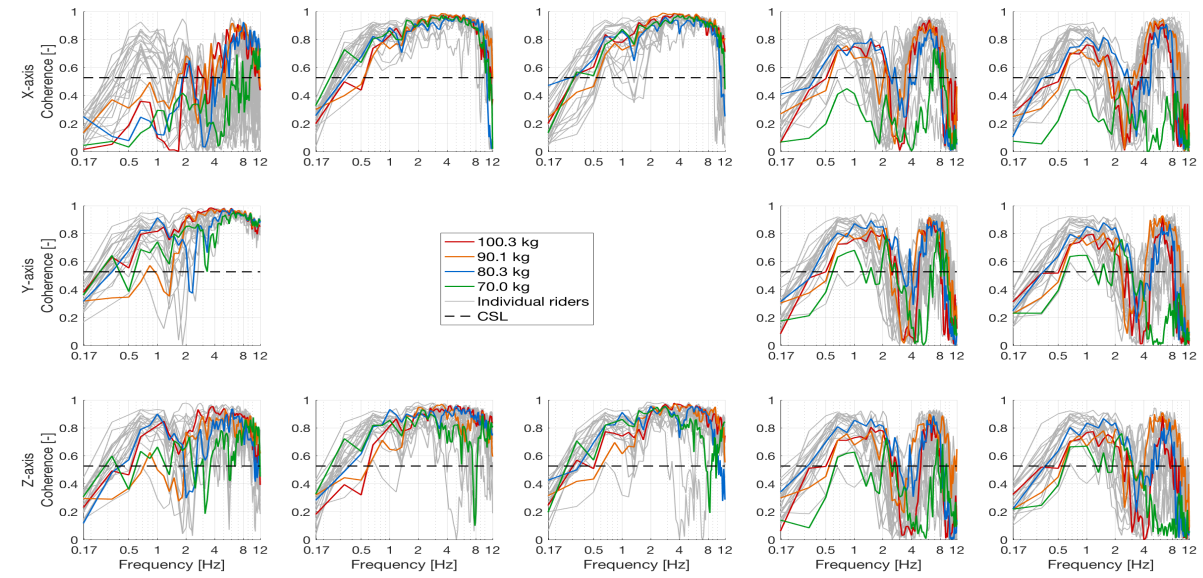

(c) Coherence

Figure G.1: The apparent mass transfer functions $M(f)$ of 24 individual participants for the sway motion (Y, lateral) at the seat post, foot pegs and handlebars. (a) gain, (b) phase and (c) coherence. The coloured lines indicate 4 riders with specific body weights. The black dashed line in the coherence plots indicate the CSL (= 0.53).

H

Appendix H: Individual rotational STS transfer functions

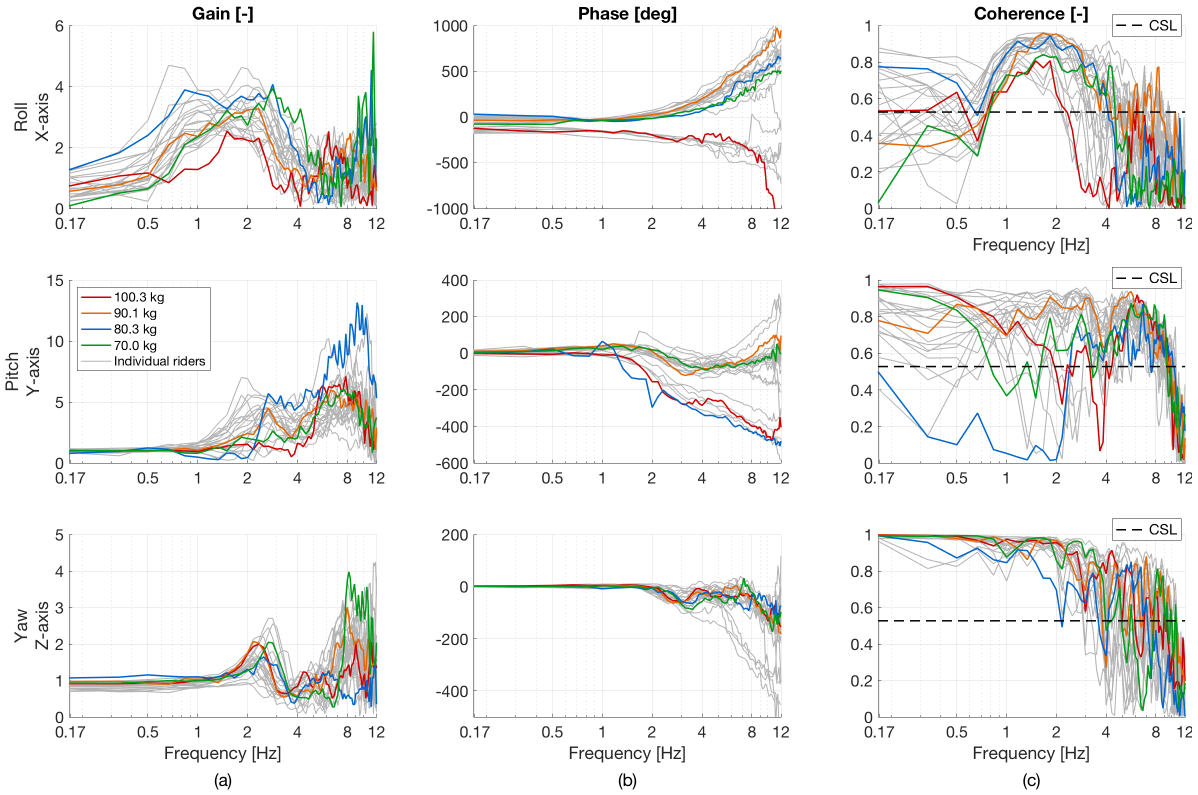

Figure H.1: The rotational seat-to-sternum (STS) transfer functions $T_{rot}(f)$ of 24 individual riders for the roll (around X-axis), pitch (around Y-axis) and yaw motion (around Z-axis). (a) gain, (b) phase and (c) coherence. The coloured lines indicate riders with specific body weights. The black dashed line in the coherence plots indicates the CSL (= 0.53).

I

Appendix I: Roll individual apparent mass transfer functions

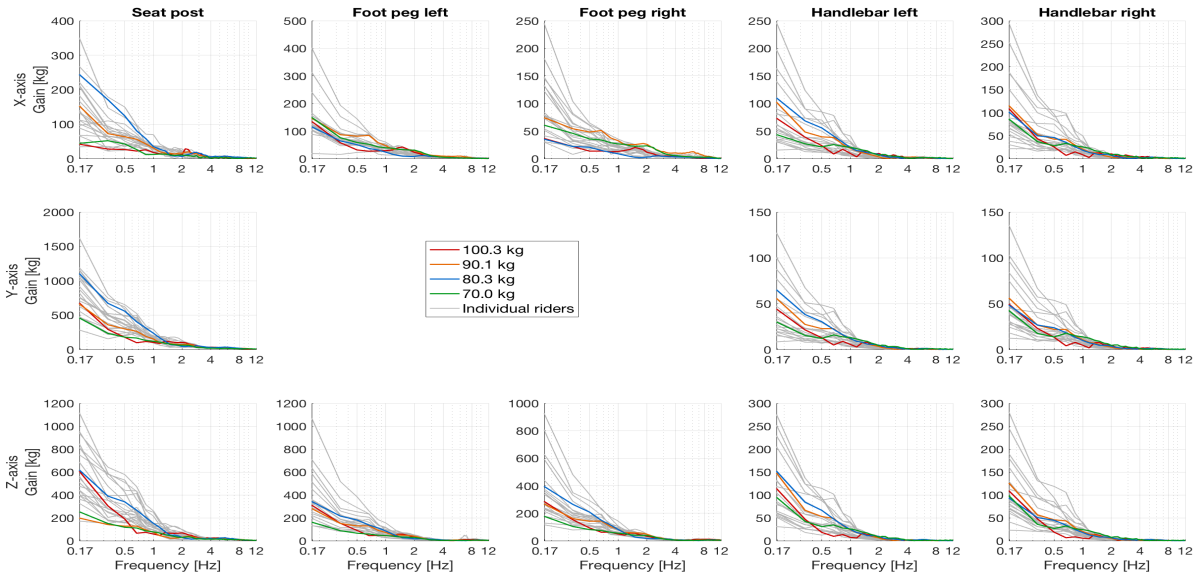

(a) Gain

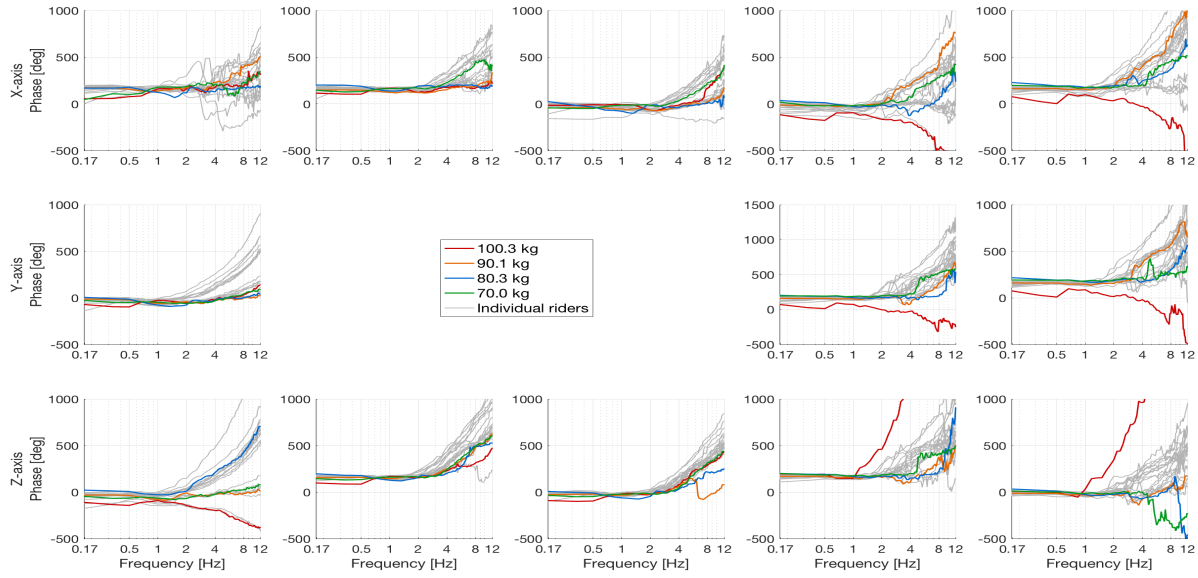

(b) Phase

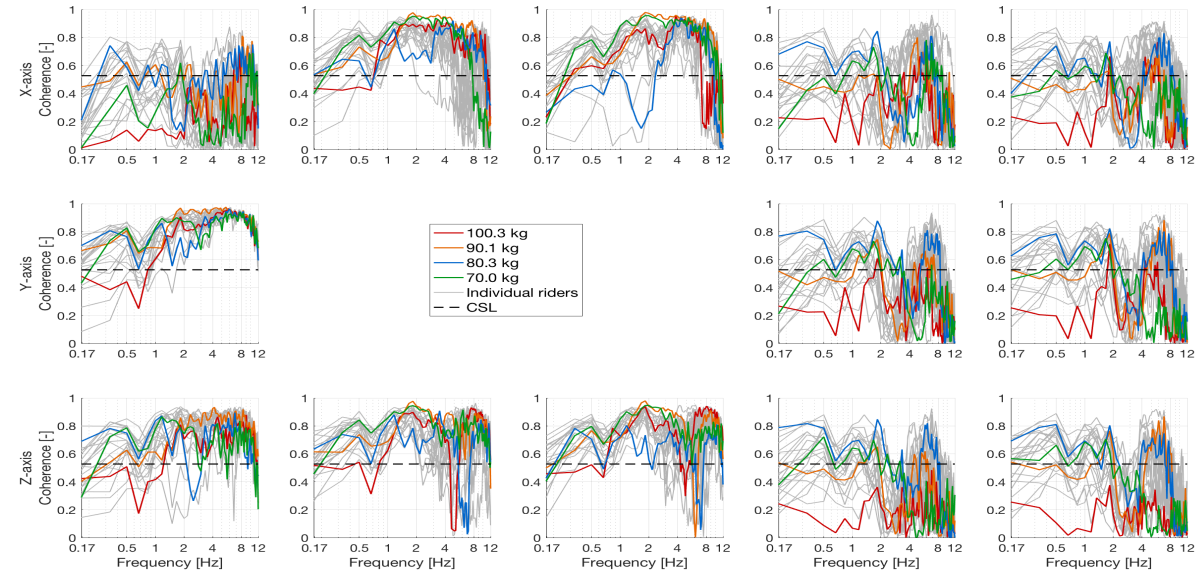

(c) Coherence

Figure I.1: The apparent mass transfer functions $M(f)$ of 24 individual participants for the roll motion (around X-axis) at the seat post, foot pegs and handlebars. (a) gain, (b) phase and (c) coherence. The coloured lines indicate 4 riders with specific body weights. The black dashed line in the coherence plots indicate the CSL (= 0.53).

J

Appendix J: Pitch individual apparent mass transfer functions

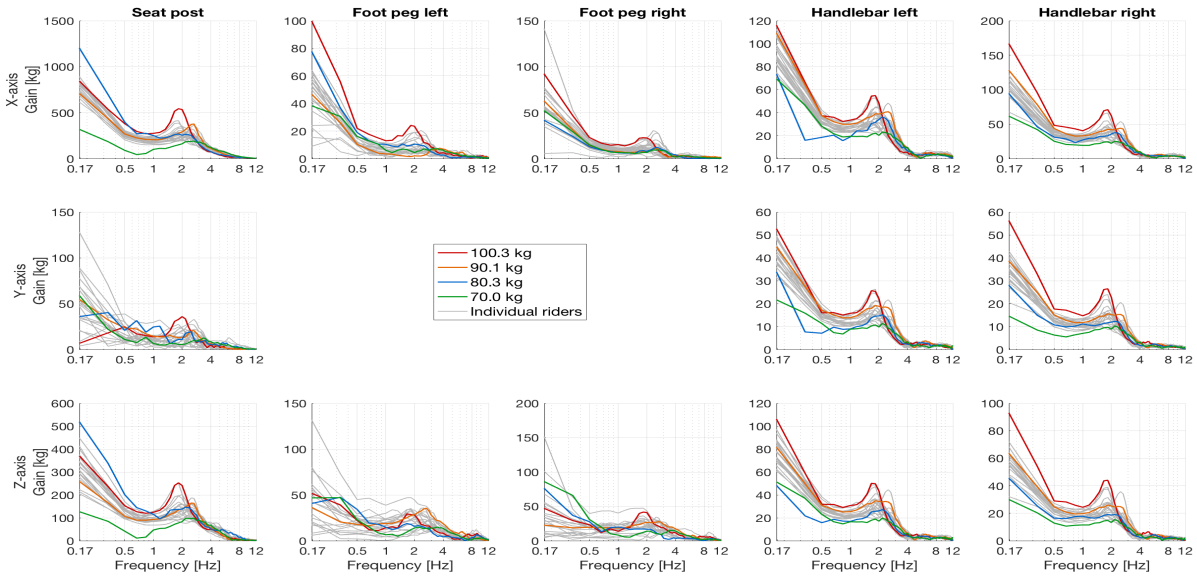

(a) Gain

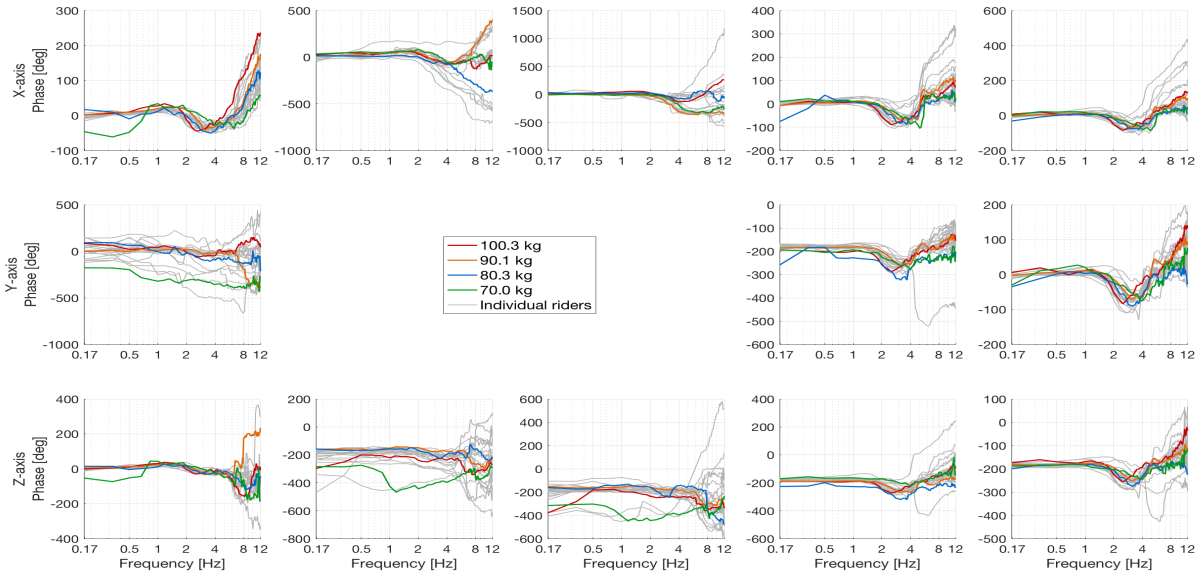

(b) Phase

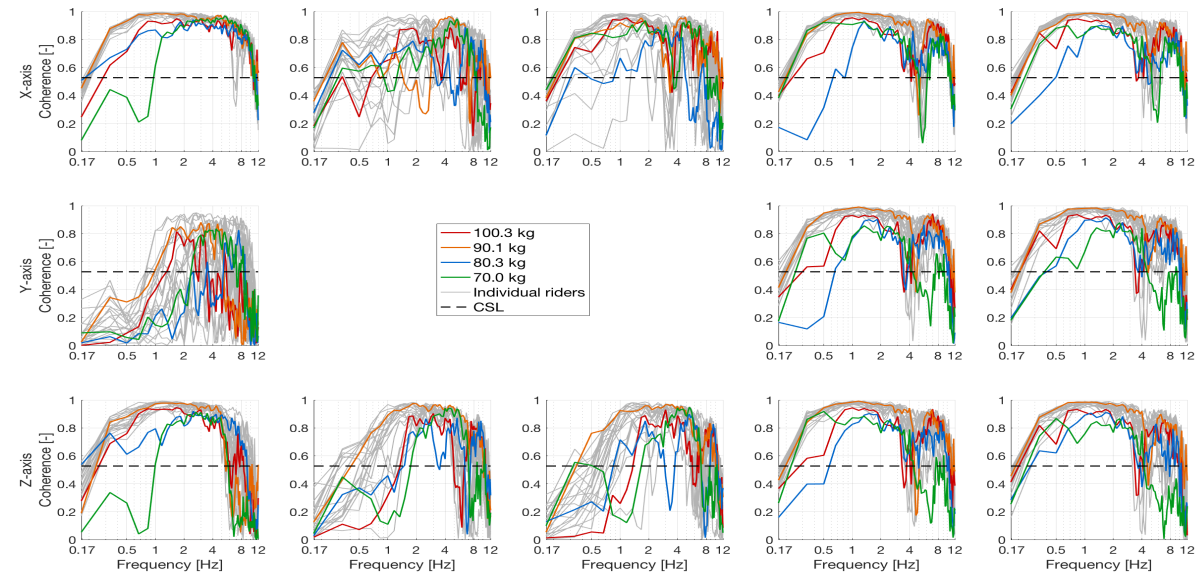

(c) Coherence

Figure J.1: The apparent mass transfer functions $M(f)$ of 24 individual participants for the pitch motion (around Y-axis) at the seat post, foot pegs and handlebars. (a) gain, (b) phase and (c) coherence. The coloured lines indicate 4 riders with specific body weights. The black dashed line in the coherence plots indicate the CSL (= 0.53).

K

Appendix J: Yaw individual apparent mass transfer functions

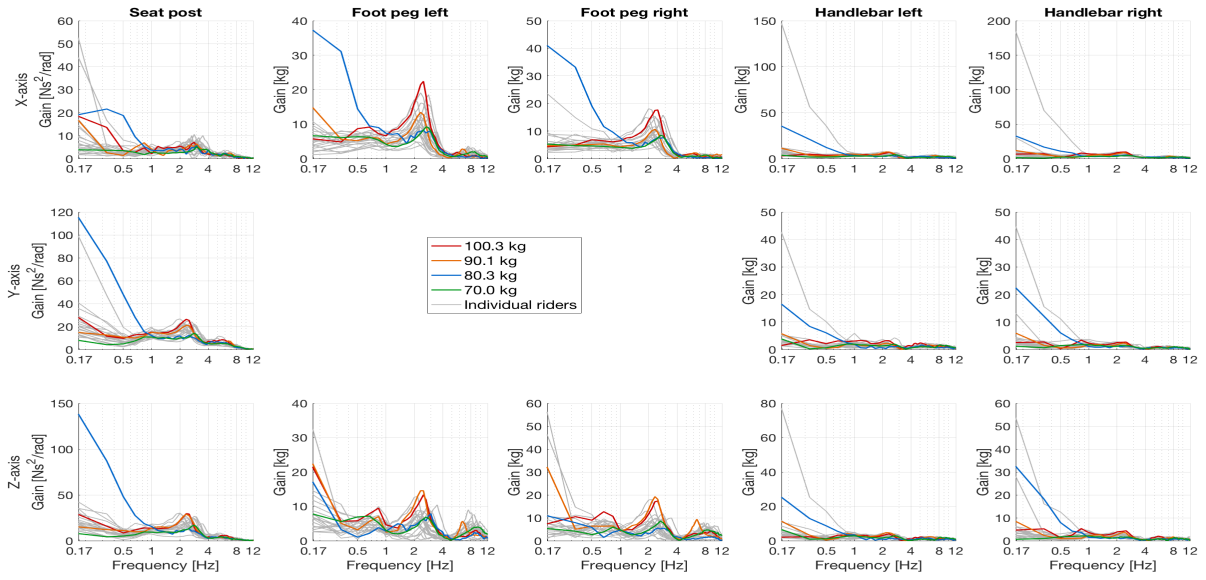

(a) Gain

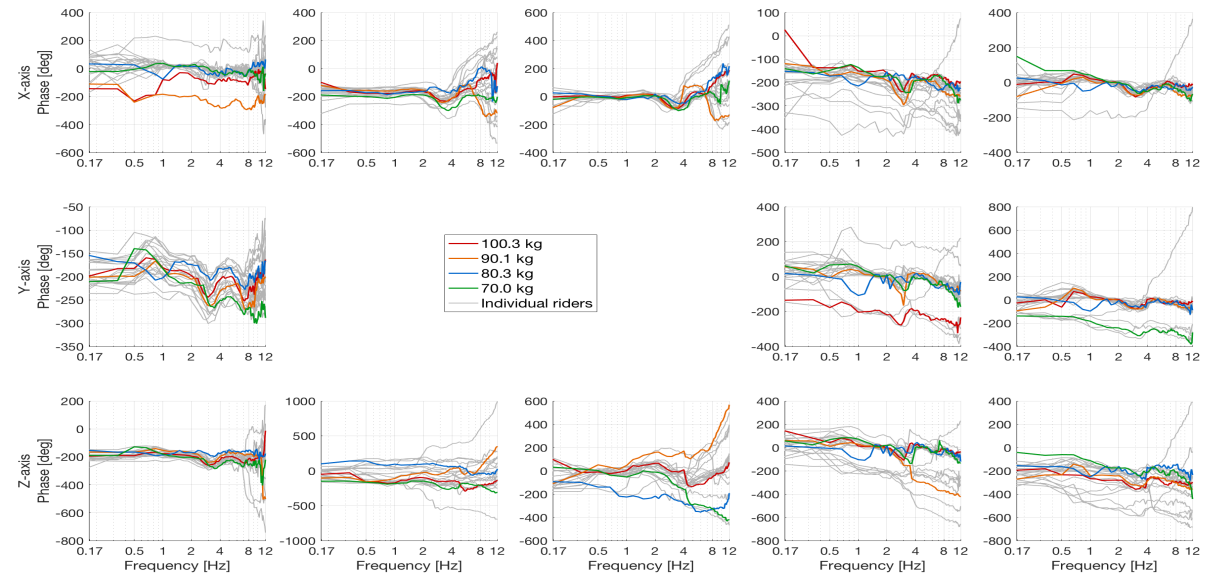

(b) Phase

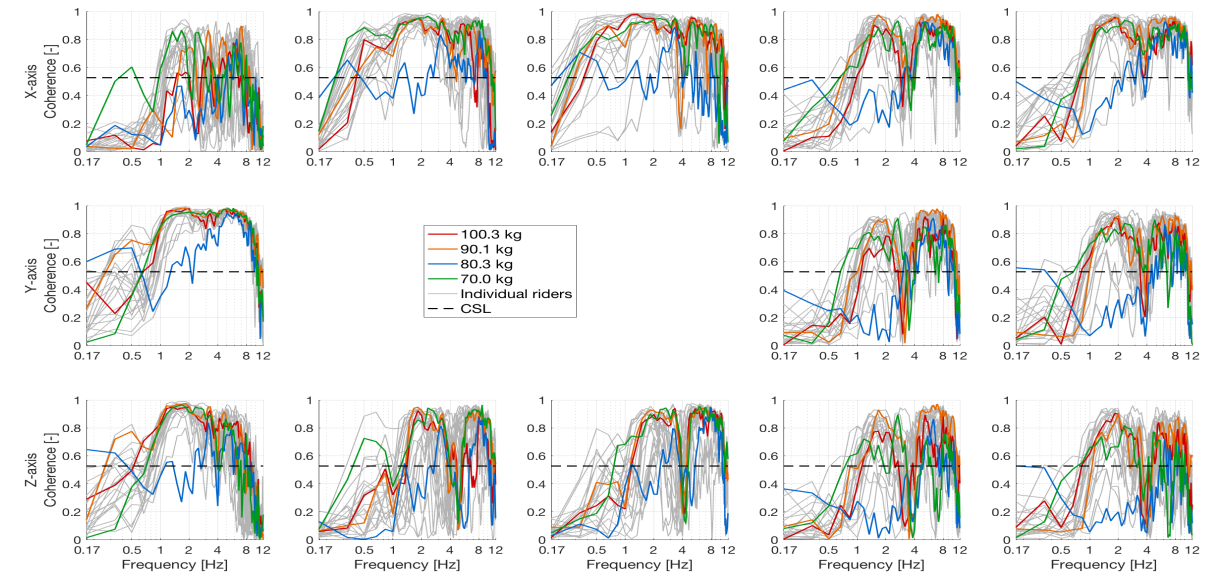

(c) Coherence

Figure K.1: The apparent mass transfer functions $M(f)$ of 24 individual participants for the yaw motion (around Z-axis) at the seat post, foot pegs and handlebars. (a) gain, (b) phase and (c) coherence. The coloured lines indicate 4 riders with specific body weights. The black dashed line in the coherence plots indicate the CSL (= 0.53).